THE EFFECT OF INTERMEDIATE THERMOMECHANICAL TREATMENTS ON THE FATIGUE PROPERTIES OF TWO 7XXX ALUMINUM ALLOYS

A THESIS

Presented to

The Faculty of the Division of Graduate Studies

by

Robert Edward Sanders, Jr.

In Partial Fulfillment

of the Requirements for the Degree

Doctor of Philosophy

in the School of Chemical Engineering

Georgia Institute of Technology

July, 1978

THE EFFECT OF INTERMEDIATE THERMOMECHANICAL

TREATMENTS ON THE FATIGUE PROPERTIES

OF TWO 7XXX ALUMINUM ALLOYS

Approved:

Dr. Edgar A. Starke, Jr.
Chairman

Dr. Miroslav Marek

Dr. Pieter Muije

Date approved by Chairman: 8/2/78

ACKNOWLEDGEMENTS

The author would like to express his deepest gratitude to his thesis advisor, Dr. Edgar A. Starke, Jr. Dr. Starke's patience and guidance during the course of the investigation made this research an invaluable educational experience. The comments and suggestions of Drs. M. Marek, P. Muije, S. B. Chakrabortty and J. T. Berry are also appreciated. Helpful discussions with his friends and colleagues, Dr. F. S. Lin, Dr. T. H. Sanders, Jr., E. J. Coyne, Jr., and J. G. Rinker are gratefully acknowledged by the author.

The financial support and cooperation of Lockheed-Georgia Company made the completion of this research possible. The author would like to particularly thank Mr. R. W. Milling, who administered the research contract. Special thanks go to W. M. McGee, who provided much-needed technical support and knowledgeable advice during the research program. The assistance of Ron Michael, Dave Anderson, and Jack Hunter of Lockheed-Georgia are also appreciated.

The author would like to thank the Alcoa Technical Center and the Army Materials Laboratory who provided the materials used in this research. Discussions with J. T. Staley, D. A. Mauney, R. R. Sawtell, Dr. J. Waldman, and H. Sulinski were extremely helpful during the course of this investigation.

The assistance of Ms. Rebecca Petty, whose art work added much to the presentation of this research, is deeply appreciated. The

capable typing of Ms. Darlene Coyne is also acknowledged.

Special thanks go to the brothers of Beta Theta Pi at Georgia Tech for their support and fellowship during the many non-working hours. Finally, the author would like to dedicate this work to his family, Mr. and Mrs. R. E. Sanders, and sister, Sally, whose love and encouragement made the completion of this research possible.

TABLE OF CONTENTS

LIST OF ILLUSTRATIONS

LIST OF TABLES

SUMMARY

The effect of different ingot processing techniques on the microstructure, monotonic and fatigue properties of 7050 and 7475 aluminum alloys has been investigated. Properties of these alloys after processing by newly-developed intermediate thermomechanical treatments (ITMT) were compared to those of hot-rolled materials which received commercial type processing.

ITMT materials of the two alloys were studied in both the as-recrystallized (AR) and as-recrystallized plus hot-rolled (AR+HR) conditions. Microstructures of the AR variants were highly recrystallized with very fine equiaxed grains. AR+HR materials were partially recrystallized with an elongated pancake-type grain morphology. Hot-rolling of the two alloys, used to simulate commercial processing, produced lamellar, largely unrecrystallized microstructures. The 7050 experimental materials were more fully recrystallized than their 7475 counterparts due to the presence of different dispersoid phases and slight differences in processing conditions.

Hot-rolled variants of the experimental alloys exhibited the best overall combination of fatigue properties of the materials studied. The predominantly unrecrystallized microstructures of hot-rolled 7050 and 7475 promoted a high-energy-absorbing transgranular fracture mode and led to superior resistance to fatigue crack propagation and unstable fracture. The more recrystallized ITMT materials experienced

a higher degree of intergranular fracture which contributed to higher fatigue crack growth rates and lower fracture toughness values. The presence of a large volume fraction of Al_2CuMg in ITMT variants of 7050 was particularly detrimental to the fracture resistance of this alloy.

Total low cycle fatigue and high cycle fatigue lives of the experimental materials were relatively unaffected by changes in microstructure produced by ingot processing. However, quantitative metallography showed that the crack initiation resistance of AR variants was somewhat improved over that of the hot-rolled materials. Crack initiation at slip bands, which occurs extensively in the unrecrystallized hot-rolled microstructure, is severely limited by the fine grain size and random texture produced by AR-type ITMT processing.

The fatigue crack propagation data of the present investigation showed that the presence of residual stresses in un-stretched plate material could markedly affect crack growth rates. A method was suggested to correct for residual stresses in WOL-type specimens and obtain a rough approximation for an "effective" ΔK. Upon the application of this method, the corrected 7475 fatigue crack propagation data was compared to the results of a predictive equation based on low cycle fatigue and microstructural parameters. The relationship correctly predicted the relative order of fatigue crack propagation resistance for the three 7475 experimental materials.

CHAPTER I

INTRODUCTION

The extensive use of age hardenable 7XXX aluminum alloys at high strength levels, i.e., greater than 520 MPa (75 ksi), has been hampered by poor secondary properties of toughness, stress corrosion resistance, and fatigue resistance, particularly in the short transverse direction. The importance of these materials in airframe construction[1-6] and Army armament items[7-11] has stimulated recent attempts to improve these properties. Some secondary property improvements have been obtained by employing slight changes in alloy chemistry[12,13], different grain refining elements[13], or removal of the impurity elements Fe and Si[3,14,15]. Such research has led to the development of alloys[3,14] with improved fracture toughness and stress corrosion resistance compared to the extensively used 7075. However, significant improvements in fatigue resistance have not been realized as yet.

Microstructure control through modification of conventional primary processing methods has been examined as a way of upgrading the properties of these alloys. These methods, called thermomechanical treatments (TMT) may be divided into two classifications: (1) Final Thermomechanical Treatments (FTMT),[2,4,5,16-23] which are applied to the wrought material and are also known as thermomechanical aging (TMA) practices[19], and (2) Intermediate Thermomechanical Treatments

(ITMT)[7-11,24], which are specialized ingot processing techniques applied before the final working operation. The FTMT processing sequence normally consists of solution heat treatment, quench, pre-aging, cold or warm work, and final aging. The dislocation structure introduced during the working operation is presumably stabilized by heterogeneous precipitation during the final aging step. Various types of FTMT have produced increased strength levels in 7XXX materials, but have been much less successful in improving fracture toughness and fatigue crack growth resistance[2,4,5]. Some workers have noted that FTMT does not necessarily offer a more attractive combination of mechanical properties than can be obtained by modifications in alloy purity[18] and heat treatment[2].

The application of ITMT to 7XXX alloys can result in a fine-grained recrystallized microstructure through the use of special ingot processing techniques. Conventional processing of commercial alloys typically results in highly-elongated grains with resulting directional mechanical properties. Consequently, poor fracture resistance in the short transverse direction has long been a problem in 7XXX thick plate material. Workers at the Frankford Arsenal Army Materials Laboratory and The Instituto Sperimentale dei Mettalli Leggeri (ISML) have developed an ITMT which uses a relatively low temperature (250°-270°C) deformation followed by a high-temperature recrystallization step to obtain fine-grained structures. Additional studies at Frankford Arsenal have produced ITMT materials in both the as-recrystallized (AR) and as-recrystallized plus hot-rolled (AR+HR) conditions. The AR material has a fine, completely recrystallized grain structure. A final hot-rolling

step applied to AR material produces the partially-recrystallized microstructure of the AR+HR material. The application of ITMT processing to 7075 has resulted in improved properties of elongation, toughness and short transverse stress corrosion resistance[7,24]. Subsequently, ITMT has been applied to a wide variety of aluminum alloys[8,9]. Several studies[1,7,24,25] have pointed to the possibilities of achieving improved fatigue properties through the application of ITMT to 7XXX series alloys. However, to date, there has not been a systematic study of the fatigue performance of ITMT materials. The present work was undertaken to clarify the role of grain structure produced by ITMT on the fatigue properties of two high-strength 7XXX aluminum alloys.

CHAPTER II

REVIEW OF THE LITERATURE

Second-Phase Particles in 7XXX Aluminum Alloys

The strength, toughness, and other mechanical properties of the 7XXX (Al-Zn-Mg-Cu) alloys are determined to a large degree by the second-phase particles present in the microstructure. The frequency, distribution, and morphology of these particles are controlled by the alloy composition and the thermal and mechanical processes applied to the ingot during the fabrication of a wrought product. Three types of second-phase particles are ordinarily found in precipitation-strengthened 7XXX aluminum alloys[6]: (a) Strengthening precipitates (~0.001 to 0.5 μm), (b) Dispersoid particles (0.01 to 0.5 μm), and (c) Constituent particles (~2 to 50 μm). The origin of these particles in the microstructure and their effect on the mechanical properties of these alloys will be discussed in more detail below.

Strengthening Precipitates and Deformation Behavior of 7XXX Alloys

The achievement of high yield strengths in 7XXX aluminum alloys is made possible by a precipitation hardening mechanism. For aging at temperatures of commercial importance, the precipitation sequence[26] is:

Supersaturated solid solution → G.P. zones → η' → η

The GP zones result from statistical variations in the concentrations of solute (Zn, Mg, and Cu) atoms, forming regions of short range order[27]. The zones are spherical or ellipsoidal in shape depending on solute chemistry and completely coherent with the aluminum matrix. The exact structure and composition of the zones are unknown. Some controversy seems to exist regarding the presence of η' in the sequence, but Gjonnes and Simensen[27] after a transmission electron microscopy study stated that they established its presence "without a doubt." The η' phase is hexagonal, platelike and coherent with the {111} planes of the aluminum matrix. The hexagonal η phase, $MgZn_2$, is completely incoherent with the matrix and is the equilibrium phase in 7XXX alloys of commercial importance.

Increasing the copper content of 7XXX alloys has been shown to markedly affect precipitation and mechanical properties. Copper enters directly in the precipitation sequence and increases the temperature range of GP zone stability[28,29]. The results of Sanders and Starke[30] showed that the addition of copper to an Al-Zn-Mg alloy increased the frequency of GP zone nucleation and accelerated the GP zone $\rightarrow \eta'$ transition during artificial aging at 120°C. The addition of copper to Al-Zn-Mg alloys has also been shown to increase the strength and stress corrosion cracking resistance.

The types of dislocation-precipitate interactions occurring in the Al-Zn-Mg system and the resultant mechanical properties of these alloys are markedly affected by the precipitate type, size, and spacing. Dislocations may cut through the coherent particles, such as GP zones, or by-pass larger incoherent η particles. For alloys deforming by a

cutting mechanism, an increase in shear stress may occur due to dislocation interactions with precipitate stress fields, disordering of ordered particles, and differences in elastic moduli or stacking fault energies between precipitates and matrix[26,31]. The looping mechanism, proposed by Orowan[32], is based on the stress required for dislocations to by-pass particles, leaving dislocation loops. Hirsch[33] has described a series of dislocation movements involving cross slip to explain the Orowan process. Quantitatively the two mechanisms have been described by Gerold[34]. The strengthening effect of the particles is calculated for looping by:

$$\Delta\tau_o = \frac{2T}{bR} \cdot \left(\frac{f}{2}\right)^{\frac{1}{2}}, \text{ and} \qquad (1)$$

for cutting,

$$\Delta\tau_o = \frac{F}{b^2} \cdot \frac{F'}{2T} \cdot \frac{f}{2} \cdot \left(\frac{R}{b}\right)^{\frac{1}{2}}, \qquad (2)$$

where:

$\Delta\tau_o$ - is the increase in shear stress due to the dispersion,

F - is the average maximum force before particle shearing,

F' - is a measure of relative particle strength and F = F'R/b,

T - is the line tension of the dislocation,

f - is the volume fraction of the particles,

R - is the particle radius, and

b - is the Burger's vector of the dislocation.

An aging curve shown in Figure 1 may be interpreted in terms of precipitate-dislocation interactions. The as-quenched hardness of the alloy is very low. Cross slip readily occurs and the alloy deforms homogeneously, i.e. with a wavy slip mode. As the alloy is aged to peak hardness, hardness increases due to the growth of shearable GP zones and the precipitation of η'. Dislocations shear the closely-spaced precipitates and become concentrated on individual slip planes, resulting in a planar slip mode[35]. Cross slip is limited and narrow localized dislocation bands are observed. At peak hardness, the microstructure consists of GP zones, semi-coherent η', and some η. As overaging occurs, most of the microstructure consists of widely-spaced incoherent η particles, and looping becomes the dominant deformation mechanism. With further over-aging the hardness decreases as predicted by Equation 1. The occurrence of looping in the overaged alloy results in a more homogeneous, wavy type of slip[35,36]. Thomas and Nutting[36] have proposed that the wavy slip character of overaged alloys is due to the promotion of cross slip in the vicinity of incoherent particles.

Ductility has been shown to vary inversely with hardness for age-hardened aluminum alloys. Originally, some workers[36] attributed the brittleness associated with peak-aged aluminum alloys to preferred deformation and fracture in soft precipitate-free-zones (PFZ's) adjacent to grain boundaries. The formation of PFZ's in these alloys is affected by many variables, including alloy composition, homogenization temperature, and aging conditions[37]. PFZ's are

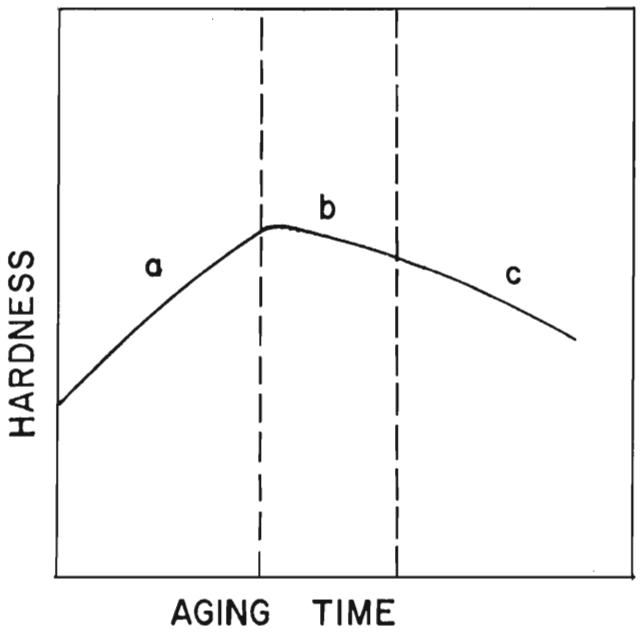

a. Underaged: shearing, GP zones.

b. Peak hardness: shearing, all types of precipitates.

c. Overaged: looping, widely-spaced incoherent precipitates.

Figure 1. Schematic Aging Curve for Age-Hardening 7XXX Aluminum Alloys.

often accompanied by large η grain boundary precipitates, which have also been cited as a source of brittleness in Al-Zn-Mg type alloys[38]. However, Ryum et al.[37] have shown that brittleness associated with peak-hardened alloys is due to the presence of localized dislocation bands in the matrix, rather than deformation within the PFZ. The impingement of these dislocation bands on grain boundaries sets up high local stresses, resulting in intergranular fracture and a reduction in ductility. Grain-boundary precipitates can effectively weaken grain boundaries and reduce ductility by promoting void formation at the particle/matrix interface during deformation[38]. Consequently, to insure good ductility in commercial 7XXX alloys, processing is controlled to obtain fine grain structures and minimize the occurrence of large grain boundary precipitates.

The improved homogeneity of deformation observed in overaged 7XXX alloys may be the basis for obtaining better stress corrosion cracking (SCC) resistance and somewhat improved toughness[39]. The superior properties are attributed, as in the case of ductility, to the reduction in planar slip and accompanying intergranular fracture found in peak-aged alloys. Some early alloys, e.g. 7079, experienced severe strength reductions when overaged to improve SCC resistance. However, most modern 7XXX alloy compositions allow overaging to produce acceptable fracture toughness and SCC resistance with only 15-20% loss of strength. These overaged conditions have been accepted widely in commercial practice and are generallly achieved by a two-step artificial aging sequence in which the initial aging (usually at 120°C) is followed by a final higher-temperature aging step in the 150°-170°C range. The commercially

important overaged conditions for 7XXX alloys are the T76 and T73 tempers. The latter designation refers to the more overaged condition.

Workers have recently extended the correlations found between slip character and monotonic deformation to the problem of fatigue. These developments will be discussed in a later section regarding the effects of microstructure on fatigue in 7XXX alloys.

Dispersoids in 7XXX Alloys

The presence of dispersoid particles in high-strength 7XXX alloys is due to the addition of small amounts of chromium (0.3% max.), manganese (0.8% max.), or zirconium (0.2% max.) to the alloy composition[14]. These elements have extremely low solubility in aluminum and are precipitated from supersaturated solid solution during ingot solidification. During subsequent heat treating and working operations, they cannot be completely redissolved but may undergo alteration in particle size and distribution. Dispersoid phases found in commercial 7XXX alloys are $Al_{12}Mg_2Cr$(E phase),$Al_{20}Mn_3Cu_2$, and Al_3Zr. The $Al_{12}Mg_2Cr$ amd $Al_{20}Mn_3Cu_2$particles generally range in size from 0.02 to 0.05 μm. The Al_3Zr particles are usually somewhat smaller (<0.02μm).

During fabrication of wrought products, dispersoids inhibit recrystallization and grain growth in 7XXX alloys. Grain boundaries are effectively "pinned" by dispersoid particles during thermal and mechanical operations, ideally resulting in an unrecrystallized microstructure in thick sections. In commercial practice, however, partial recrystallization often occurs in spite of the dispersoids. The extent of recrystallization depends upon the severity and temperature of the mechanical operations and the temperature and duration (to some extent) of the

thermal treatments. This effect allows for the possibility of grain structure modification by intermediate thermomechanical treatments (to be discussed later).

The effects of dispersoids on the mechanical properties of 7XXX alloys may be interpreted by their effects on grain structure and subsequent microstructure/property analyses. Dispersoids have little effect on strength in 7XXX alloys since this property is primarily governed by the closely-spaced hardening precipitates. (However, one study[25] did report a slight yield strength increase, ~40 MPa, attributed to the presence of Al_3Zr when zirconium was added to an Al-Zn-Mg alloy). The toughness of 7XXX alloy plate material has been shown to be inversely related to the degree of recrystallization[3,14]. Thus, fine dispersoid distributions which promote an unrecrystallized structure are preferable for improved fracture resistance[1,3,14]. The unrecrystallized structure promotes a high energy absorbing transgranular fracture mode in preference to the low energy intergranular fracture of recrystallized materials[39].

Staley's[14] results indicate that the amount of dispersoid forming element in 7XXX alloys should be held to the minimum required for the attainment of the desired grain structure. Crack propagation energy was found to decrease linearly with increasing chromium content in 7075 sheet. This was attributed to a void sheet formation[40] mechanism in which microvoids form at dispersoids and coalesce to link fractured constituent particles. The same study [14] also showed that substitution of zirconium for chromium as the dispersoid-former results in increased toughness in 7475-type alloys. However, this

result was not substantiated when standard K_{IC} specimens were tested.

Quench sensitivity in 7XXX alloys occurs when a significant number of solute atoms are tied up in the formation of $Al_{12}Mg_2Cr$ or $Al_{20}Mn_3Cr$ dispersoids[39]. With a smaller amount of solute available to participate in the age hardening sequence, strength is reduced. Zirconium, which forms Al_3Zr, has been shown to reduce quench sensitivity in 7XXX alloys. Since Al_3Zr does not tie up solute atoms in dispersoid formation, desirable strength levels can be maintained.

Constituent Particles

Constituent particles in 7XXX aluminum alloys may be: (a) insoluble compounds resulting from the presence of the impurity elements iron and silicon, or (b) partially soluble intermetallic particles composed of the major alloying elements. The first type of particles, identified primarily as Al_7Cu_2Fe, $FeAl_6$, and Mg_2Si[14], separate during ingot casting, and may be up to 30 μm in the longest dimension. These particles are often found strung out in the primary fabrication direction of wrought products and often contribute to a mechanical fibering effect. The partially soluble intermetallics of the second type result from incomplete solution of the primary alloying elements during heat treatment and fabrication. In some cases, complete solution of these particles is impossible since non-equilibrium melting may occur before a sufficiently high solutionization temperature is reached[14]. The chief consituent phase of this type in 7XXX alloys is Al_2CuMg[6].

It is generally agreed that the fracture of consituent particles under stress leads to preferential paths for crack advance and reduced

toughness[14,39]. It has been shown that decreasing Fe and Si levels in 7XXX alloy compositions can markedly increase toughness values. Consequently, "cleaner" alloys such as 7475 and 7050 have been introduced which take advantage of higher purity levels, in part, for the achievement of improved fracture toughness[3,39]. Since the presence of Al_2CuMg has also been shown to be significantly detrimental to toughness in 7XXX alloys[14], careful control of alloy chemistry, thermal treatments, and deformation processing is necessary to avoid this effect. It is possible, within limits, to modify the size, distribution and volume fraction of Al_2CuMg to obtain improved toughness[14].

Fatigue Testing

Strain-Controlled Low Cycle Fatigue Testing

The fatigue problem has historically been approached by subjecting standard specimens to cyclic loading and measuring cycles to failure. This type of stress-constrolled testing results in the typical "S-N" curve shown in Figure 2(a) and has long been used to rank materials for engineering applications[41]. However, in many applications,e.g. some aerospace components, automobile parts, or pressure vessels[41], it is often desirable to obtain fatigue data at low cyclic lives, where resistance to cyclic strains, rather than stresses, is of primary importance. Consequently, the use of strain-controlled low cycle fatigue (LCF) testing has become an important tool for the evaluation of a material's response to cyclic loading at or above the material's yield strength[42].

During a LCF test conducted at a constant strain amplitude, the

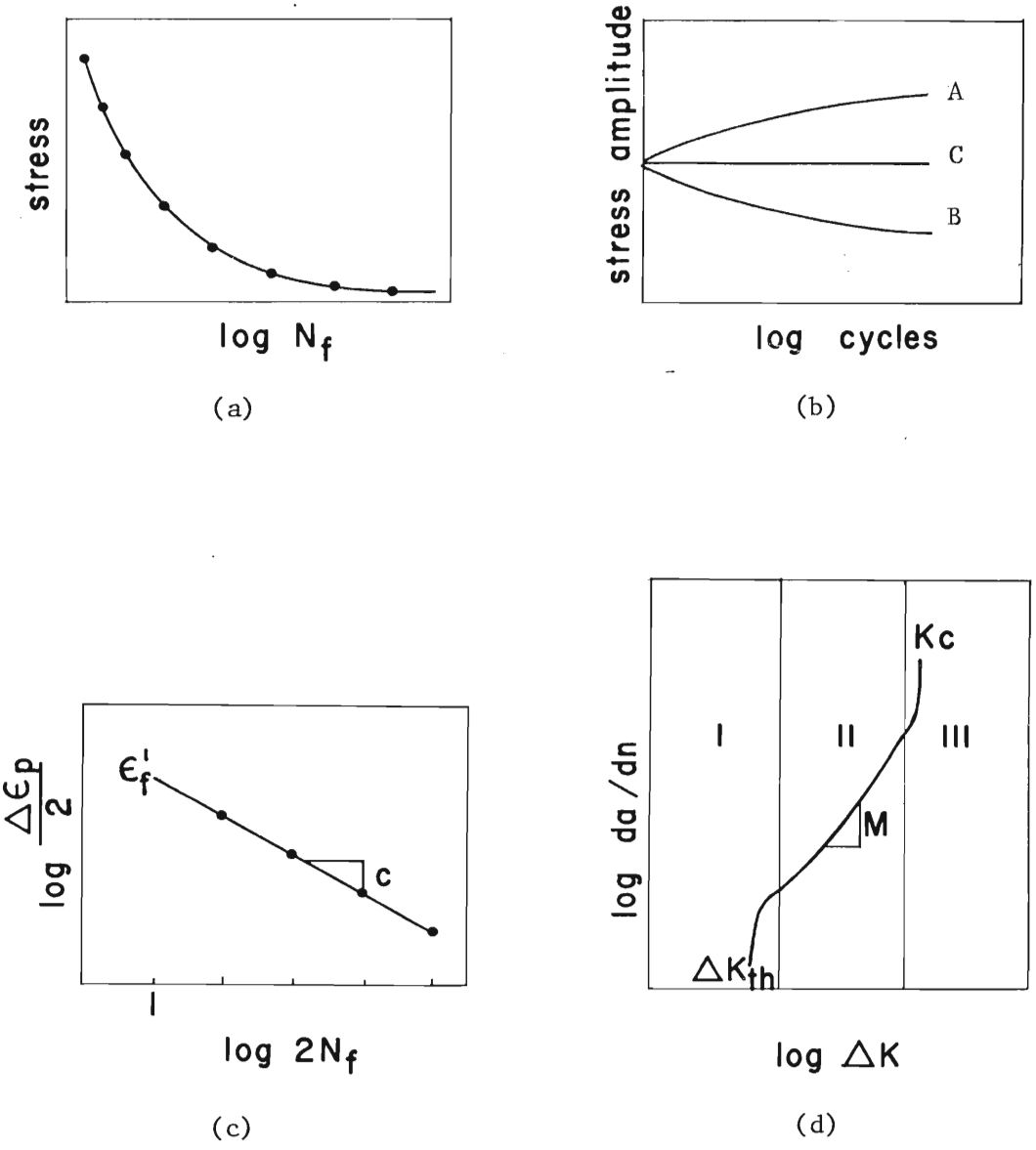

Figure 2. Various Empirical Treatments of Fatigue Data: (a) Typical S-N curve, (b) Cyclic hardening-softening curve, (c) Coffin-Manson plot, and (d) da/dN versus ΔK treatment of FCP data.

stress amplitide is monitored, leading to a plot of stress amplitude versus cycles such as in Figure 2(b). A material's stress response during a LCF test may be: (1) cyclic hardening (curve A in Figure 2(b)), (2) cyclic softening (curve B), or (3) saturation (curve C). From a number of LCF tests conducted at different strain amplitudes, a cyclic stress-strain curve may be plotted from the empirical relation shown in Equation 3.

$$\sigma_a = k' \left(\frac{\Delta\varepsilon_p}{2}\right)^{n'} \tag{3}$$

where:

σ_a - tensile stress amplitude at saturation,

$\frac{\Delta\varepsilon_p}{2}$ - plastic strain amplitude at saturation,

n' - cyclic work hardening exponent.

Engineers have recently begun to use the cyclic stress-strain curve in the design of parts subjected to fatigue loading since the monotonic stress-strain curve may not give a true representation of a material's cyclic strength.

The treatment of strain-controlled LCF data can also be accomplished through the use of the empirical Coffin-Manson[43,44] relationship, Equation 4.

$$\frac{\Delta\varepsilon_p}{2} = \varepsilon'_f \cdot (2N_f)^{-c} \tag{4}$$

where:

ε'_f - fatigue ductility coefficient,

$2N_f$ - twice the number of cycles to failure,

c - fatigue ductility exponent.

A graphical representation of the Coffin-Manson plot is shown in Figure 2(c). The value of ε'_f is taken at $2N_f = 1/2$[43], or $2N_f = 1$[45], and has been often equated with the value of ε_f, the true strain to fracture in a monotonic tensile test. However, in aged aluminum alloys, ε'_f has often been observed to be considerably larger than ε_f. The value of c has typically been observed to range from -0.5 to -0.7 for most aged aluminum alloys. Sanders and Starke[25] showed that the value of c was sensitive to aging treatment and large differences in grain structure for Al-Zn-Mg-type alloys. Other investigators have shown that considerable deviations from linearity occur in the Coffin-Manson plots of aluminum alloys particularly at long LCF lives[30,43,46,47]. Typically observed LCF lives at low strain amplitudes were much shorter than predicted by extrapolation from the high strain amplitude portion of the curve. Many explanations have been offered to explain the failure of Coffin-Manson plots to predict LCF data of aluminum alloys. However, most often, these phenomena were attributed to microstructural effects which caused strain localization (i.e., non-homogeneous deformation) at low plastic strain amplitudes.

Fatigue Crack Propagation Testing

Recent fatigue studies of aluminum alloys have been aimed at improving the resistance to fatigue crack propagation (FCP). This approach has been made necessary by the high probability of the existence of material or manufacturing defects as crack initiation sites in actual structures. Consequently, crack growth rates are the primary determinant of total fatigue life in such structures.

Experimentally, the most common measurement of material susceptibility to FCP is based upon the determination of crack growth rate, $\frac{da}{dN}$, as a function of ΔK, the stress intensity range. The most generally accepted crack growth equation has been proposed by Paris et al.[48] and is shown in Equation 5:

$$\frac{da}{dN} = C \cdot (\Delta K)^M \tag{5}$$

where:

$\Delta K = K_{max} - K_{min}$; K is the stress intensity factor,

C and M = experimentally determined parameters.

Values for M found in the literature usually range between 2 and 4. Extensive reviews of the FCP literature may be found in References 46 and 49. Equations used to calculate K for various specimen designs are given in Reference 49.

The basic FCP behavior of aluminum alloys are generally defined

by plots of log $\frac{da}{dN}$ versus log ΔK as shown in Figure 2(d). Fatigue crack propagation in Region I of Figure 2(d) is said to exhibit a "threshold" effect, i.e. there is a ΔK_{th} below which fatigue cracks will not propagate. In Region II, da/dN varies with ΔK according to the Paris equation. FCP rates in Region III deviate from the predictions of Paris as they asymptotically approach a limiting value of fracture toughness, K_c. The acceleration of FCP rates in this region is often attributed to a transition to plane stress in Region III from plane strain in Region II. From the comparison of da/dN versus ΔK data, the effects of such variables as heat treatment, processing variables, and environment on FCP may be investigated.

Microstructural Effects on Fatigue in 7XXX Alloys

Cyclic Stress-Strain Response

Since the advent of strain-controlled LCF testing, a great deal of effort has been devoted to the study of microstructural effects on cyclic stress-strain behavior. The observation that various aluminum alloys cyclically harden or soften was typically attributed to the type of precipitate structure present in the alloy. The work of Calabrese and Laird[50,51] has been most helpful in understanding the precipitate-dislocation interactions which control cyclic stress-strain response during LCF. They strain-cycled an Al-4Cu alloy containing different precipitate structures and correlated their results to TEM observations. The authors noted that the microstructures containing shearable GP zones cyclically hardened to a saturation state and then softened. They

correlated the behavior to an increase in dislocation density (hardening) followed by the accumulation of dislocations into discrete bands (softening). The authors attributed the softening to a scrambling of the ordered zones by the to and fro motion of dislocations on their glide planes. The reduction in order of the zones destroys their hardening capabilities, leading to the accumulation of dislocations in planar bands. For strain-controlled cycling of microstructures containing a fine dispersion of incoherent plate-like precipitates, they noted very little work hardening, followed by immediate saturation of the stress amplitude. No cyclic softening was observed. From TEM observations, they determined that dislocations are stored at the plate-matrix interfaces and the saturation stress is determined by the shuttling of dislocations between the plate-like precipitates. In microstructures containing very coarse incoherent precipitates, dislocation cells are formed and the cyclic stress-strain response is similar to that for single phase materials. The saturation stress is accounted for by the shuttling of dislocations between cell walls.

While the previous work is important in deriving mechanisms for cyclic stress-strain response, it has been observed[52] that commercial 7XXX alloys, in contrast to the binary alloys just described do not undergo cyclic softening by precipitate-dislocation interactions. Laird[52] attributes this effect to the strain homogenization induced by the presence of dispersoids and the commercial processing which tends to produce a less-ordered, "scrambled" structure. Another study[53] has reported cyclic

softening in 7XXX alloys subjected to commercial-type processing. However, the author pointed out that the softening was not a result of repeated precipitate-shearing by dislocations, but was due to extensive micro-cracking on the specimen surface during latter stages of the LCF test.

Crack Initiation and Stage I Propagation

Microstructural effects on fatigue failure in aluminum alloys can be interpreted as they relate to the two stages of the fatigue process: (a) crack initiation, and (b) crack propagation. Microstructural features such as grain size and second phase particles can significantly alter these processes during fatigue of 7XXX alloys.

Crack initiation often takes place in smooth specimens by a process of slip band decohesion. Persistent slip bands (PSB's), which are formed during cyclic loading, intersect the specimen surface and become the sites for the occurence of intrusions and/or extrusions[49]. One dislocation model which accounts for this phenomenon is the random-walk mechanism in which a series of random, irreversible displacements on the primary glide plane within the PSB leads to the development of a notch peak topography[49]. A slip ratcheting mechanism postulates a repetitive movement of screw dislocations with each cycle that, depending upon the sign of the dislocation, forms an intrusion or extrusion. After the initiation of a crack, Stage I crack propagation occurs in which the crack grows along the slip band. Due to the crystallographic nature of both events, it is extremely difficult to separate crack initiation and

Stage I growth. Consequently, it is often necessary to choose an arbitrary measure of length for a crack before we can say that crack initiation has occurred.

In age-hardened 7XXX alloys, precipitate structures which control slip mode can significantly affect crack initiation processes. Hunter and Fricke[54] noted that increasing magnesium additions to aluminum alloys promoted localized deformation and decreased high cycle fatigue life even though static strength was increased. Another study[55] showed that the fatigue life of Al-Cu-Mg was improved by the addition of ~0.1-0.2 micron sized incoherent particles. Dislocation structures in such alloys were much more homogeneous than the banded PSB structures found in pure Al-Cu-Mg with no incoherent particles. Finney's[56] results showed that a planar slip mode in Al-Cu-Mg actually increased fatigue life due to an increased degree of slip reversibility. The two studies may seem somewhat contradictory since the beneficial effects on fatigue resistance of the two types of particles (coherent and incoherent) arise from different mechanisms. In recent studies, Grosskreutz[57], Fine[58], and Calabrese and Laird[50] have proposed that a microstructure containing a fine, closely-spaced coherent dispersion to increase yield stress and large particles to homogenize the deformation would yield good fatigue resistance. Sanders and Starke[25] have recently studied the relationship between microstructure and low cycle fatigue resistance in two Al-Zn-Mg type alloys. Their results indicated that microstructures which promote homogeneous slip (e.g., small grain sizes, incoherent precipitates) lead to improved low cycle fatigue life, since the

elimination of planar slip tends to delay crack initiation at high strain amplitudes. However, their data also predicted that, for long fatigue lives, slip reversibility may be the most important factor for increasing fatigue life.

The concept of slip mode is essential to the explanation of grain size effect on fatigue crack initiation. Thompson and Backofen[59] attributed grain size effects on high cycle fatigue to the propagation of Stage I cracks. They pointed out that, in planar slip materials, dislocation motion accompanying crack growth is not impeded until a grain boundary is encountered. In wavy slip materials, dislocation cell structures hinder Stage I crack growth and eliminate the grain size effect.

Laird and Feltner[60] attributed grain size effects on LCF to the nucleation and growth of Stage I cracks at grain boundaries. As the severity of surface deformation increases during a fatigue test, folding occurs at grain boundaries to accommodate differences in strain between adjacent grains[61]. The folds become more severe until Stage I cracks are initiated. As the stress intensity at the tip of the Stage I crack increases grain boundaries become the dominant factor in controlling the severity of folding and resultant Stage I cracking. A similar argument was offered by Feltner and Beardmore[62] who proposed that slip offsets and resultant stresses developed at grain boundaries are smaller in fine-grained materials (regardless of slip mode). Thus, the occurrence of crack initiation is delayed and LCF life is increased for smaller grain sizes. However, the authors cited data to show that very large reductions in grain

size are necessary to obtain rather limited improvements in LCF life. They observed that achievement of increases in the cohesive strength of grain boundaries would also be beneficial to LCF resistance.

Stage II Crack Propagation

Propagation of Stage II fatigue cracks takes place in a direction perpendicular to that of the applied tensile stress. Laird[63] has proposed that, due to the intense plastic deformation occurring at the crack tip, Stage II cracks produce characteristic fatigue striations with each cycle by a plastic blunting mechanism. However, the absence of fatigue striations when FCP occurred in a vacuum[64] led to other proposed mechanisms[65,66]. These mechanisms have been reviewed in more detail elsewhere[53].

Features most often observed on FCP fracture surfaces of 7XXX alloys include both ductile and brittle striations[67]. The ductile striations are smooth and continuous, and are usually found normal to the macroscopic FCP direction. Brittle striations often are not recognized as striations since they are wider and flatter than the ductile variety. They often appear to be almost quasi-cleavage in nature and are often found to be associated with river patterns perpendicular to the crack growth direction.

The effects of microstructural features on FCP in 7XXX alloys is still somewhat unclear. Some studies indicated that alloy composition and aging treatment can significantly affect FCP rates, particularly in the presence of corrosive environments[2,46,68]. Under corrosion-fatigue conditions, alloys with shearable precipitates

exhibited marked acceleration of FCP compared to inert environments. Other studies showed, however, that FCP rates are relatively unchanged by differences in alloy chemistry or heat treatment[69,70].

The role played by constituent particles, e.g. Al_7Cu_2Fe or Al_2CuMg, in the FCP process is fairly well-established at high ΔK (>20MPa$m^{\frac{1}{2}}$). In this stress intensity range, constituent particles initiate voids in the plastic zone ahead of the crack and FCP is accelerated by the link-up of these voids. At lower ΔK, some workers[71] argue that inclusions may actually retard FCP by causing the crack to deviate from its preferred path normal to the applied stress. This conclusion finds support in recent spectrum loading tests[72], in which alloys with higher constituent contents showed significantly slower growth rates than purer materials following periodic overloads. However, a recent thorough study[6] of microstructural effects on FCP in 7XXX alloys showed no effects of constituent particles at low to intermediate ΔK.

There is some controversy regarding the effect of grain structure on Stage II FCP. By changing dispersoid distribution via different homogenization practices, Rosenfield et al[1] modified the grain size, shape, and degree of recrystallization (DR) of a wide variety of 7XXX alloys. They found that smaller grain size and more unrecrystallized microstructures led to reduced FCP rates. An equally comprehensive study[6], on the other hand, found that FCP rates were insensitive to large changes in grain size. It is probable that grain size effects of FCP in commercial 7XXX alloys are contingent upon such variables as temper (slip mode), inclusion content

(mechanical fibering), fracture mode (intergranular or transgranular), and possibly texture.

Thermomechanical Treatments for 7XXX Alloys

Efforts to obtain improved fracture toughness and fatigue resistance have led to the application of various thermomechanical treatments (TMT) during processing of 7XXX alloys. For convenience, the discussion of TMT may be divided into two classifications: (1) Final Thermomechanical Treatments (FTMT), which are applied to the wrought product, and (2) Intermediate Thermomechanical Treatments (ITMT), which are applied to the ingot before final working. Developments in the application of TMT to 7XXX alloys will be examined with particular emphasis on their potential to affect fatigue properties.

Final Thermomechanical Treatments are applied to aluminum alloys after the final hot working operation. The sequence of operations during FTMT consists of a pre-aging step, followed by a cold- or warm-working step, followed by a final aging step. The significant increases in strength derived in alloys from FTMT result from the dense dislocation network introduced during the mechanical working operation. The final aging step supposedly leads to heterogeneous nucleation of η' on dislocations, resulting in a pinning effect which, according to Osterman[16], stabilizes the dislocation network. (However, it should be noted that, at the temperature (120°C) used for the second aging step in the original investigation of this type[16], the probability of heterogeneous

precipitation of η' is low. This temperature is below the GP zone solvus[73] for 7075 where homogeneous decomposition of the alloy normally occurs. Consequently, pinning of dislocations by η' is not expected to result in a major strengthening effect).

Early studies of 7XXX alloys subjected to FTMT concentrated on the determination of S-N curves for these materials. Osterman[16] reported a significant increase in fatigue strength of 7075 when a FTMT was applied. The improvement in fatigue resistance was attributed to the increased homogeneity of deformation occurring in the FTMT alloys. According to Osterman, the dislocation network provides sites for slip initiation throughout the microstructure and prevents the formation of narrow dislocation bands. The homogenization of deformation leads to an increased resistance to crack initiation, and consequently to improved fatigue life. Osterman's data also showed that the improved fatigue resistance is not simply due to the increased strength of FTMT 7075. The endurance ratio (fatigue strength/UTS) of the FTMT material is significantly higher (0.27 vs. 0.22) than that of the commercially processed 7075. Avitzur[74] stated that the improvement in fatigue properties observed by Osterman could be a result of the elimination of precipitate-free-zones (PFZ's) adjacent to grain boundaries by the FTMT. PFZ's have previously been cited as the causes for intergranular fracture and loss of ductility in Al-Zn-Mg type alloys. However, Osterman[75] pointed out, in support of his original interpretation, that PFZ's in commercial-type alloys are very small and that FTMT did not have an appreciable effect on the fracture mode of 7075.

However, the effect of FTMT on fatigue life of 7XXX-series alloys has not been conclusively established. Two studies[23,76] showed increases in fatigue life due to FTMT application similar to the results of Osterman's[16] work, while two other studies[4,17] showed slightly poorer fatigue resistance for FTMT-7000 series alloys. Another study[18] concluded that FTMT "does not appear to offer very much potential for improving the fatigue strength of 7075" and pointed to the necessity of using higher purity alloys to obtain increases in fatigue resistance. Recent results[52] for the cyclic stress-strain response of FTMT 7XXX alloys showed that the dislocation structure introduced during FTMT was unstable and led to serious cyclic softening during strain-controlled LCF. Laird[52] also concluded that any benefits in fatigue resistance from the application of FTMT to 7XXX alloys are unlikely.

Other studies[2,5] have attempted to evaluate the FCP resistance of FTMT 7XXX alloys. Hyatt[2] found that overaged microstructures and higher purity were as beneficial to crack growth resistance as any FTMT employed in his studies. Thompson and Zinkham[5] showed that significant improvements in FCP resistance were realized by higher purity levels as well as the application of FTMT to 7075. SEM observations revealed a larger incidence of crack branching and undulations in the FTMT material, but no basic change in the mode of crack propagation compared to the commercial 7075. Hence, the authors proposed that the lower crack growth rates observed in FTMT 7075 are due to a more tortuous fatigue crack path.

Intermediate Thermomechanical Treatments

Initial work in the area of processing aluminum ingots showed that substantial increases in ductility and toughness could be obtained by a reduction of undissolved second phases in these alloys[77,78]. These improvements were achieved by the use of "cleaner" (e.g., lower Fe and Si content) materials and more effective homogenization heat treatments. It was shown that a smaller dendrite arm spacing in the ingot material facilitated homogenization and led to improved mechanical properties after hot working.

The most recent developments in the field of ITMT have been aimed at the production of fine, homogeneous grain structures in these alloys[7,24]. Conventional processing received by commercial alloys results in highly-elongated grains and often in directional mechanical properties. Poor fracture resistance in the short transverse direction has long been a problem in 7XXX thick plate material[7]. DiRusso et al.[24] state that the elongated "pancake" grains of commercially-processed 7075 result from the precipitation of E phase particles prior to hot working, allowing the as-cast ingot structure to be retained as the primary determinant of final wrought grain morphology. An ITMT was developed by DiRusso et al.[24] (ISML-ITMT) which retained most of the Cr in solid solution during a partial homogenization and low temperature deformation step, thus making the Cr ineffective in preventing recrystallization into a fine grain structure. A subsequent homogenization step precipitates the Cr as the E phase and stabilizes the fine structure.

Additional studies at Frankford Arsenal[7] showed that the maintenance of Cr in solid solution prior to deformation is not necessary in order to obtain a fine, recrystallized grain structure. Their process, designated FA-ITMT[7], uses a long time ingot homogenization to precipitate the Cr as E phase and an annealing step to precipitate the major alloying elements, Zn, Mg, and Cu, as coarse particles prior to deformation. When the alloying elements are retained in solid solution before working (with Cr present as E phase), fine grain structures are not obtained. The mechanism by which the distribution of major alloying elements affected the final wrought grain structure was not explained by the authors.

The goal of achieving significant increases in the mechanical properties of 7XXX aluminum alloys through the use of ITMT has been attained to some degree. Significant increases in elongation[7], toughness[24], and stress corrosion resistance[24] of ITMT-processed 7075 have been reported. Slight increases in yield strength were observed, even though the reduction in grain size was very great. However, this result may be expected since the grain sizes of these materials are very large in comparison to the spacing of the hardening precipitates (GP zones and η').

Several studies[5,7,24,25] have pointed to the possibilities of achieving some improved fatigue properties through the application of ITMT to 7XXX alloys. However, to date, there has been no systematic study of the fatigue performance of these materials. One recent work[11] has evaluated the potential of ITMT for improving corrosion FCP resistance of 7XXX forgings. Zola[11] reported superior performance

of ITMT alloys in 3.5% NaCl solution. However, the 7475 ITMT FCP data was compared to data for 7075-T73, which leaves some doubt as to whether FCP resistance was improved by ITMT or by the different alloy composition and purity levels of 7475.

CHAPTER III

EXPERIMENTAL PROCEDURES

The aluminum alloys used in this research were produced by the Alcoa Technical Center, Alcoa Center, Pennsylvania. The chemical compositions in weight percent of the alloys are shown in Table 1. Part of the 7050 ingot was treated by ITMT at the Pitman Dunn Laboratory, Frankford Arsenal. As-recrystallized (AR) and as-recrystallized plus hot-rolled (AR+HR) 7050 ITMT materials were received as 25.4mm plate in the T6X1 condition. (The T6X1 temper is an experimental high-strength aging condition discussed by Staley[13] in a previous study). The 7050 material which was hot-rolled (HR) to simulate commercial processing was produced by Alcoa as 38.1mm plate and was received in the F, as fabricated, temper. Specimen blanks of the 7050 HR material were subsequently heat-treated to the T6X1 temper. The production of the 7475 materials (AR, HR, and AR+HR) was done as part of a previous investigation[10]. These materials were received as 38.1mm plate in the T6 condition. Processing schedules for the ITMT materials are shown schematically in Figure 3. Exact processing details for the HR materials are considered proprietary[10], but commercial hot-rolling temperatures for 7XXX alloys are usually in the 400°-450°C range. Heat treatment and aging schedules for the experimental materials are shown in Table 1. Solutionizing treatments

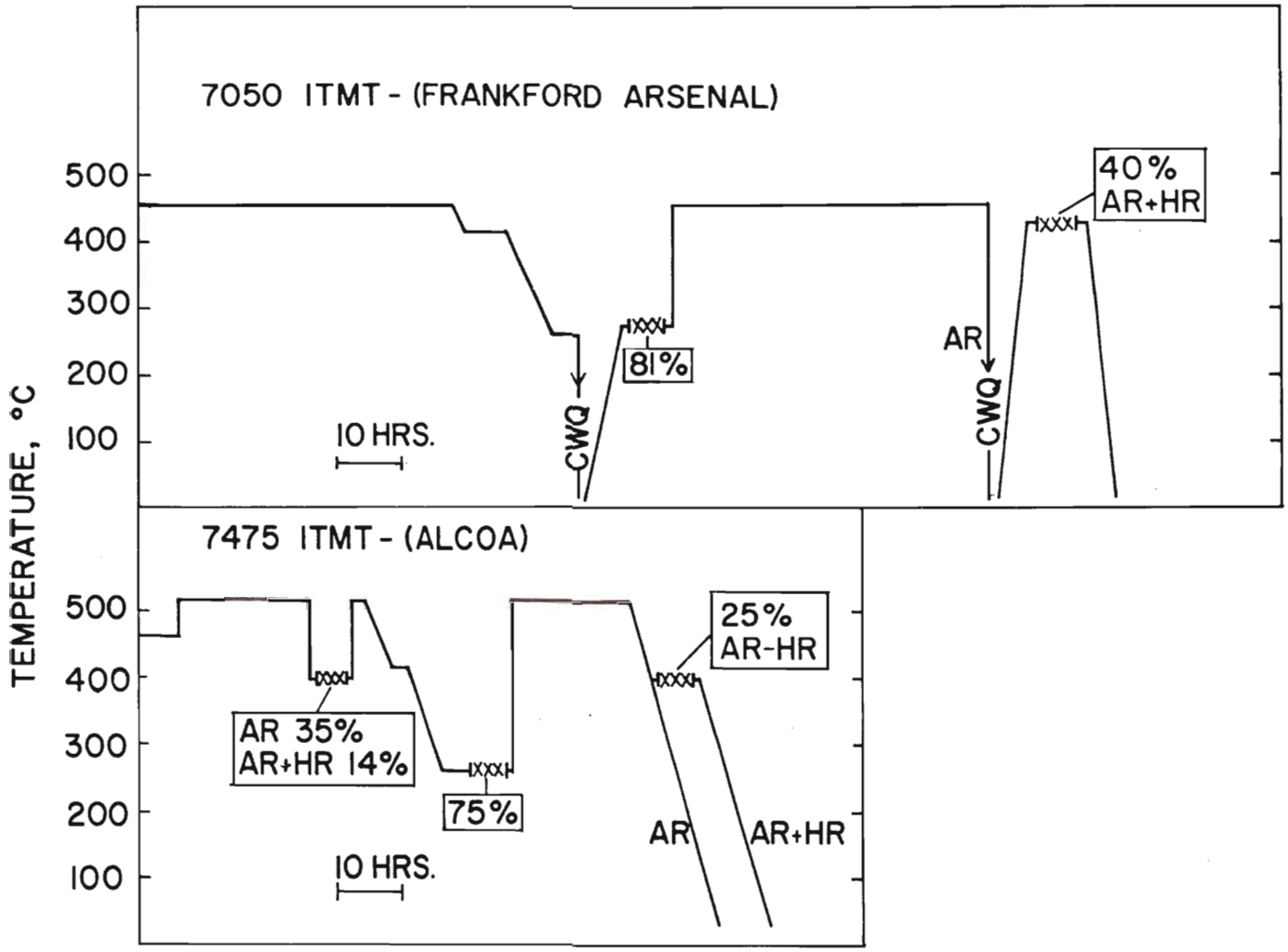

Figure 3. ITMT Processing Schedules for 7050 and 7475.

Table 1. Chemical Composition and Heat Treatments of Experimental Alloys

Chemical Composition

	Si	Fe	Cu	Mg	Zn	Ti	Zr	Cr
7050	0.01	0.02	2.35	2.45	6.42	0.01	0.11	--
7475	0.06	0.12	1.65	2.35	5.79	0.01	--	0.23

Heat Treatment

	7050-T6X1	7475-T6
Solution Treatment	3h/477°C Cold Water Quench	2h/516°C Cold Water Quench
Natural Age (Room Temperature)	5 days	4 days
Artificial Age	4h/121°C 4h/168°C	24h/121°C

were carried out in a molten salt bath. Aging treatments for the 7050 materials were done in a silicone oil bath. 7475 materials were heat-treated by Alcoa in circulating air furnaces.

Samples were cut from the central portions of the plates and polished for metallographic examination of the three principal sections. In order to quantitatively determine the degree of recrystallization in the material, an HNO_3 etching technique was found to be preferable to the conventionally used Keller's etch. Specimens were etched 3-5 minutes in a 25% HNO_3-75% water solution at 70°C. After this treatment, subgrain and grain boundaries were readily visible, thus greatly enhancing the contrast between recrystallized and unrecrystallized areas. From microphotographs, simple point count techniques were used to determine the percentage of recrystallized material in the microstructure. Quantitative metallography was also used to determine the percentage of second phases in the microstructures. Foils for transmission electron microscopy (TEM) were prepared by standard techniques from the aged experimental materials. Scanning electron microscopy (SEM) was also used to examine the metallographic samples.

Flat-plate ASTM[79] tensile specimens and cylindrical low cycle fatigue (LCF) and high cycle fatigue (HCF) specimens, shown in Figure 4, were prepared from the heat-treated materials with the gage lengths parallel to the rolling direction of the plates. (In an effort to conserve 7475 material, it was necessary to use smaller LCF and HCF specimens). All fatigue specimens were designed in accordance with a new ASTM recommended practice[80]. Two sides of each tensile specimen

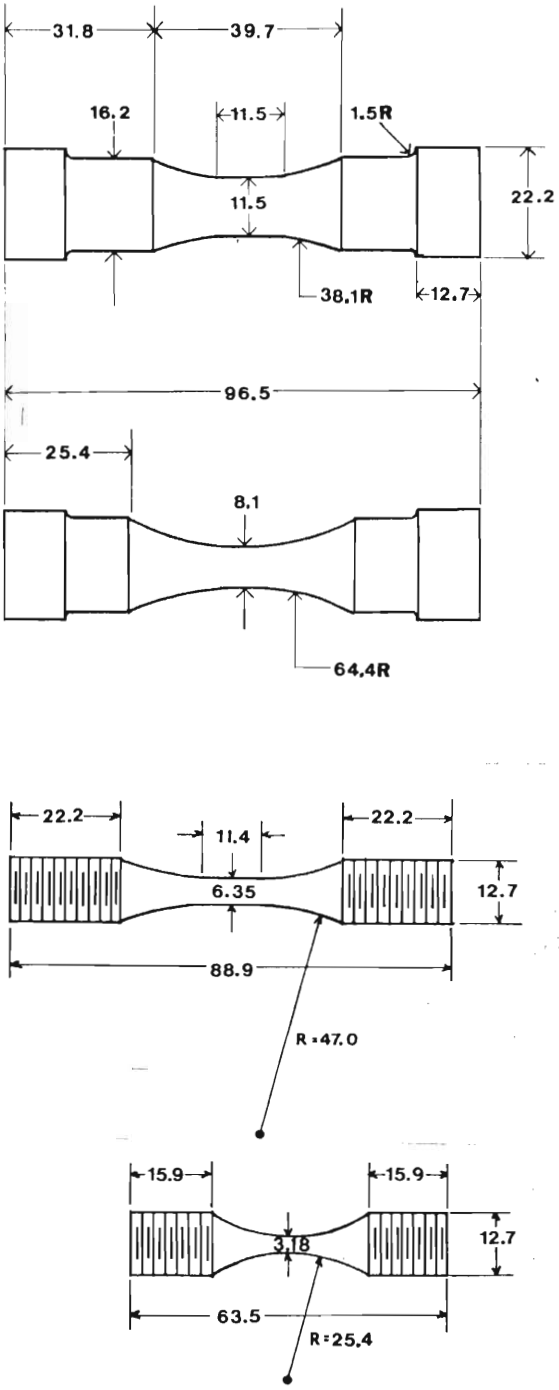

Figure 4. Axial Fatigue Specimen Designs: (a) 7050 LCF, (b) 7050 HCF, (c) 7475 LCF, and (d) 7475 HCF.

were polished to facilitate observations of surface deformation. The surfaces of the fatigue specimens were ground by hand with 600 grit emery paper, then hand polished with billiard cloths impregnated with 6μ and 1μ diamond paste. The surface of each fatigue specimen was examined at 35X with a binocular microscope to insure that all circumferential scratches and machine marks were removed from the specimen. Several LCF specimens were electropolished to make possible replication and observation of specimen surfaces at various intervals during strain-controlled testing.

The fatigue testing was performed on two closed loop servohydraulic Materials Testing Systems (MTS) with capacities of 22,690 and 10,000 Kg under total strain control. The frequency of each test was adjusted so that a constant strain rate was maintained using a sawtooth-type command signal. The strain was controlled using a 10 mm extensometer attached to the specimen. Small strips of cellophane tape were applied to the specimen surface to prevent the sharp knife edges from cutting the specimen. Self-aligning hydraulic grips were used on the larger testing machine to insure proper alignment of the specimen with respect to the loading axis. A Wood's metal reservoir was used with the smaller test system. A dry air (R.H. < 0.2%) atmosphere was used for both LCF and HCF tests. The HCF tests were conducted at 10 Hz in sinusoidal fully-reversed tension/compression loading.

A standard WOL type compact tension specimen (H/W = .486)[81], shown in Appendix A, was selected for the FCP studies. The nominal thickness of the 7050 specimens was 6.35 mm. 7475 FCP

specimens were 9.50 mm in thickness. The specimens were machined so that crack growth measurements were obtained for both T-L and L-T orientations[82]. FCP testing was performed on a 10,000 Kg closed loop MTS system at 10 and 20 Hz in the same dry air atmosphere used for the axial fatigue tests. A minimum/maximum stress ratio (R) of 0.1 was used for the FCP tests. Crack length was monitored visually to within $\pm$0.01 mm using a Gaertner travelling microscope. Plots of FCP rate (da/dN) versus stress intensity range (ΔK) were made from the raw crack length versus cycles data.

Pole figure data was collected on a Siemens x-ray unit equipped with an oscillating goniometer. Fixed time increments were used to collect intensity data at angles ranging from 0° to 80° with the plate surface. Analysis and plots of the data were made using a computer program developed at this laboratory. Residual stress measurements were made on several samples using a back reflection technique.

CHAPTER IV

RESULTS AND DISCUSSION

Microstructure

The microstructures of the experimental alloys are shown in Figures 5 and 6. The 7050 AR material, Figure 5(a), consisted of very small (0.02 mm) recrystallized grains. The 7050 AR+HR microstructure was considerably less recrystallized than the AR material, with the "pancake"-type grain morphology typical of hot-rolled materials. The 7050 HR material was also partially (45%) recrystallized, consisting of coarse, recrystallized grains and areas of unrecrystallized subgrains as shown in Figures 5(c) and 7. Results of degree of recrystallization (DR) and grain size measurements are shown in Table 2. Since the AR+HR and HR 7050 materials both contained large amounts of unrecrystallized material, grain sizes shown in Table 2 are merely estimates of recrystallized grain dimensions obtained by a linear intercept technique.

The microstructures of the 7475 materials were considerably less recrystallized than their 7050 counterparts, as evidenced by comparison of Figures 5 and 6 and the DR measurements in Table 2. The 7475 AR material was only 62% recrystallized (compared to 94% DR for 7050 AR) and the aspect ratios (length/width) of many of the grains were as high as 4:1 (compared to 1:1 for 7050 AR). The

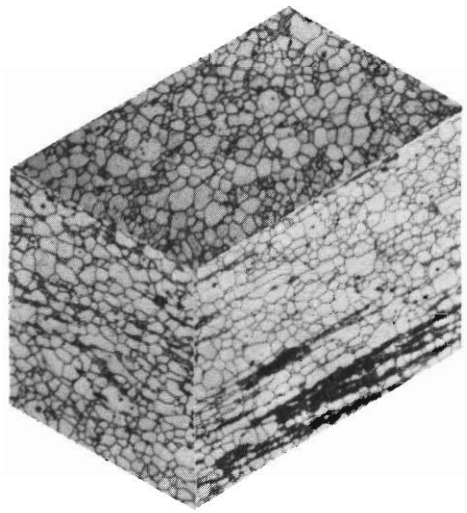

(a)

(b)

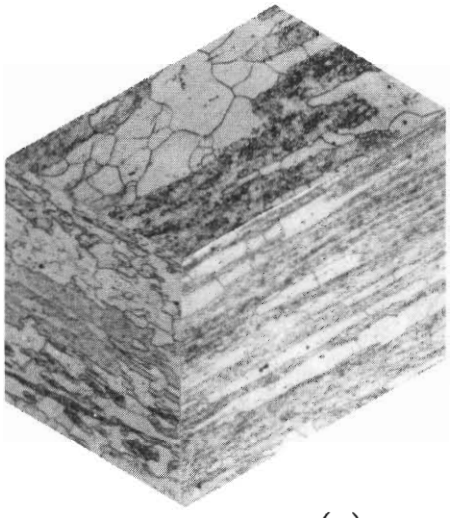

(c)

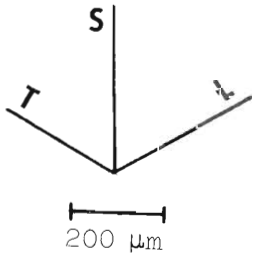

Figure 5. Microstructures of 7050 Experimental Materials: (a) AR, (b) AR+HR, and (c) HR.

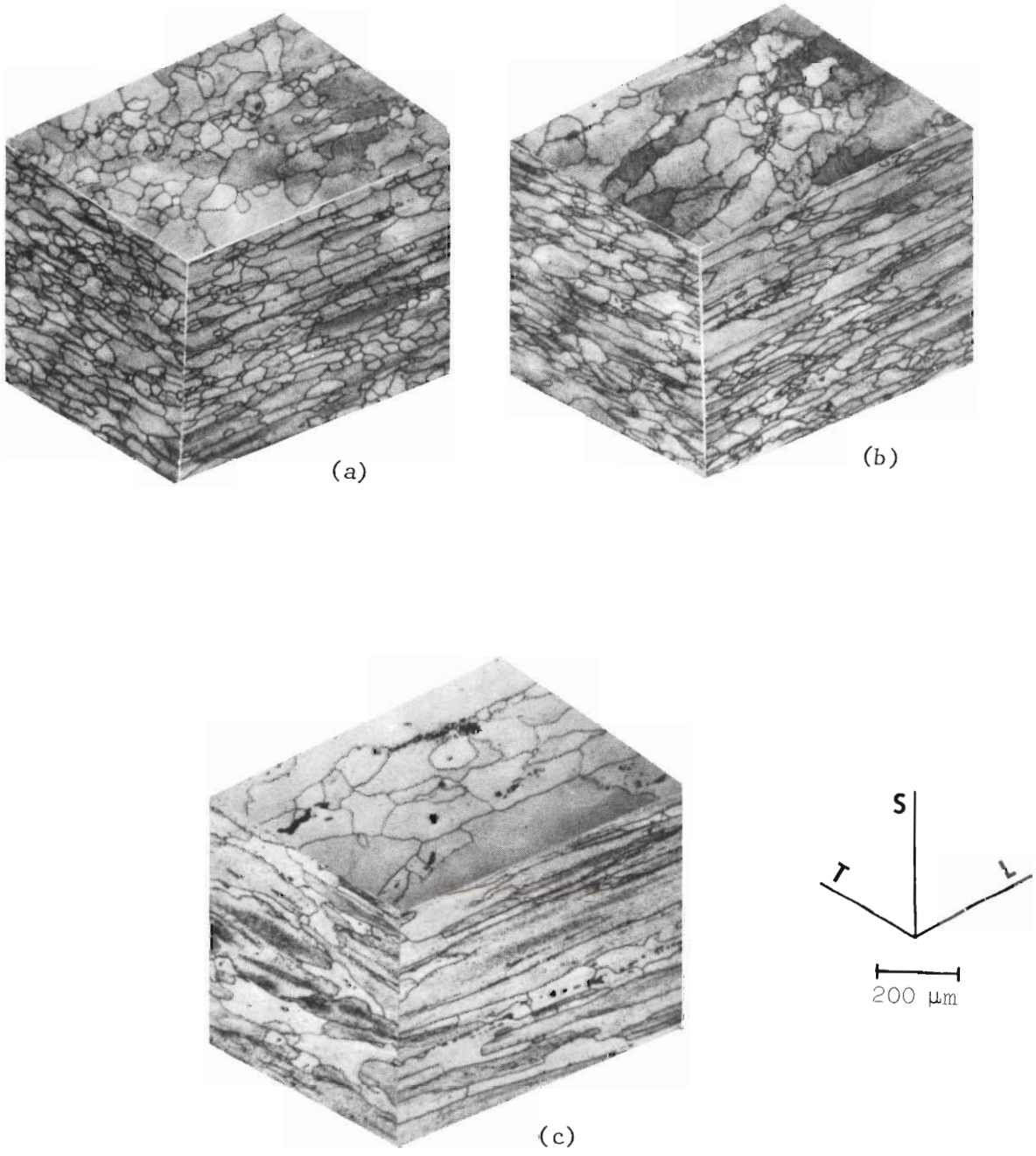

Figure 6. Microstructures of 7475 Experimental Materials: (a) AR, (b) AR+HR, and (c) HR.

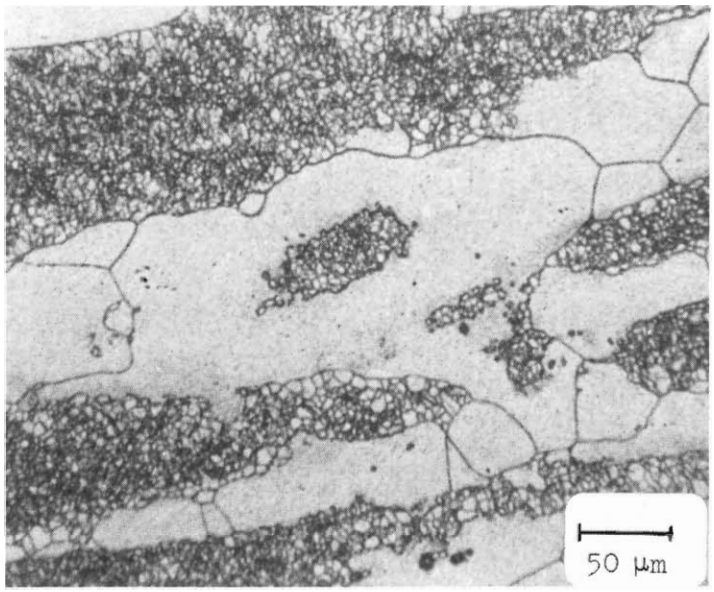

(a)

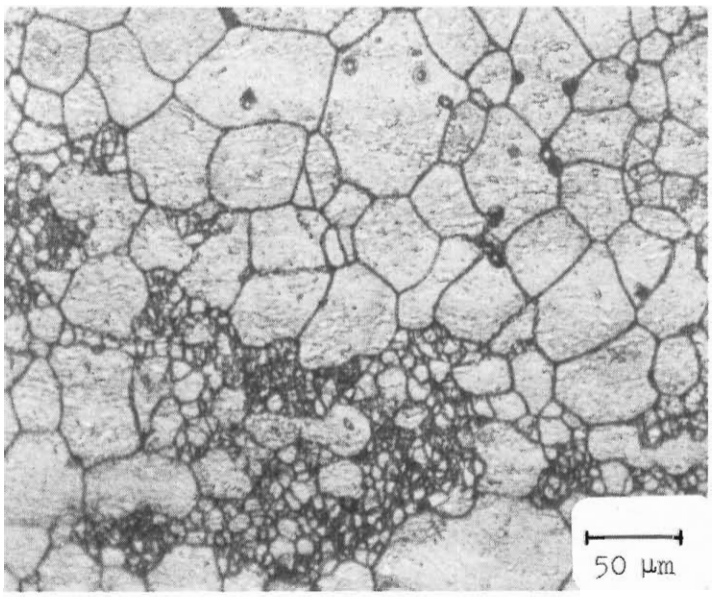

(b)

Figure 7. Grain and Subgrain Structures in the 7050 Alloy: (a) HR, and (b) AR, 25% HNO_3 Etch.

Table 2. Microstructure of Experimental Materials

	Average Grain Diameter (mm)			Degree of Recrystallization (%)
	Short T	Long T	R.D.	
7050				
AR	0.018	0.022	0.024	94
AR+HR	0.046	0.077	0.074	68
HR	0.078	0.085	0.107	45
7475				
AR	0.019	0.031	0.039	62
AR+HR	0.027	0.064	0.130	10
HR	0.023	0.071	0.187	16

microstructures of both 7475 AR+HR and 7475 HR are essentially unrecrystallized, with "packets" of subgrains elongated in the rolling direction of the plate.

The AR materials of both alloys achieve their predominantly recrystallized structures as a result of the low temperature deformation steps in their ITMT processing schedules shown in Figure 3. The large amount of strain energy introduced into the ingot at relatively low deformation temperatures provides a large driving force for recrystallization to occur during later heat treatments. Grain growth during homogenization is hindered by the action of the dispersoid phases ($Al_{12}Mg_2Cr$ in 7475 and Al_3Zr in 7050).

The HR variants of the experimental alloys achieve partially recrystallized structures due to the use of hot-rolling in the 400°-450°C range as the only deformation process in the fabrication of the plate. At the hot-rolling temperature, the dispersoid particles inhibit, but do not completely prevent recrystallization. Partial recrystallization occurs following hot-rolling during the solution treatment, which results in the duplex grain morphology shown in Figures 5 through 7. The "unrecrystallized" areas of Figure 7 are, in all probability, regions which contain both subgrains (with low angle boundaries) and very fine recrystallized grains (with high angle boundaries). Due to the very fine nature of this mixed structure and the impracticability of distinguishing between the two components, entire regions of this nature have been designated "unrecrystallized" for the purposes of this investigation. As in the case of the HR material, the high temperature hot-rolling

step in the processing of the AR+HR material results in a partially recrystallized microstructure.

The structures of the AR+HR materials, Figures 5(b) and 6(b), indicate that recrystallization prior to hot-rolling produces a finer unrecrystallized structure than hot-rolling alone. 7050 AR+HR has a somewhat higher DR (68% vs. 45%) than 7050 HR and has a finer recrystallized grain size. 7475 AR+HR has a slightly finer grain size and approximately equal DR compared to 7475 HR.

TEM of the experimental materials showed that the different responses of 7050 and 7475 to processing (i.e., different microstructures) were most likely related to the type, volume fraction, and distribution of dispersoid phases. Subgrains in the 7050 materials appeared to be completely recovered (i.e., no dislocation debris) as shown in Figure 8. Al_3Zr particles were most probably observed, but were randomly distributed and were not often in evidence at subgrain boundaries. By contrast, the 7475 materials showed a high density of large (up to 0.5 μm) E phase particles. Figure 9 shows that the E phase has been very effective in "pinning" subgrains and preventing recrystallization despite the higher temperature (516°C vs. 477°C) heat treatments. The presence of dislocation debris in the 7475 materials also indicates that the E phase has hindered dislocation motion and recovery during heat treatment after deformation.

The particles which appear dark in the 7050 microstructures of Figure 5 were determined by energy dispersive x-ray analysis to be extremely copper-rich. The particles are probably undissolved $S(Al_2CuMg)$ phase, similar in appearance to those observed in

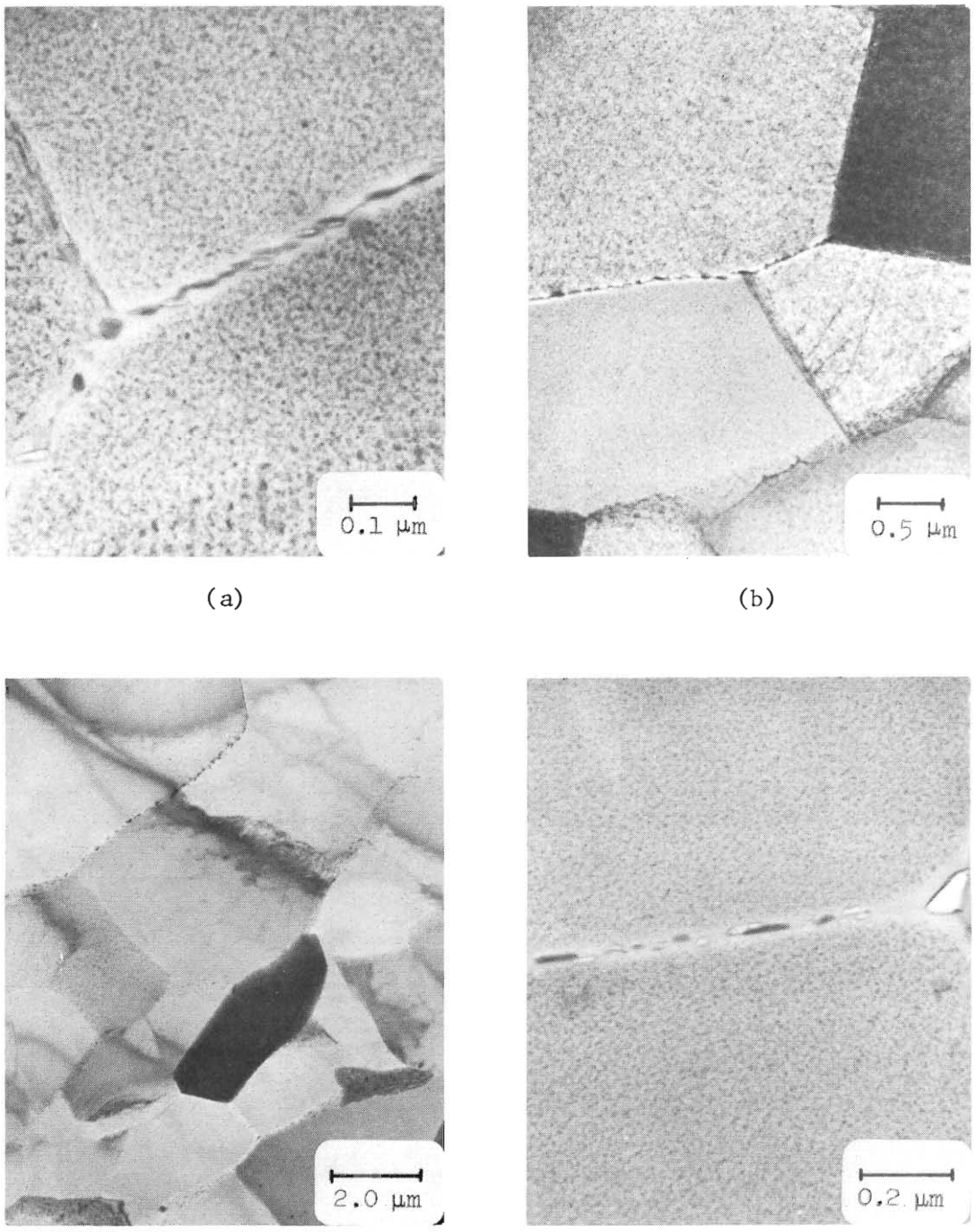

Figure 8. Transmission Electron Micrographs of 7050-T6X1: (a) AR, (b) AR+HR, (c) and (d) HR.

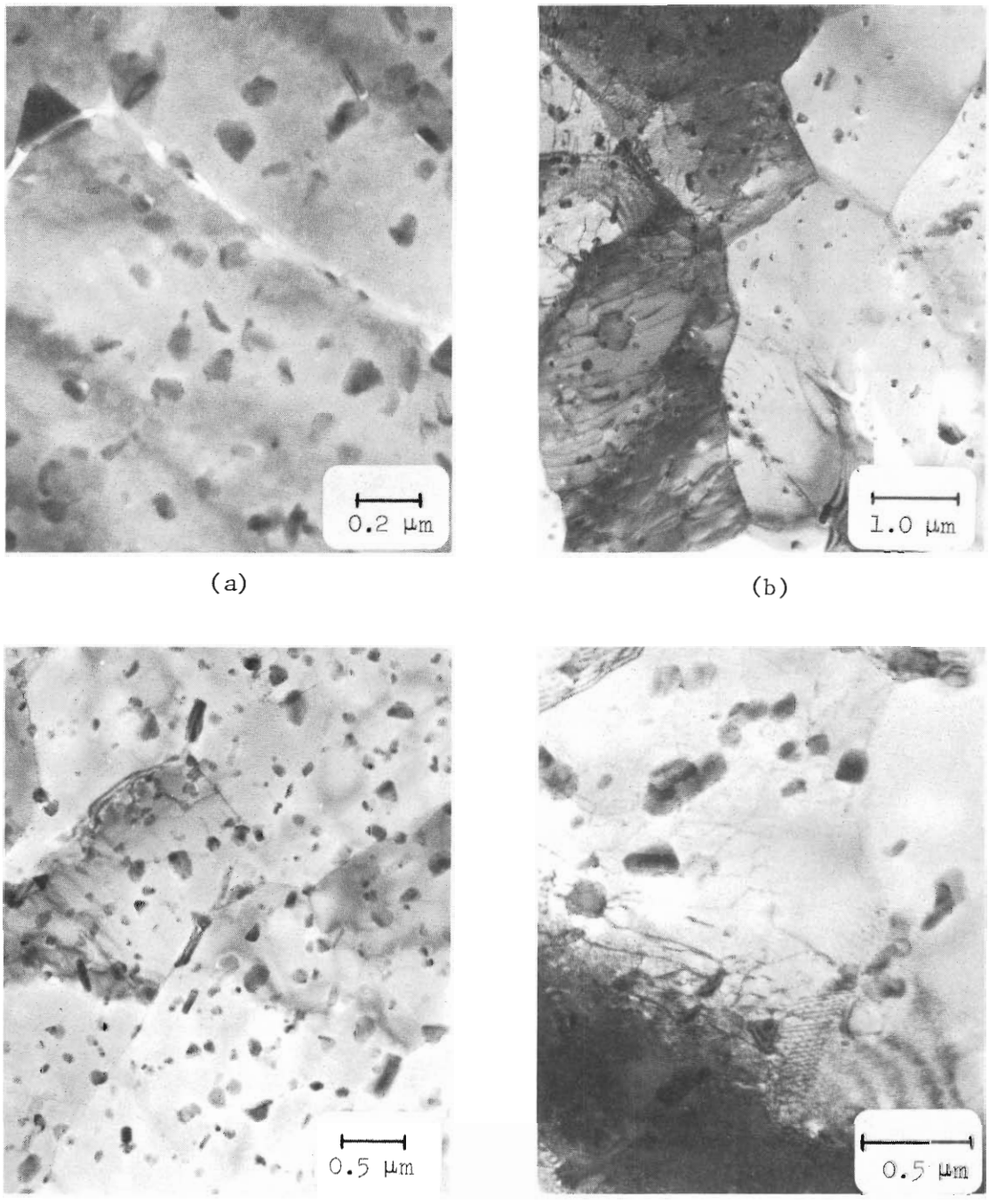

Figure 9. Transmission Electron Micrographs of 7475-T6: (a) AR, (b) AR+HR, (c) and (d) HR.

previous investigations[14,83]. The AR material appeared to have a significantly larger volume fraction of these particles associated with the grain boundaries than either the HR or AR+HR materials. Quantitative metallography showed the overall volume fraction of Al_2CuMg particles in 7050 to be 1.78% for AR, 1.33% for AR+HR and 0.34% for HR. The differences in volume fraction and distribution of these phases can best be explained in terms of the alloy composition and ingot processing. The copper content of the 7050 alloy (2.35%) is higher than that of most other typical 7XXX alloy compositions. Communications with other workers[84] suggest that a three-step heat treatment in the 477°-488°C range can be used to completely dissolve Al_2CuMg in alloys of similar composition. However, the copper content of the alloy also necessitates extreme care in heat treatment to avoid the problem of nonequilibrium melting[84]. Thermal treatments at excessive temperatures can cause melting at the Al_2CuMg-matrix interface before complete solution of the alloying elements occurs. Consequently, the thermal treatment temperatures used in this investigation were somewhat lower than that required for solution of all copper-rich phases.

The appearance of Al_2CuMg in 7050 AR is probably aided by the furnace cooling step in the ingot processing schedule, Figure 3. By cooling slowly from 413°C to 260°C, precipitation of Al_2CuMg can occur before rolling at 274°C. Since the particles precipitate before the recrystallized grain structure is determined, they are essentially trapped as intergranular constituent particles. Neither the recrystallization treatment at 454°C nor the solution treatment at

477°C is sufficient to redissolve the particles. The distribution of Al_2CuMg in the AR+HR material seems to be more uniform than that found in the AR material. The particles, as in the HR material, are randomly distributed and seem to have no particular tendency to be associated with the grain boundaries. This is probably due to the fact that hot-rolling aids in the mechanical redistribution of the Al_2CuMg particles.

Al_2CuMg was not noted to be an important constituent in the microstructure of the 7475 materials. A few Al_2CuMg particles were observed during optical metallographic examination, but the vast majority of constituents were insoluble particles (Al_7Cu_2Fe, Mg_2Si, $FeAl_6$) due to the presence of Fe and Si impurities in the 7475 composition. These particles were up to 10 μm in size and often appeared to be strung out in the rolling direction of the plate. Quantitative metallography revealed no significant differences in volume fraction (0.9%) of these phases between the three 7475 materials. The absence of Al_2CuMg in the 7475 microstructure can be attributed to the lower Cu content of 7475 and the thermal and mechanical processing received by the alloy. The higher temperature (516°C) used for thermal treatment of 7475 is commonly used by Alcoa[84] to insure effective solution of all major alloying elements.

A general observation to be made from the microstructures shown in Figures 5 and 6 is that the variants of 7050 are considerably more recrystallized than their 7475 counterparts. This result is probably due to the differences in grain-refining dispersoids and processing schedules for the two alloys. Other workers[8,9] have

studied the effectiveness of Cr and Zr as grain refiners in 7XXX alloys. In these studies, it was shown that Zr-bearing alloys developed equiaxed, fully recrystallized structures in the AR condition and suffered from extensive grain growth upon hot-rolling of the AR material. By contrast, the elongated partially recrystallized grains of AR Cr-bearing alloys did not undergo grain growth after hot-rolling. Thus, the larger values of DR observed for the 7050 materials may quite possibly be due to the less-effective action of Al_3Zr compared to $Al_{12}Mg_2Cr$ in preventing recrystallization. It should also be noted that, at zirconium levels higher than that of the present study (0.11%), more effective grain refinement was observed[9].

However, it cannot be stated unambiguously that differences in dispersoid type and volume fraction are the only causes for the different responses of 7050 and 7475 to ITMT in the present study. The different processing temperatures and deformation steps may also have contributed to the observed microstructural differences. For instance, 7050 AR was produced with a 81 per cent reduction at 274°C whereas 7475 AR experienced a 75 per cent deformation step at 260°C. Another consequence of the different ITMT schedules for the two alloys is the presence of Al_2CuMg particles in the 7050 alloy. These 3-5 μm particles, precipitated during slow cooling of the ingot to the deformation temperature, may have served as nucleation sites for recrystallization in the 7050 alloy.

Measurements of preferred orientation (texture) of the six experimental materials are shown in Figures 10 through 12. Both 7050 and 7475 AR materials, Figure 10, had essentially random textures,

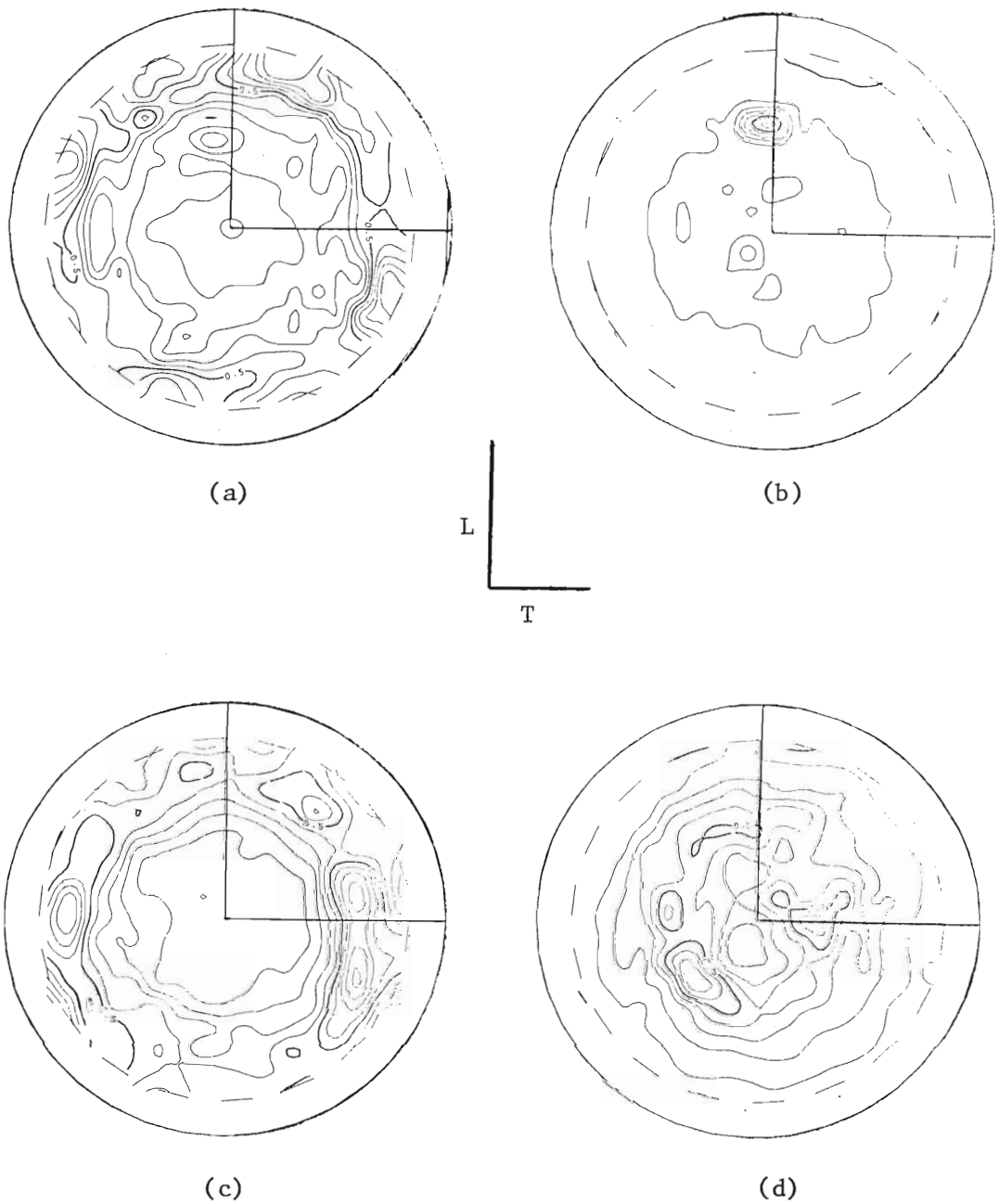

Figure 10. Pole Figures of As-Recrystallized (AR) Experimental Materials: (a) 7050 (200), (b) 7050 (220), (c) 7475 (200), and (d) 7475 (220).

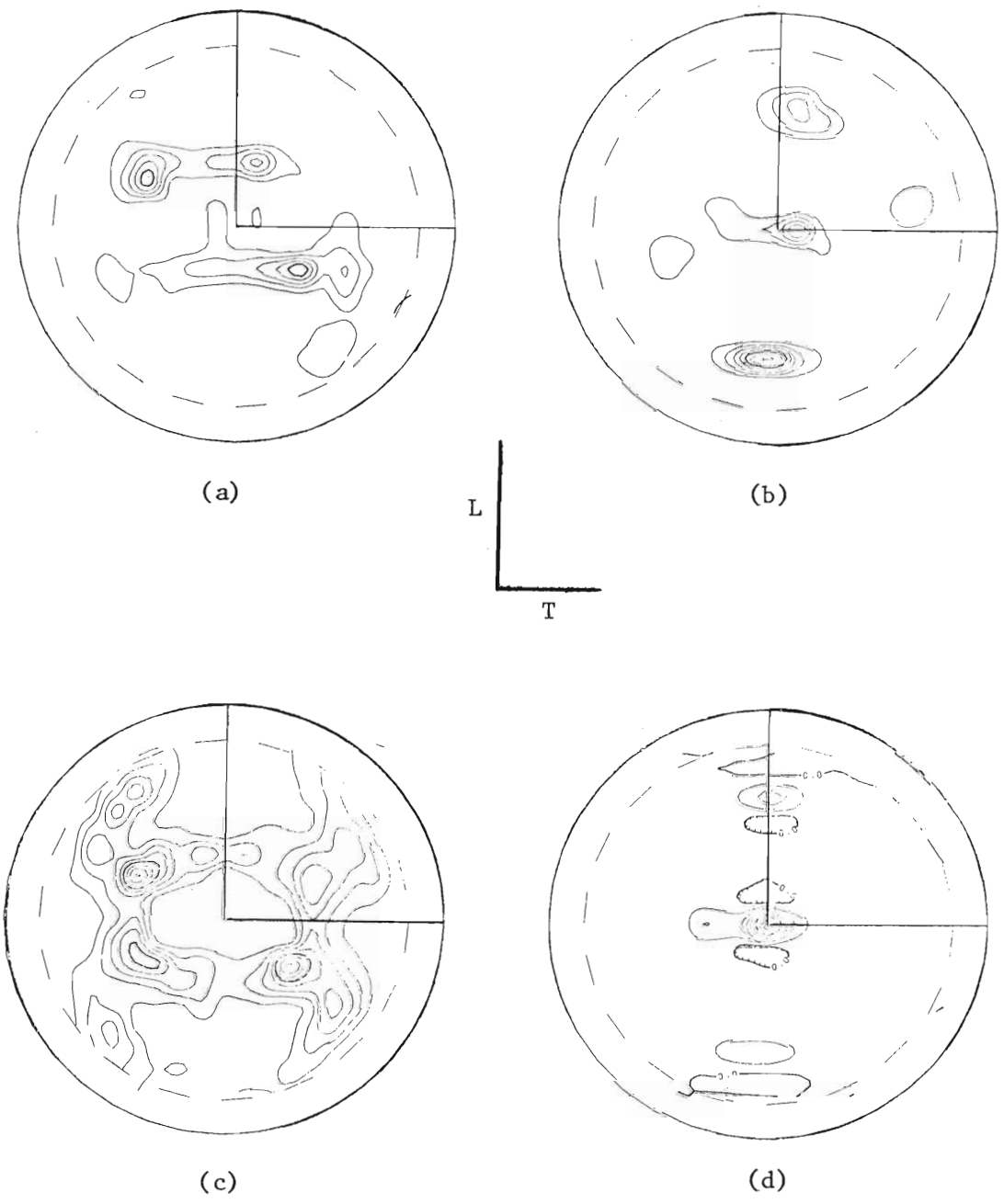

Figure 11. Pole Figures of Hot-Rolled (HR) Experimental Materials: (a) 7050 (200), (b) 7050 (220), (c) 7475 (200), and (d) 7475 (220).

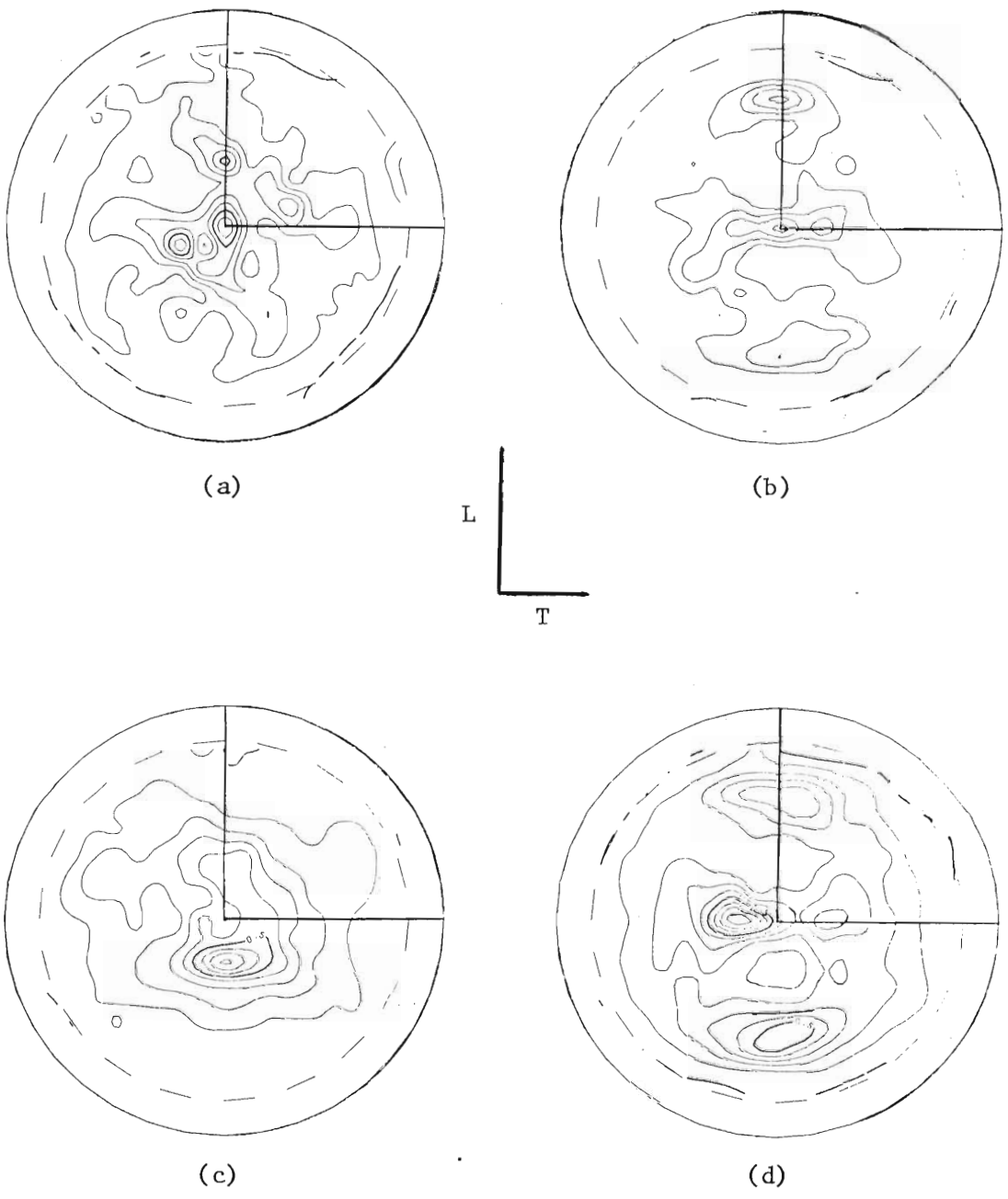

Figure 12. Pole Figures of As-Recrystallized Plus Hot-Rolled Experimental Materials: (a) 7050 (200), (b) 7050 (220), (c) 7475 (200), and (d) 7475 (220).

with no discernible preferred orientation. Figure 11 shows that HR materials of both 7050 and 7475 had textures close to (110)[1$\bar{1}$2], i.e. the (110) parallel to the plate surface and the [1$\bar{1}$2] parallel to the plate rolling direction. Comparison of Figures 11 and 12 shows that the AR+HR materials had textures similar to those of HR. However, the AR+HR textures were less pronounced than those observed in plates produced by hot-rolling alone.

Monotonic Properties and Fracture Toughness

Tensile and fracture toughness parameters for the experimental materials are shown in Table 3. Yield strengths of the 7050 ITMT materials were slightly higher than those of the HR material. The ductility of 7050, as indicated by the elongation and reduction in area values, was relatively unchanged by the different types of processing. However, the ductility of 7475 increased with the production of more equiaxed, recrystallized structures. Strengths of the 7475 materials were roughly equivalent, with the HR material being slightly stronger. Toughness, as indicated by K_{IC} or K_Q appeared to be the parameter most sensitive to changes in processing of the two alloys. The toughness indicators appear to vary inversely with the degree of recrystallization in agreement with earlier results by Staley[14]. The determination of K_{IC} and K_Q are described in Appendix B.

The lack of a grain size effect on strength in 7050 and 7475 is not surprising in view of the fact that the grain and subgrain sizes of these alloys are very large compared to the spacing of the hardening

Table 3. Monotonic and Fracture Toughness Properties

	Yield Strength (MPa)	Elongation (%)	Reduction in Area (%)	K_{IC}* (MPa$\sqrt{m}$)		K_Q (MPa$\sqrt{m}$)
				T-L	L-T	
7050						
AR	576	10.8	28	20.6	20.6	-
AR+HR	565	10.2	-	24.7	25.5	-
HR	552	11.1	31	26.3	28.8	-
7475**						
AR	467	17.9	32	-	-	35.6
AR+HR	487	17.1	28	-	-	32.9
HR	504	15.0	19	-	-	44.1

Data for Yield Strength, Elongation, and Reduction in Area are for specimens tested in the longitudinal direction.

*Data supplied by Frankford Arsenal, courtesy of H. Sulinski and J. Waldman(8).

**7475 data supplied by Alcoa, courtesy of J. E. Vruggink(10). K_Q values are designated as such because ASTM (82) restrictions for plane strain K_{IC} test were not met. (See Appendix B).

precipitates in 7XXX materials. The large volume fraction of GP zones, η' and η, shown in Figures 8 and 9, impede dislocation motion as discussed earlier and serve as the primary strengthening agents in the two alloys. This lack of a grain-boundary strengthening effect has been reported previously[7].

The monotonic fracture surfaces shown in Figure 13 are helpful in explaining the effect of microstructure on the ductility and fracture properties of 7050. The ductilities of 7050 AR and 7050 HR are remarkably similar in light of the almost exclusively intergranular fracture observed for 7050 AR, Figure 13(a). By contrast, the HR variant of 7050 exhibits a mixed-mode, but predominantly ductile fracture appearance. Brittle fracture, such as that in Figure 13(a) would be expected to cause a serious loss of ductility in the fine-grained AR material. However, it appears that the reduced grain size of 7050 AR has overcome the embrittling effect of intergranular fracture; probably by increasing the homogeneity of deformation. The examination of polished tensile specimens strained 5%, Figure 14, substantiates this result. The AR material shows a very uniform distribution of strain between grains. Coarse slip lines, indicative of pronounced inhomogeneous deformation, are not observed on the surfaces at the magnification of Figure 14(a). In the 7050 HR material, Figure 14(b), some slip lines are observed and the macroscopic distribution of strain appears to be more inhomogeneous, i.e., some areas of the specimen are highly deformed while others show no deformation at all. Since fracture will initiate locally in areas which have reached a critical strain, the fine-grained microstructure of the 7050 AR

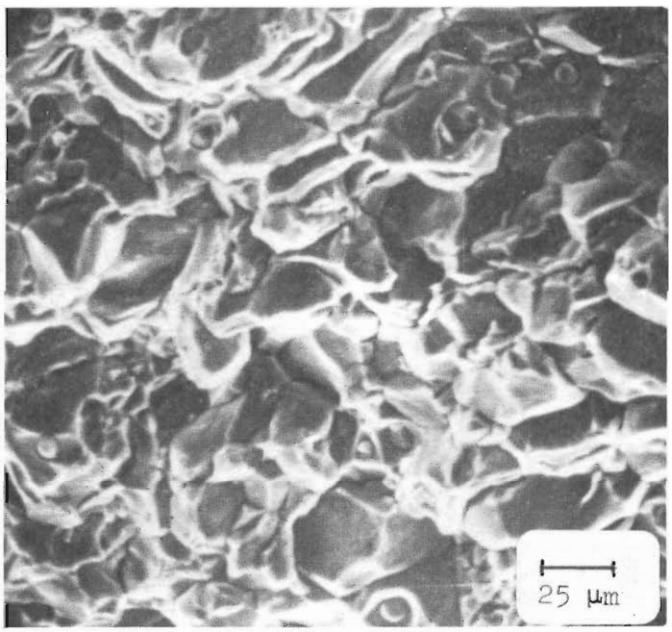

(a)

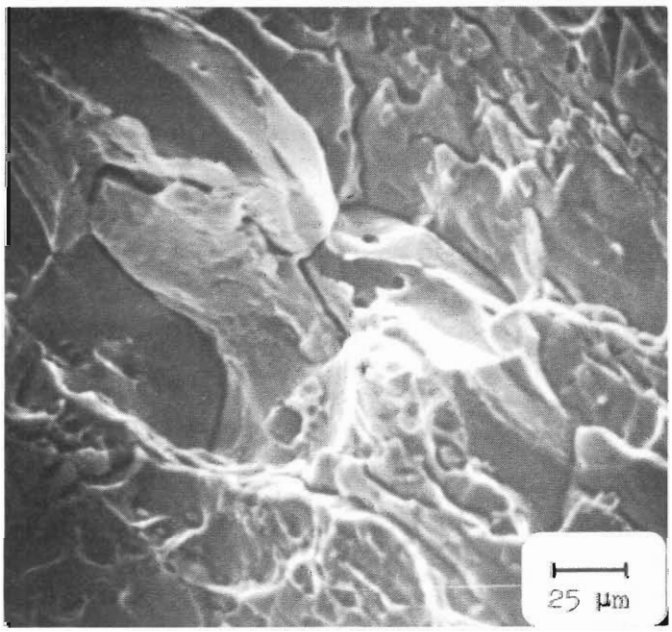

(b)

Figure 13. Scanning Electron Micrographs of 7050 Tensile Fracture Surfaces: (a) AR, and (b) HR.

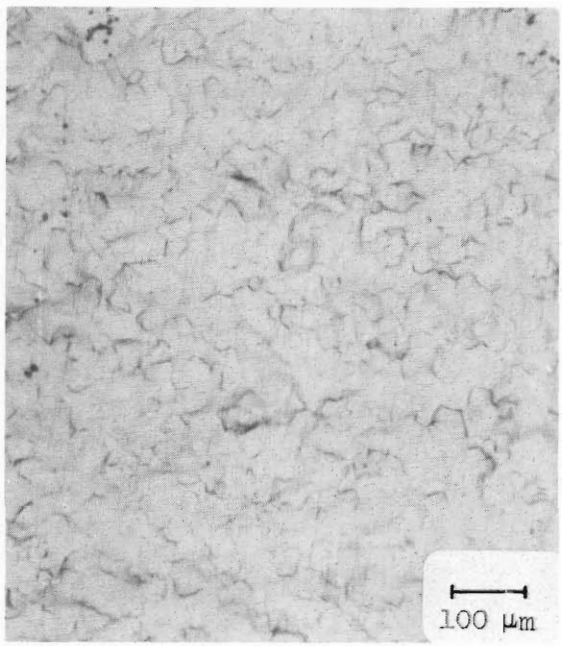

(a)

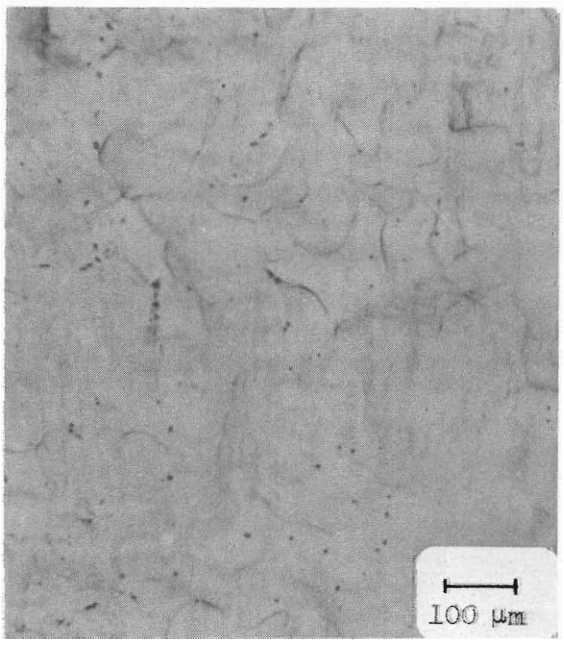

(b)

Figure 14. Observations of Deformation on Polished Surfaces of 7050 Specimens Strained 5.0% in Tension: (a) AR, and (b) HR.

is desirable since it provides for a more uniform distribution of strain. Thus, homogeneous deformation compensates for the detrimental effect of intergranular fracture and contributes to the overall good ductility observed for the AR ITMT material.

A similar explanation is offered for the increase in ductility observed for the ITMT 7475 materials. Though the unrecrystallized structure of 7475 HR promotes higher energy transgranular fracture, Figure 15, the increased homogeneity of strain shown by more recrystallized structures, Figure 16, offsets this effect to produce increases in ductility. It should be noted that the positive effects of ITMT on ductility are dependent on the type of dispersoid present in the alloy. 7050 AR, with Al_3Zr, shows intergranular fracture, a more homogeneous distribution of strain, but no overall ductility improvement. On the other hand, the recrystallization of 7475 in the presence of E phase dispersoids produces intergranular fracture, more homogeneous deformation, and a marked ductility improvement.

Though equivalent strength and ductility were maintained in 7050 AR and equivalent strength and improved ductility were achieved in 7475 AR, recrystallization had a negative effect on fracture resistance of both alloys. This result is in agreement with previous work[14] which showed showed that the production of unrecrystallized structures in 7XXX plate materials was desirable for maintenance of optimum fracture toughness. Unrecrystallized subgrain structures promote a high energy transgranular fracture mode in contrast to the low energy intergranular fracture observed in recrystallized materials as shown in Figures 13 and 15. The TEM results of Figure 17, which show

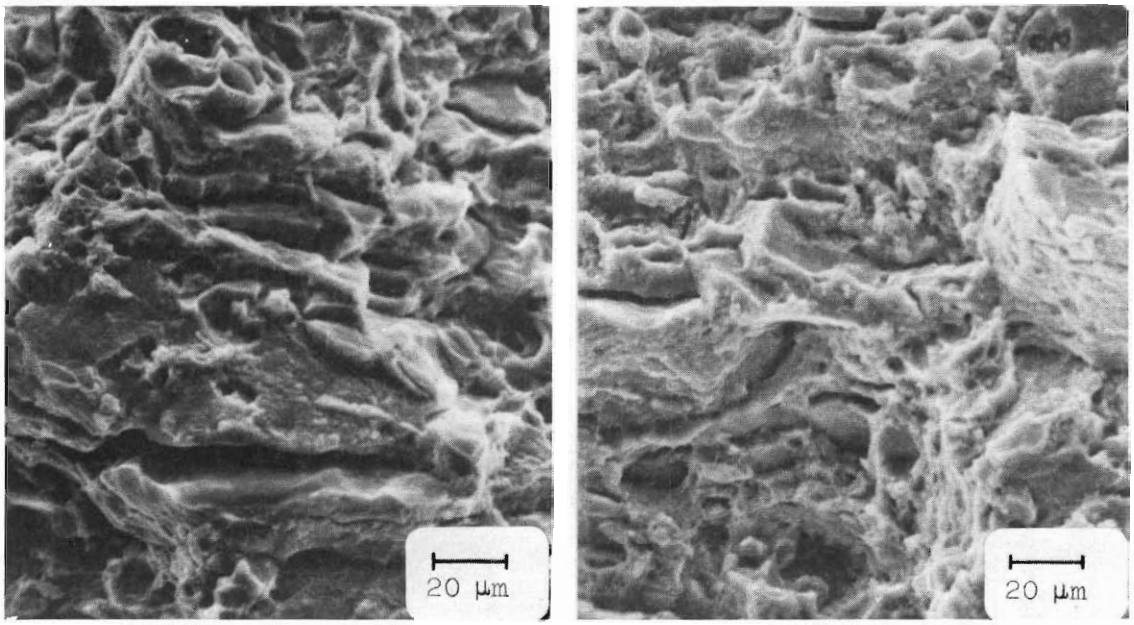

(a) (b)

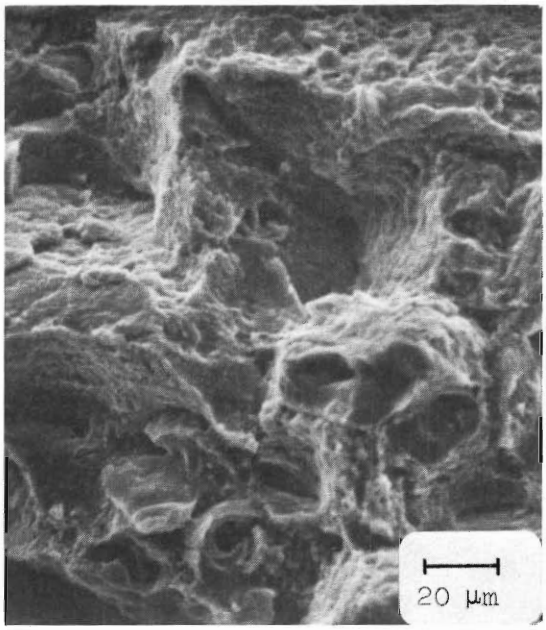

(c)

Figure 15. Scanning Electron Micrographs of 7475 Tensile Fracture Surfaces: (a) AR, (b) AR+HR, and (c) HR.

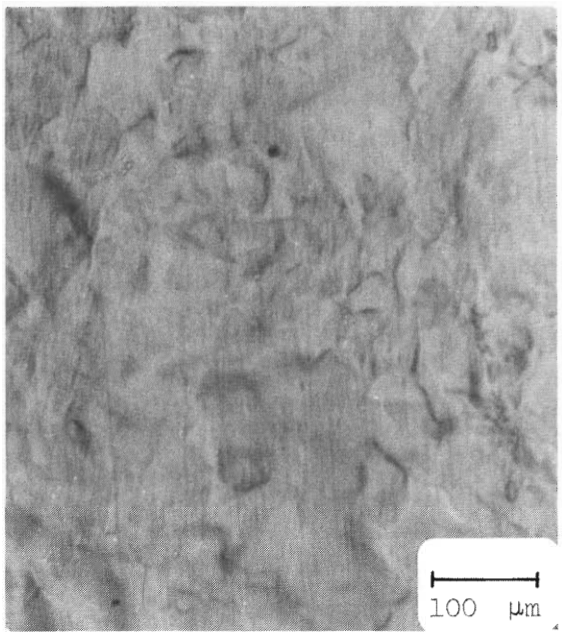

(a)

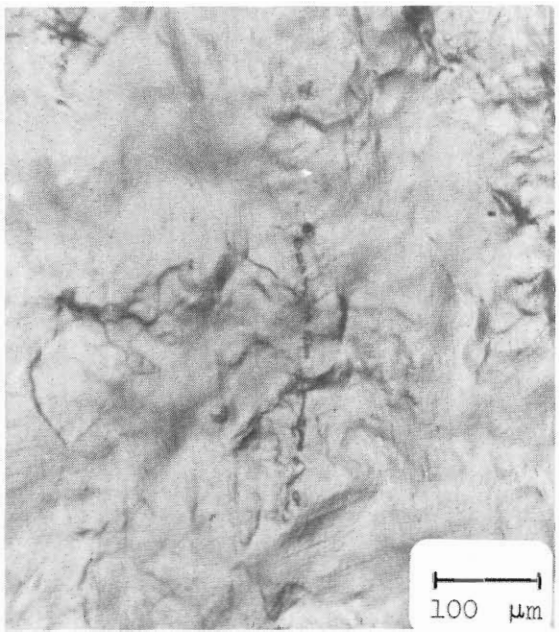

(b)

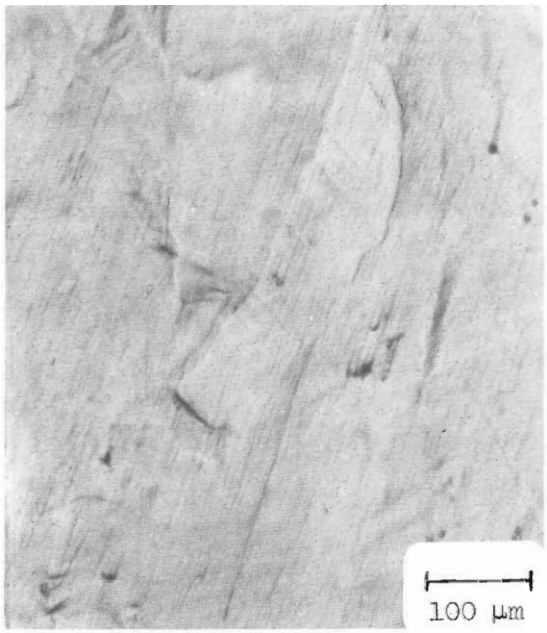

(c)

Figure 16. Observation of Deformation on Polished Surfaces of 7475 Specimens Strained 5.0% in Tension: (a) AR, (b) AR+HR, and (c) HR. Stress axis is vertical.

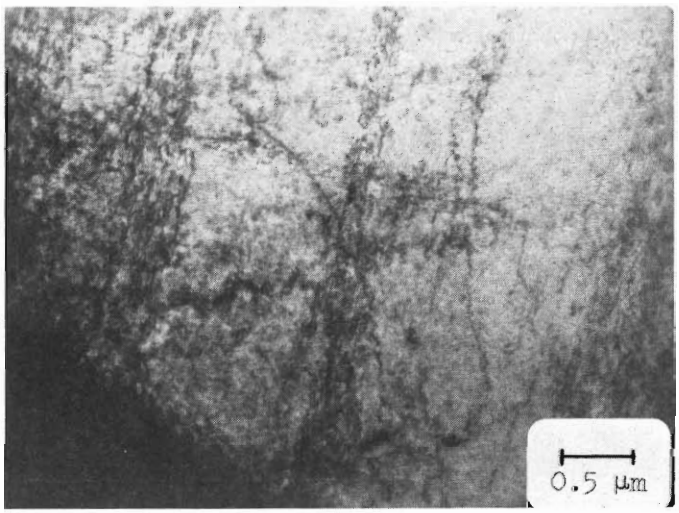

(a)

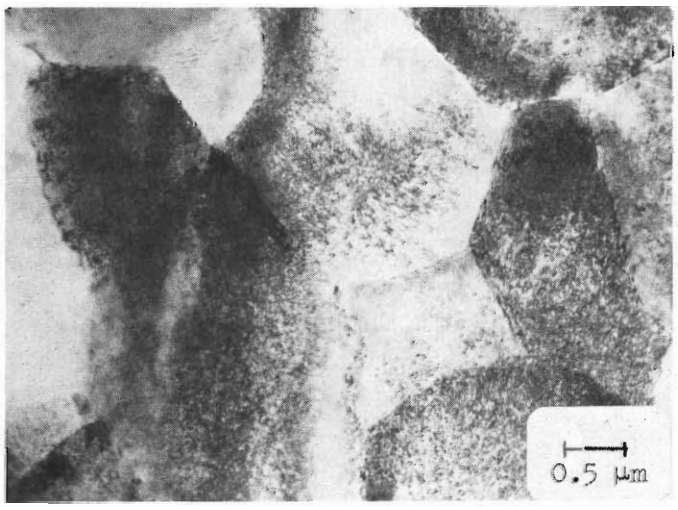

(b)

Figure 17. Transmission Electron Micrographs of 7050 AR Specimen Strained 5.0% in Tension: (a) planar dislocation arrays observed in recrystallized grains of both AR and HR, and (b) homogeneous deformation typically observed in subgrains of both materials.

dislocation structures in deformed 7050 specimens, support the above argument. In areas where recrystallized grains are present, Figure 17(a) planar dislocation bands are observed. These bands can lead to large stress concentrations at grain boundaries and contribute to intergranular fracture[37]. Deformation in unrecrystallized regions is more homogeneous on a microscopic scale as shown in Figure 17(b). Consequently, unrecrystallized structures should be expected to increase fracture resistance by homogenizing deformation on a micro scale and promoting ductile transgranular fracture.

From the study of tensile deformation and fracture in these alloys, it is evident that two opposing factors must be balanced in order to attain the optimum combination of properties. The macroscopic homogeneity of deformation (on a grain size scale) must be maintained so that localized fracture is delayed and ductility enhanced. (This is favored by fine, recrystallized structures, e.g. 7050 AR). However, the optimum resistance to fracture requires a maximum-energy-absorbing transgranular mode, a condition which is met by unrecrystallized structures. The presence of subgrains homogenizes deformation on a microscopic scale and reduces the occurrence of dislocation banding which leads to low-energy intergranular fracture. Perhaps the recent development of powder metallurgy alloys[85], with grain sizes on the order of several microns, may provide structures more suitable for achieving optimum ductility and fracture toughness in 7XXX alloys.

The role played by constituent particles in determining the fracture properties of the experimental materials should not be

overlooked. The Al_2CuMg particles, which may be observed on the fracture surfaces in Figure 13(a) can be highly detrimental to fracture toughness. When present at grain boundaries, as in 7050 AR they probably have the worst possible effect on toughness since they aid in low energy intergranular fracture. This is reflected in part by the low K_{IC} value for this processing condition. Hahn and Rosenfield have noted that similarly sized (1-10 μm) constituent particles are extremely detrimental to fracture toughness in 7XXX materials. Constituent particles fracture easily during deformation and facilitate void formation during crack extension. Consequently, they reduce the energy required for fracture, as reflected in the K_{IC} value. The same mechanism can be used to explain the effect of Fe- and Si-rich constituents on the fracture toughness of 7475. These particles are also in the size range considered to be detrimental to toughness and the volume fraction of these consituents is approximately 0.9% for each of the three 7475 materials. Particles of this type fractured during tensile deformation are shown in Figure 18.

Cyclic Properties and Fatigue Crack Initiation

The monitoring of stress response during strain-controlled LCF testing produced the results shown in Figures 19 and 20. These cyclic hardening-softening curves, plotted as the average of the tensile and compressive stresses during a LCF cycle versus number of cycles, are typical of the data obtained for the experimental materials at various strain amplitudes. A reduction in the stress amplitude was observed during the early portions of LCF tests on the

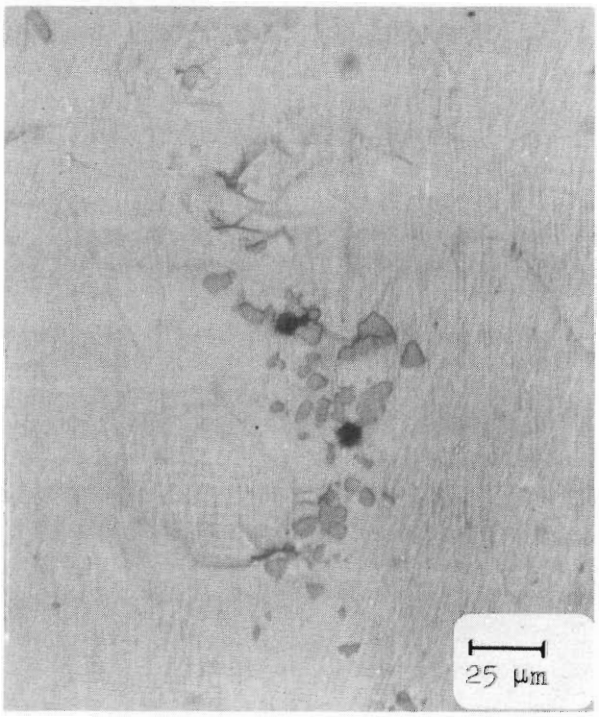

Figure 18. Fractured Al-Fe-Si Intermetallic Particles Observed on Surface of 7475 Tensile Specimen Strained 5.0% in Tension. Stress axis is vertical.

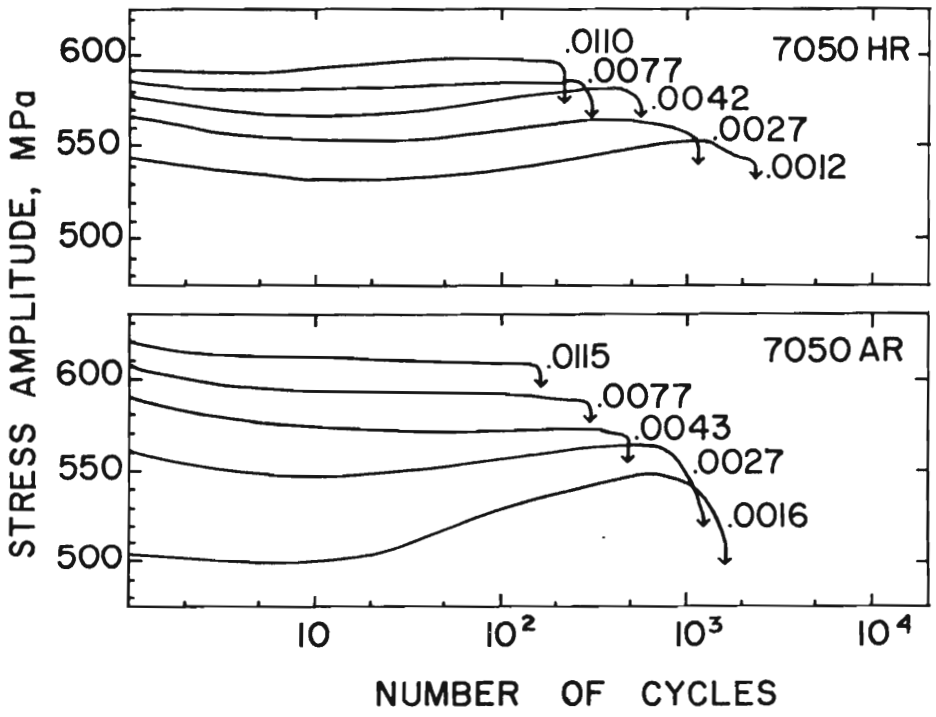

(b)

Figure 19. Cyclic Stress Response during LCF Tests of 7050 Specimens: (a) HR, and (b) AR.

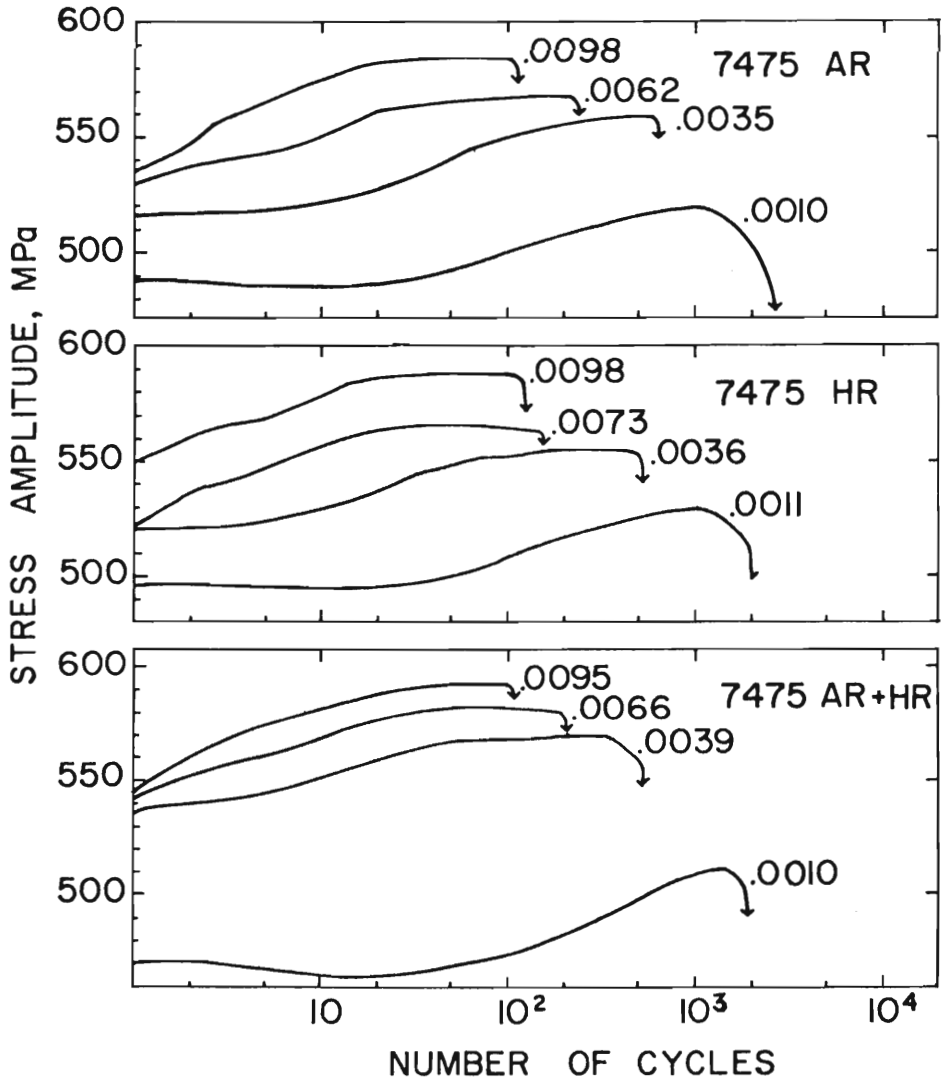

Figure 20. Cyclic Stress Response during LCF Tests of 7475 Specimens: (a) AR, (b) HR, and (c) AR+HR.

7050 alloy, Figure 19. The maximum compressive stress was slightly larger than the maximum tensile stress for the same cycle and did not show the same marked reduction with cycling exhibited by the tensile stress. This observation is interesting since no other investigators had reported cyclic softening at such high strain amplitudes in 7XXX alloys. It is believed that the reduction in stress amplitude observed is due to the relief of residual stresses present in the samples rather than a precipitate-dislocation interaction effect. Since the plates from which the specimens were cut were cold water quenched before machining, some residual stresses must be present in the specimens. An attempt was made to measure the magnitude of the stresses using x-ray techniques. The scatter in the results obtained by this method was large, but the stress values calculated were of the order of magnitude (10-40 MPa) of the observed reduction in tensile stress in Figure 19. The residual stress explanation is also supported by the fact that the softening effect varies considerably with strain amplitude. At high strain amplitudes, the residual stresses are relieved within a few cycles. At lower strain amplitudes, the effect persists for as long as 50-100 cycles. The presence of these residual stresses is not expected to significantly affect the total strain-controlled LCF life since they are removed after a small fraction of total life has expired.

After removal of the residual stresses, the cyclic stress response of the 7050 materials showed saturation or cyclic hardening at the lower plastic strain amplitudes. However, at high plastic strain amplitudes, the 7050 AR material cyclically softened slightly until failure occurred. Dislocation structures observed in thin foils were

homogeneous, giving no indication of the persistent slip band structures expected to lead to cyclic softening. The dislocation arrangement, shown in Figure 21(a), is typical of fatigue deformation in both 7050 AR and 7050 HR. The probable cause for the slight cyclic softening in 7050 AR is the extensive grain boundary cracking which developed as cycling continued. These cracks, shown in Figure 21(b), have been cited previously as the cause for cyclic softening in alloys of this type[53]. The opening and closing of these cracks under strain control allows for a gradual decrease in stress amplitude as the cracks grow prior to failure.

Cyclic hardening occurred quite extensively when the 7475 materials were subjected to strain-controlled fatigue, as shown in Figure 20. At low plastic strain amplitudes, residual stresses were probably responsible for the slight decrease or apparent saturation of the stress amplitude early in the LCF tests. At higher strain amplitudes, rapid cyclic hardening masked out the effect, if any. The origin of the cyclic hardening observed in the 7475 materials is most likely dislocation looping of dispersoid (E phase) particles. In a previous study[53], in which zirconium was used as a grain refiner, an Al-6Zn-2Mg-1.6Cu alloy displayed cyclic softening or saturation behavior at low strain amplitudes. Cyclic hardening of the magnitude observed in the present study for 7475 was generally seen for the Al-Zn-Mg-Cu-(Zr) alloy only at plastic strain amplitudes greater than 0.010. This conclusion is supported by the homogeneous deformation observed in thin foils made from fatigued 7475 specimens. Figure 22. Note the apparent pinning effect of the $Al_{12}Mg_2Cr$ particles

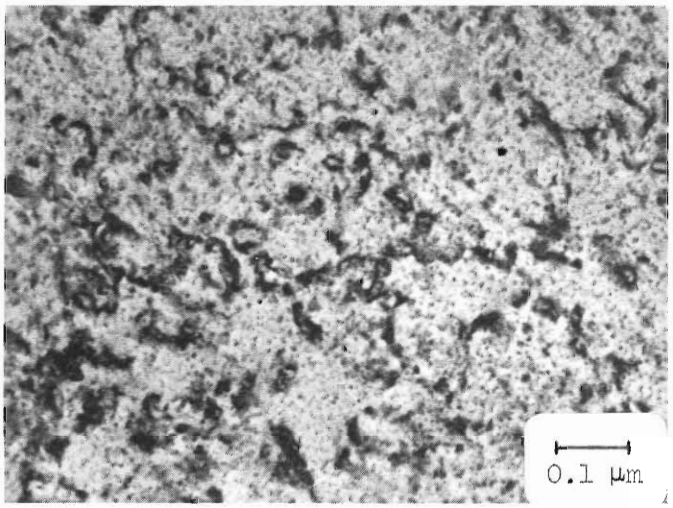

(a)

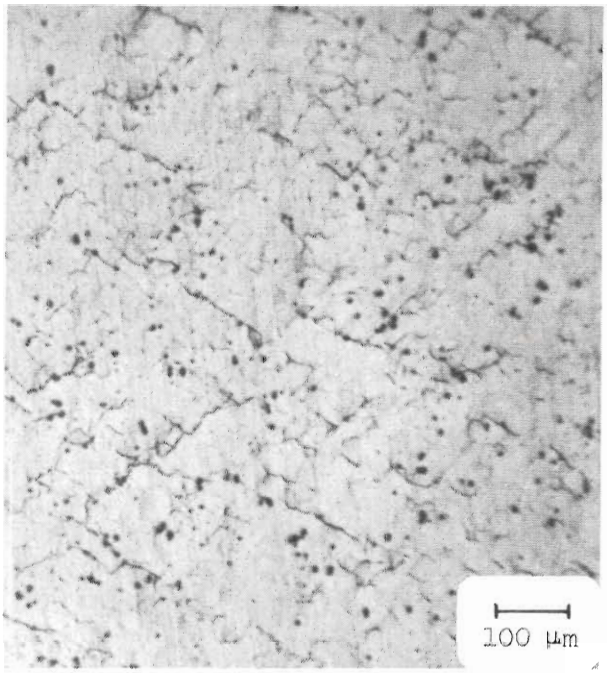

(b)

Figure 21. (a) Dislocation distribution in 7050 HR specimen cycled 1250 cycles at a total strain amplitude of 1.0%.
(b) Surface cracking in 7050 AR specimen cycled 300 cycles at a total strain amplitude of 1.2%.

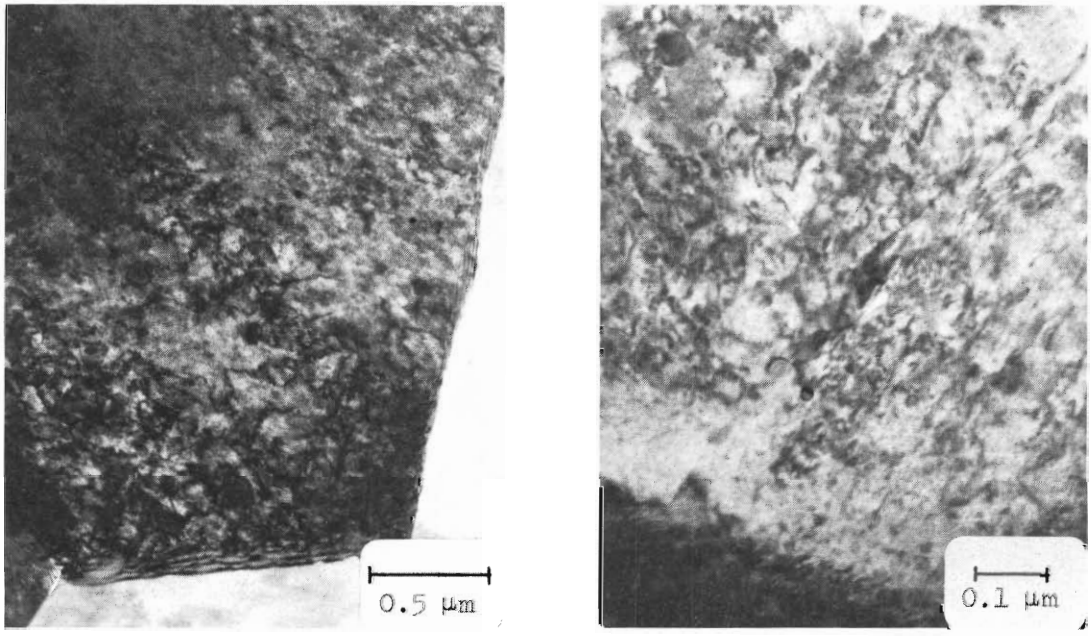

(a) (b)

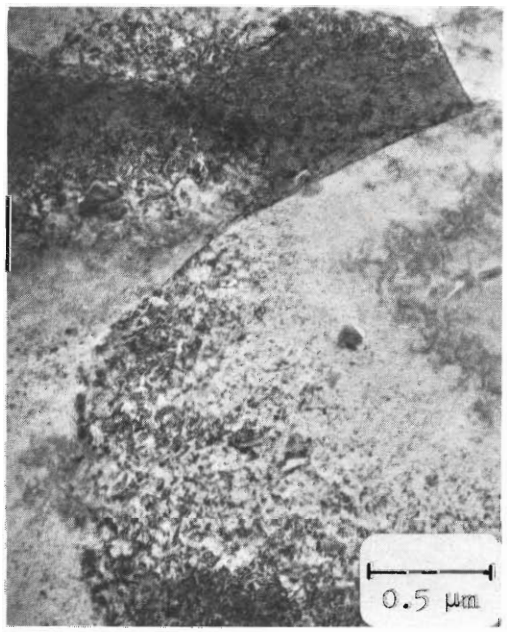

(c)

Figure 22. Dislocation Structures in Fatigued 7475 Specimens: (a) AR, 2600 cycles, $\Delta\varepsilon_p/2 = 0.10\%$, (b) HR, 1850 cycles $\Delta\varepsilon_p/2 = 0.10\%$, and (c) HR, 130 cycles, $\Delta\varepsilon_p/2 = 1.0\%$.

on dislocations. Looping of these particles would be expected to lead to cyclic hardening behavior. In fact, Laird[52] has recently proposed that the dispersoid phase in 7075 (which is the same as in 7475) plays the "dominant role in improving the cyclic stress-strain response of commercial alloys with respect to the base alloy."

The Coffin-Manson plots, shown in Figure 23, may be viewed as an indication of the resistance of a material's microstructure to crack initiation and failure in the LCF region[25]. These plots of plastic strain amplitude (taken at $\frac{1}{2} N_f$) versus reversals to failure show that, within the scatter of data, there is no significant difference in total LCF life of the 7050 AR and HR materials for the range of strain amplitudes studies. At low plastic strain amplitudes, the 7475 AR material seems to be slightly superior in LCF resistance to 7475 AR+HR and 7475 HR. The fatigue ductility exponents, -c, and the fatigue ductility coefficients, ε'_f, obtained from the Coffin-Manson plots for the LCF data are listed in Table 4. Also shown in Table 4 are values of the cyclic work hardening coefficient, n', which were calculated using a linear regression analysis from the relationship between stress amplitude and plastic strain amplitude given in Equation 3.

The failure of the Coffin-Manson relationship, Figure 23, to accurately predict LCF behavior of aluminum alloys at low plastic strain amplitudes has been observed previously[25,30,46,53]. This anomalous behavior has led some workers[86,87] to suggest that a plot of plastic work per cycle (ΔW_p) versus $2N_f$ may be more helpful in dealing with LCF data of aluminum alloys. Plots of ΔW_p versus

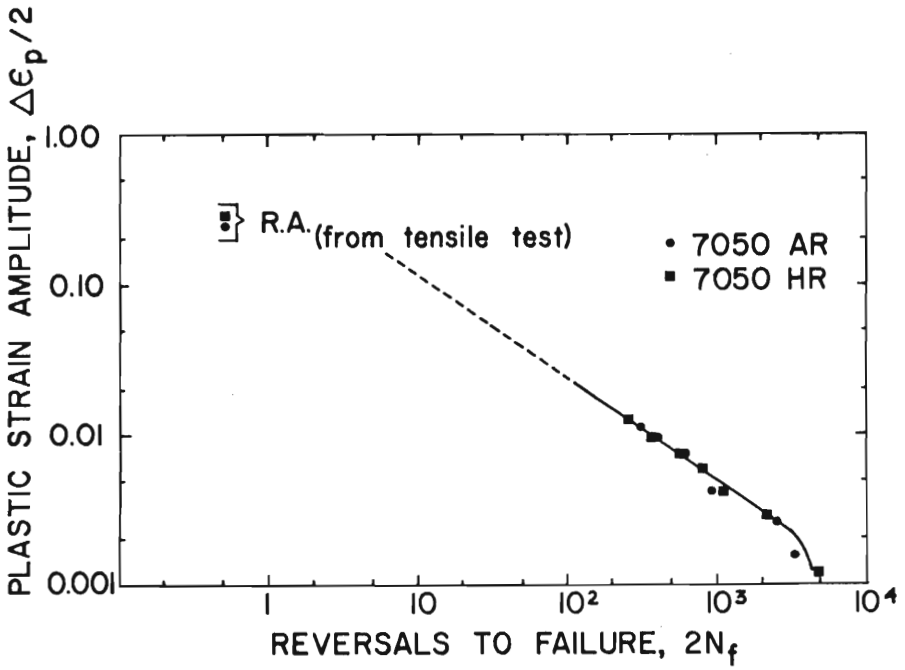

(a)

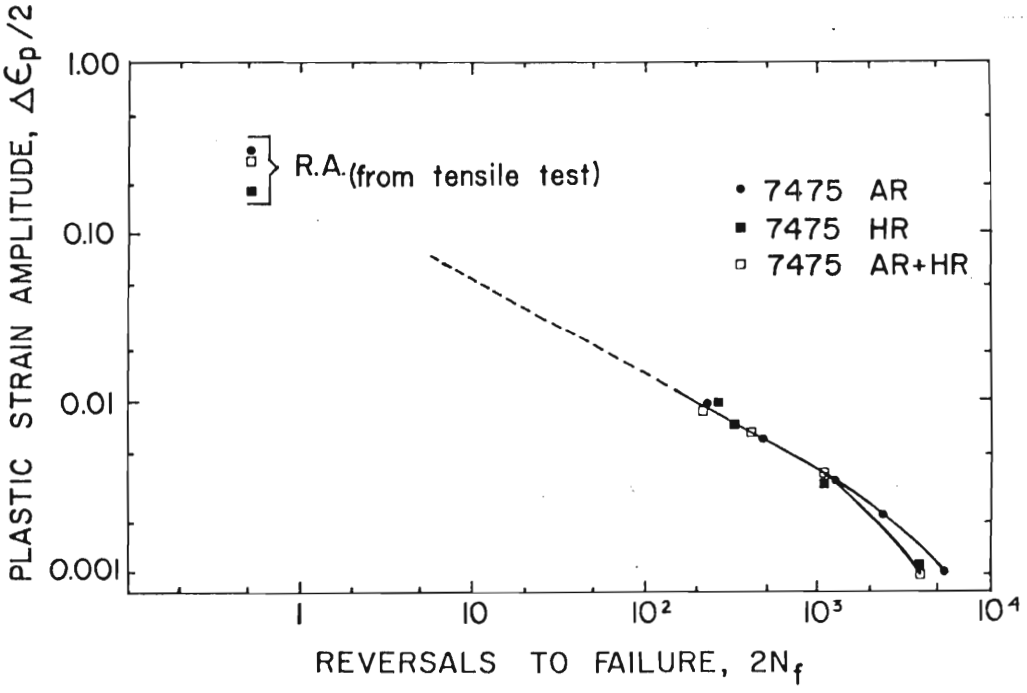

(b)

Figure 23. Coffin-Manson Plots of LCF Data for: (a) 7050, and (b) 7475.

Table 4. LCF Parameters for the Experimental Alloys

	n'	-c	ε'_f* (%)
7050			
AR	0.05	0.70	58
HR	0.04	0.70	58
7475			
AR	0.05	0.51	20
AR+HR	0.06	0.51	20
HR	0.04	0.51	20

*ε'_f determined at $2N_f = 1$

cycles were constructed for several of the 7050 LCF tests. These plots, analagous to cyclic stress response curves, are shown in Figure 24(a). From the values of ΔW_p at saturation for each test, the plots of ΔW_p versus $2N_f$ were constructed for 7050 AR and 7050 HR as shown in Figure 24(b). These curves merely reflect the similarity in fatigue behavior between the two variants of 7050 and offer no better prediction of fatigue resistance than the traditional cyclic stress response and Coffin-Manson plots. It is interesting to note from Figure 24(b) that the slope of the ΔW_p-$2N_f$ plot correlates well with the slope of the Coffin-Manson plot according to the relationship put forth by Saxena and Antolovich[87].

Microstructural explanations[30,46,88] put forth to explain the anomalous Coffin-Manson behavior are most often based upon the occurrence of strain localization, i.e., non-homogeneous deformation, at low plastic strain amplitudes. Thin foils from 7050 and 7475 samples fatigued at strain amplitudes below the break in the Coffin-Manson plot were examined. Figure 22 shows that dislocation arrangements in these foils were mostly homogeneous, with little evidence of the deformation bands reported to occur during LCF at low strain amplitudes[30,88]. When dislocation banding was observed by TEM, homogeneously distributed dislocations could be seen between the bands. Another recent LCF study of 7XXX alloys[53] also reported no TEM evidence of non-homogeneous deformation at low plastic strain amplitudes. It should be noted, however, that the failure to observe dislocation banding by TEM does not rule out altogether the occurrence of strain localization. The present investigation examined only

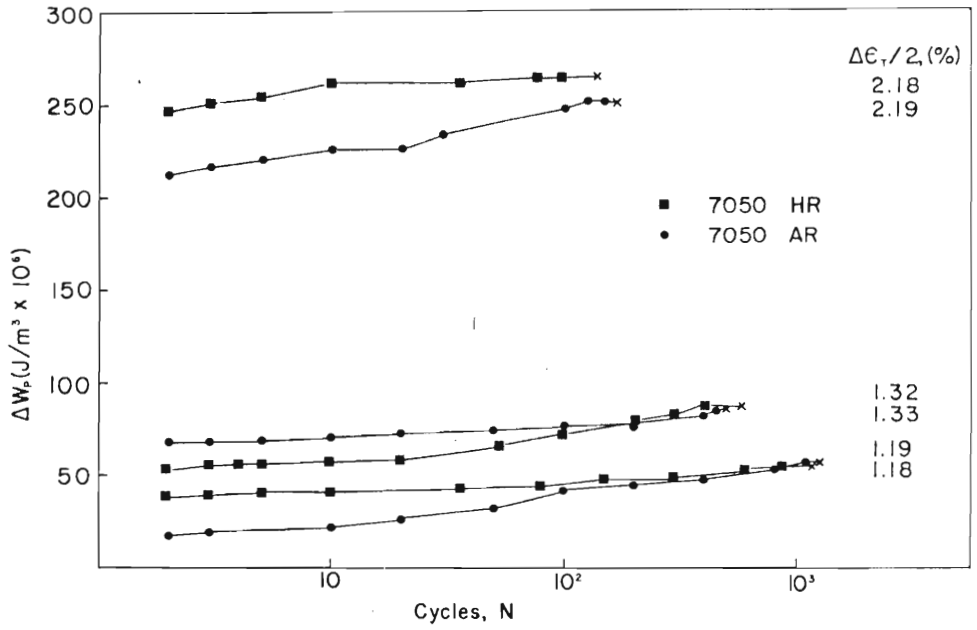

(a)

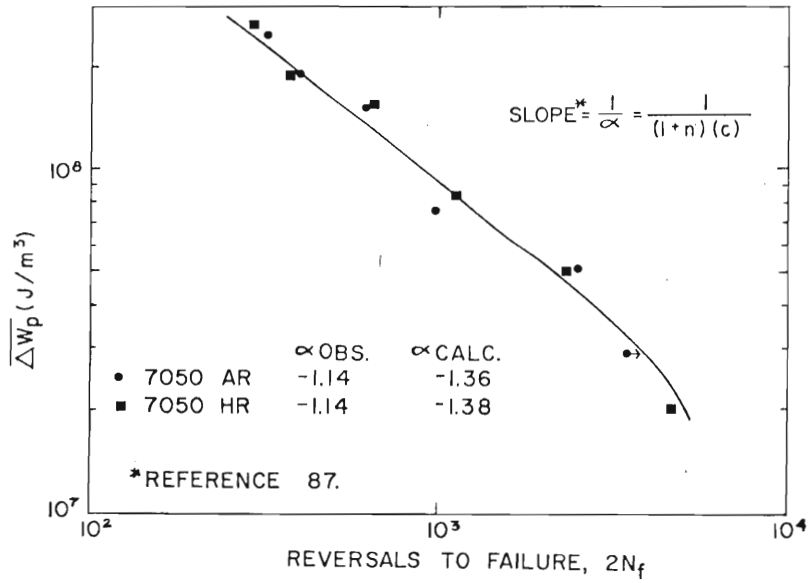

(b)

Figure 24. 7050 LCF Data Plotted in Terms of Plastic Work per Cycle (ΔW_p): (a) Cyclic stress response, and (b) $\overline{\Delta W}_p$ versus LCF life.

a limited number of foils in making this observation and may have fortuitously examined only areas which deformed uniformly. Macroscopic examination of specimen surfaces revealed that, at low strain amplitudes, some degree of strain localization must have occurred. Some grains on the specimen surface were covered with slip lines, while adjacent grains were unmarked. At higher strain amplitudes, deformation was more uniformly distributed throughout the microstructure. Thus, the results of the present investigation are in overall agreement with previous studies[30,88] which propose a strain-localization explanation of anomalous Coffin-Manson fatigue behavior in 7XXX aluminum alloys.

Stress-controlled high cycle fatigue tests (R=1.0) were conducted to assess the resistance of the experimental materials to crack initiation at long cyclic lives. Considering the 7475 data of Figure 23(b), it was felt that stress-controlled tests may possibly clarify microstructural effects on crack initiation in these materials. The results of these HCF tests, shown in Figure 25, show that there is essentially no difference in stress-controlled fatigue resistance between AR and HR variants of the two alloys.

From the Coffin-Manson plots of Figure 23 and the HCF data of Figure 25, it is evident that differences in grain structure due to ingot processing have little effect on total LCF or HCF life. However, it should be noted that the comparisons of fatigue resistance were made only on the basis of <u>total</u> fatigue life measurement. Since it is extremely difficult to pinpoint the exact time of initiation of the <u>fatal</u> crack in a LCF test, the first observation of

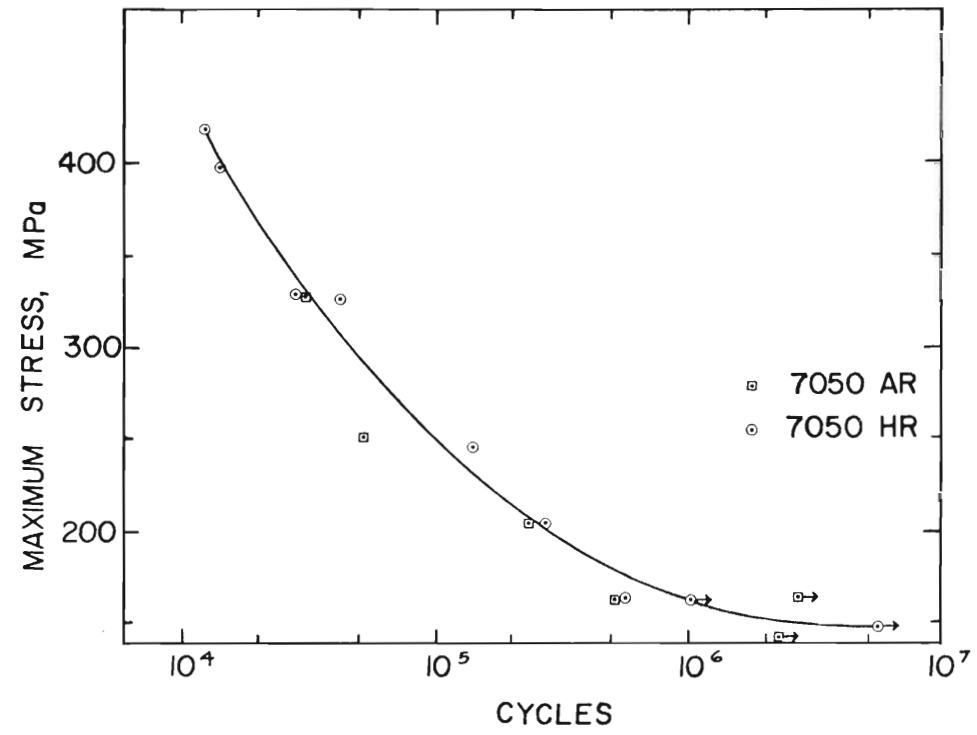

(a)

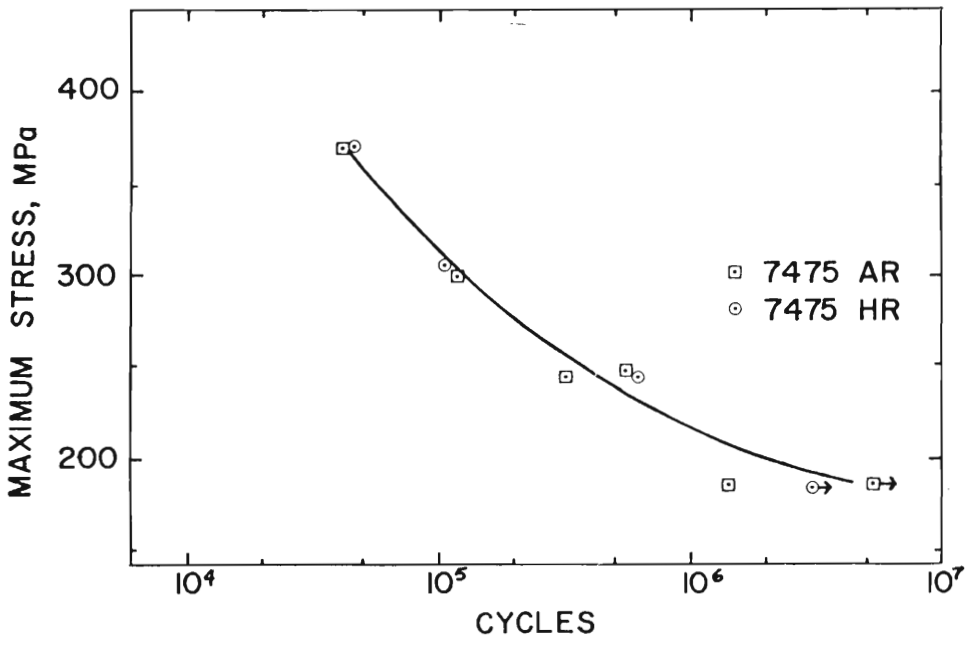

(b)

Figure 25. High Cycle Fatigue Data for: (a) 7050 and (b) 7475.

a measurable drop in tensile load after saturation occurred was taken at the time of crack initiation. Due to the marked differences in notch sensitivity between the AR and HR microstructures (particularly in 7050), it would be helpful to have a more reliable indicator of crack initiation. Once a fatigue crack was observed in a 7050 AR specimen, failure was almost immediate. At higher strain amplitudes, AR specimens sometimes failed before any noticeable drop in tensile load indicated the presence of the fatal fatigue crack. 7050 HR specimens, on the other hand, always showed a clear-cut crack initiation time and progressive growth of the crack until failure, as evidenced by the reduction in the tensile portion of the hysteresis loop. These observations were borne out by examination of fractured LCF specimens. Fracture surfaces of 7050 AR LCF specimens showed very small, if any, areas of fatigue damage while considerably larger fatigued regions were found on fracture surfaces of comparable 7050 HR specimens. From optical examination, it appeared that each LCF specimen contained only one primary crack initiation site. The fatigued areas of the LCF specimens were too small to be measured conveniently, but similar observations of the fractured 7050 HCF specimens shown in Figure 26 were easily checked by planimetric measurements. Note that the fatigued areas of the AR specimens are small (approximately 11% and 41%) compared to those of the HR specimens (17% and 55%) of similar total fatigue life. Consequently, to obtain similar <u>total</u> fatigue life, crack initiation in the AR specimens must be somewhat more difficult.

Metallographic observations of crack initiation were made to

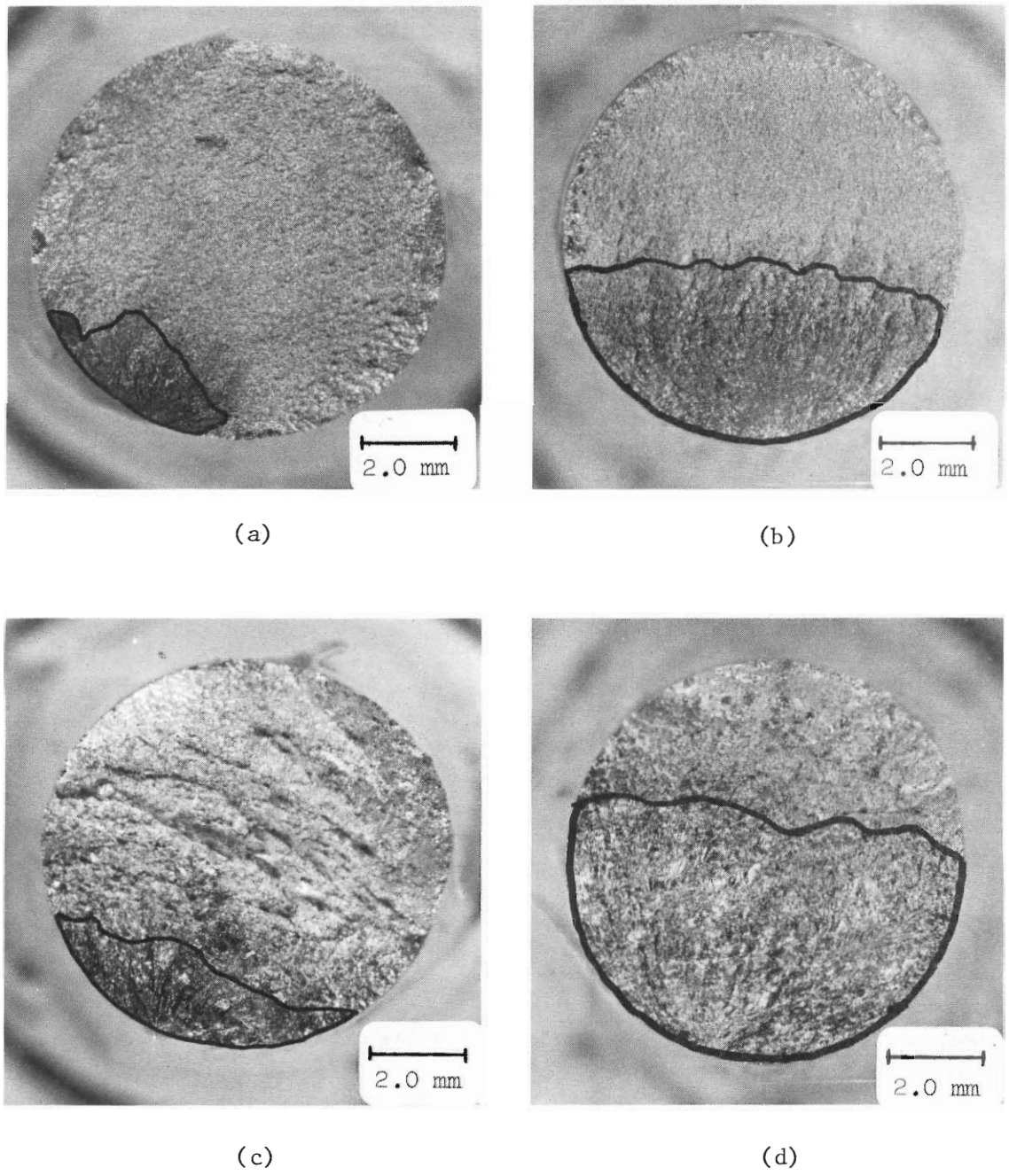

(a) (b)

(c) (d)

Figure 26. Optical Micrographs of Fractured 7050 HCF Specimens: (a) AR, N_f = 30,830, fatigued area = 11.1%, (b) AR, N_f = 514,360, fatigued area = 41.3%, (c) HR, N_f = 28,850, fatigued area = 17.2%, and (d) HR, N_f = 572,570, fatigued area = 55.0%.

determine if there was any microstructural basis for a difference in crack initiation resistance in the experimental materials. Surfaces of LCF specimens of the 7050 AR material cycled at a total strain amplitude of $\pm$ 1.2% (N_f = 1262) revealed that grain boundary cracks initiated early ($\sim$100 cycles) in the LCF test and linked up during subsequent cycling, Figures 27(a) and 27(b), until a critical crack size for failure was reached. No crack initiation at surface slip markings was observed. Crack initiation in the 7050 HR material cycled at $\pm$ 1.2% (N_f = 1165) also occurred early in the LCF test. Slip lines and intergranular cracks were observed at 100 cycles. Subsequent cycling increased the severity of slip markings and led to initiation of cracks at slip lines and link-up of grain boundary cracks until failure occurred as shown in Figures 27(c) and 27(d). Etching of the fatigued 7050 HR specimens revealed that crack initiation occurred extensively at slip lines in both recrystallized and unrecrystallized grains, Figure 28.

In order to obtain a quantitative assessment of LCF crack initiation resistance for the two 7050 materials, a detailed analysis was made of the fatigued areas shown in Figure 27. The technique, described by Underwood and Starke[89], computes L_A, the length of crack traces per unit area; N_A, the number of crack initiation sites per unit area; and $\bar{L}$, the mean crack length. These quantities, reported in Table 5, show that the severity of fatigue damage, as reflected in the number and length of cracks, is consistently less for the fine-grained 7050 AR material. Consequently, it is concluded that the AR microstructure offers superior LCF crack initiation

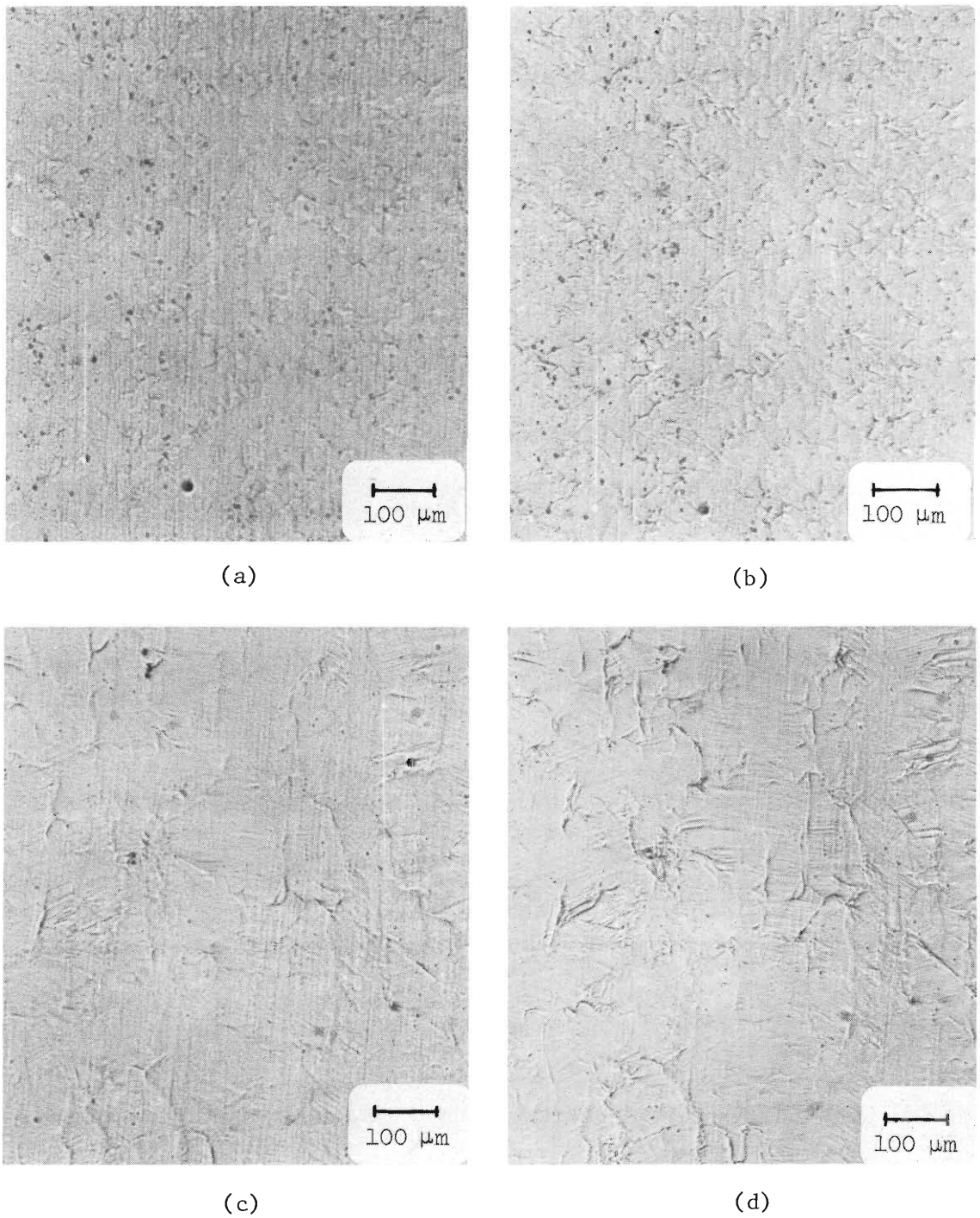

Figure 27. Observations of LCF Crack Initiation in 7050 LCF Specimens Cycled at a Total Strain Amplitude of 1.2%: (a) AR, 100 cycles, (b) AR, same area, 300 cycles, (c) HR, 100 cycles, and (d) HR, same area, 300 cycles. Stress axis is vertical.

Table 5. Quantitative Metallographic Parameters for LCF Crack Initiation

	L_A (cm^{-1})	N_A (cm^{-2})	$\bar{L}$ (μm)
7050 AR,(±1.2%)			
100 cycles	19.45	9,589	20.3
300 cycles	63.34	26,849	23.6
7050 HR,(±1.2%)			
100 cycles	35.99	11,513	31.3
300 cycles	108.82	32,740	33.2
7475 AR,(±0.98%)			
500 cycles	9.16	1,498	61
7475 HR,(±0.98%)			
500 cycles	15.27	1,519	100
7050 HRL,(±0.90%)			
600 cycles	63.82	18,083	35
7050 HRT,(±0.90%)			
600 cycles	81.66	17,868	46

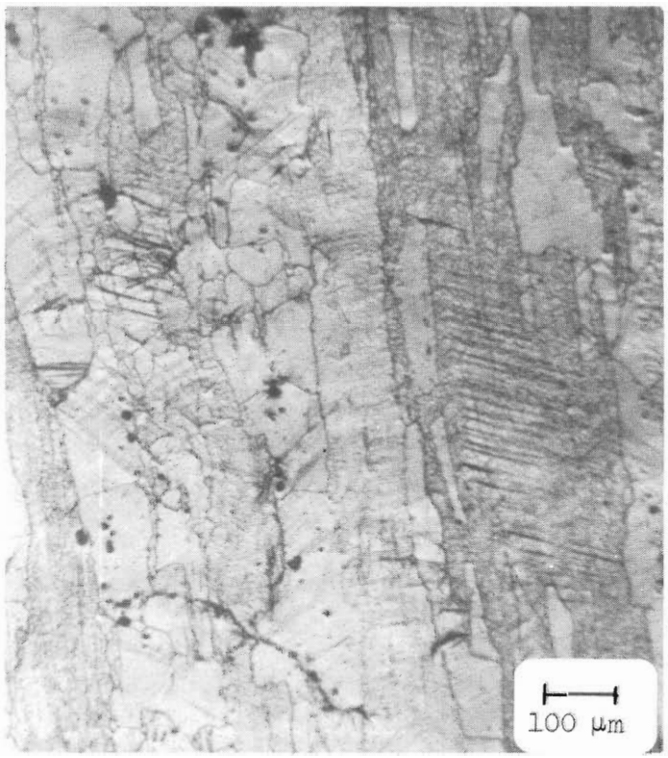

Figure 28. Etched Surface of 7050 HR Specimen Cycled at a Total Strain Amplitude of 1.2% for 300 Cycles. Stress Axis is Vertical.

resistance compared to the partially-recrystallized HR material.

Similar results were obtained for crack initiation studies of the 7475 materials. Specimens of 7475 AR and 7475 HR were strain-cycled at a total strain amplitude of $\pm$ 0.98%. Crack initiation was followed by replication of specimen surfaces at 100 and 500 cycles. Optical micrographs of replicas from these tests are shown in Figure 29. At 100 cycles, slip markings were evident in samples of both materials. Grain boundary offsets had developed in the AR material. However, no fatigue cracks were observed in either sample. Upon further cycling to 500 cycles, extensive slip band crack initiation and Stage I growth occurred in the HR material and grain boundary cracks developed in AR material. By 500 cycles, cracks had also initiated at Fe-Si intermetallic particles in both materials. These particles did not appear to change the overall character of fatigue cracking in the two variants of 7475, but only appeared to accelerate the operating processes. In 7475 AR, fatigue cracks which initiated at intermetallics followed grain boundaries during Stage I growth. Figures 29(c) and (d) show that crystallographic Stage I crack growth along slip bands occurred regardless of the original crack initiation site. The quantitative metallographic techniques described earlier were applied to the replicas to compute L_A, N_A and $\bar{L}$. As in the case of the 7050 materials, the AR variant of 7475 exhibited consistently less severe fatigue damage than its HR counterpart as shown by the values in Table 5.

Two microstrucutral features, grain size and preferred orientation, are probably responsible for this difference in crack

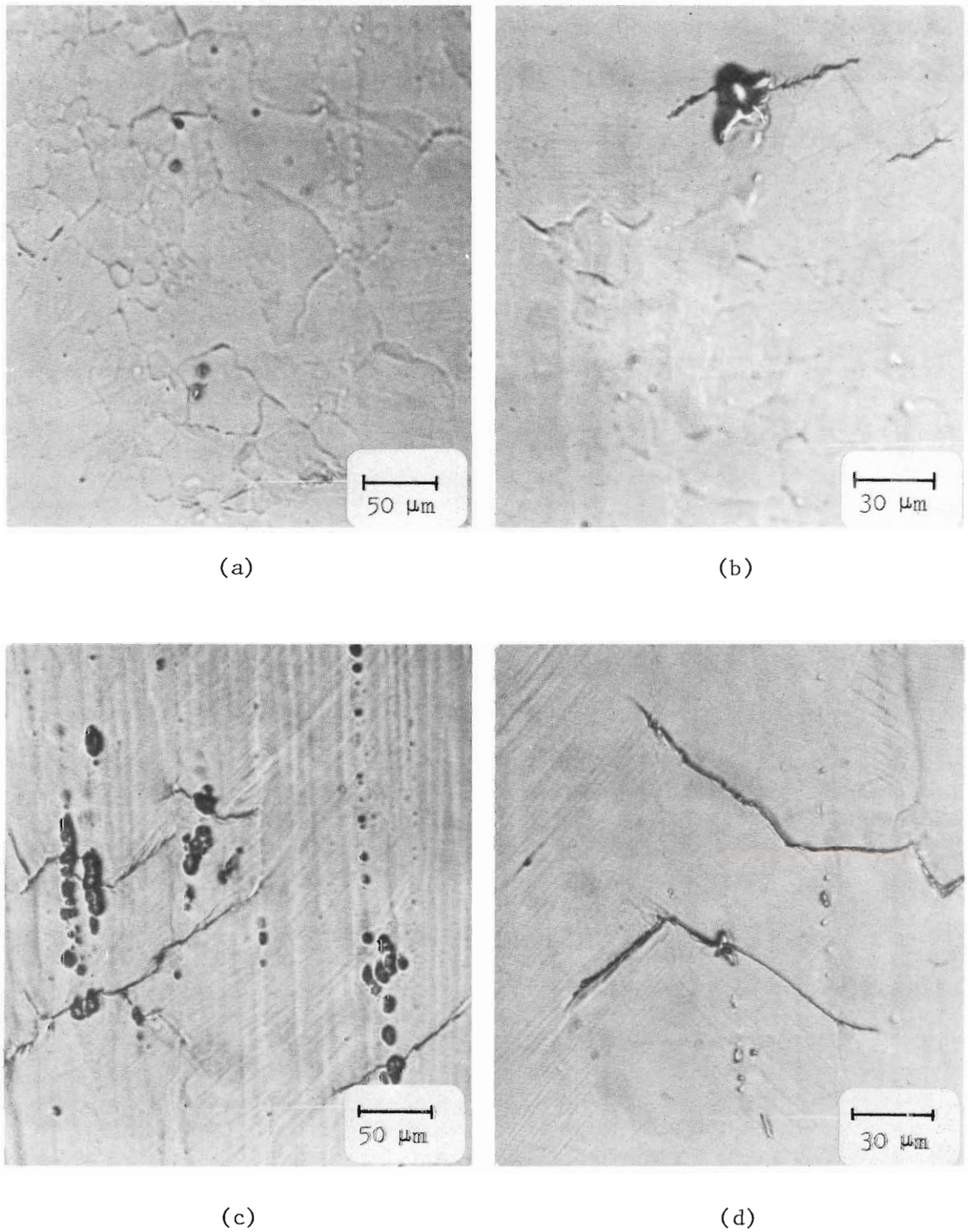

Figure 29. LCF Crack Initiation in 7475 Specimens Cycled 500 Cycles at a Total Strain Amplitude of 0.98%: (a) and (b) AR, (c) and (d) HR.

initiation behavior. During fatigue cycling, large well-developed persistent slip bands (PSB's) form in the hot-rolled materials. The formation of PSB's in these materials is aided by the degree of preferred orientation (texture) introduced into the plate by hot-rolling. The sharp (110)[1$\bar{1}$2] texture of the HR materials shown in Figure 11 provides a higher density of grains with {111} planes favorably oriented for slip when compared to the more randomly oriented AR materials. With a low degree of misorientation between adjacent grains and subgrains, their boundaries do not provide effective barriers against slip as shown in Figure 28. PSB's lead to the development of coarse surface slip lines which provide easy sites for crack initiation and Stage I crack growth. In the AR materials, high-angle grain boundaries effectively prevent the transfer of plasticity between adjacent grains. Since neighboring grains are unlikely to have similar orientations (note the random textures of Figure 10), the development of PSB's is restricted to individual grains. Surface slip markings are much less intense than observed for the HR materials and are unlikely to be crack initiation sites. Consequently, crack initiation in the AR materials occurs predominantly at the grain boundaries. As PSB's develop during fatigue and begin to intersect grain boundaries, some grain rotation, resulting in microscopic offsets, occurs to accommodate differing degrees of deformation in adjacent grains. Dislocation pile-ups at grain boundaries and grain boundary offsets probably result in the intergranular crack initiation shown in Figures 27 and 29. It also appears from these figures that the link-up of small cracks to form a larger, and eventually fatal, crack

is more difficult than crack link-up in the HR materials.

In order to determine the role of preferred orientation on the crack initiation behavior of the alloys, two 7050 HR specimens were prepared: specimen HRL with the axis parallel to the rolling direction of the plate, and specimen HRT with the axis perpendicular to the rolling direction. The specimens were strain cycled at a total strain amplitude of 0.90% for 600 cycles, after which they were examined by optical metallography. The quantitative metallographic parameters shown in Table 5 indicates that the crack initiation resistance is relatively unaffected by orientation in the 7050 HR material.

Fatigue Crack Propagation

Alloy 7050

Fatigue crack propagation data for the 7050 experimental materials, plotted as da/dN vs. ΔK, are shown in Figure 30. Over the range of ΔK studied, 5-25 $MPam^{\frac{1}{2}}$, the curves assume the sigmoidal shape typically observed for most FCP data[90]. A comparison of the data shows that the slowest crack growth rates at low ΔK values were exhibited by specimens of the HR material cut from the center of the plate (designated as HR-C on Figure 30). When the specimens were taken from the top or bottom edge of the HR plate (HR-E), crack growth rates were comparable to those of 7050 AR i.e., 3-4 times faster than the HR-C material. The limited data obtained for 7050 AR+HR showed that FCP rates were similar or slightly faster than for the AR material. At higher ΔK values, the da/dN-ΔK plots for the experimental materials converge, and the HR-C material loses its large advantage

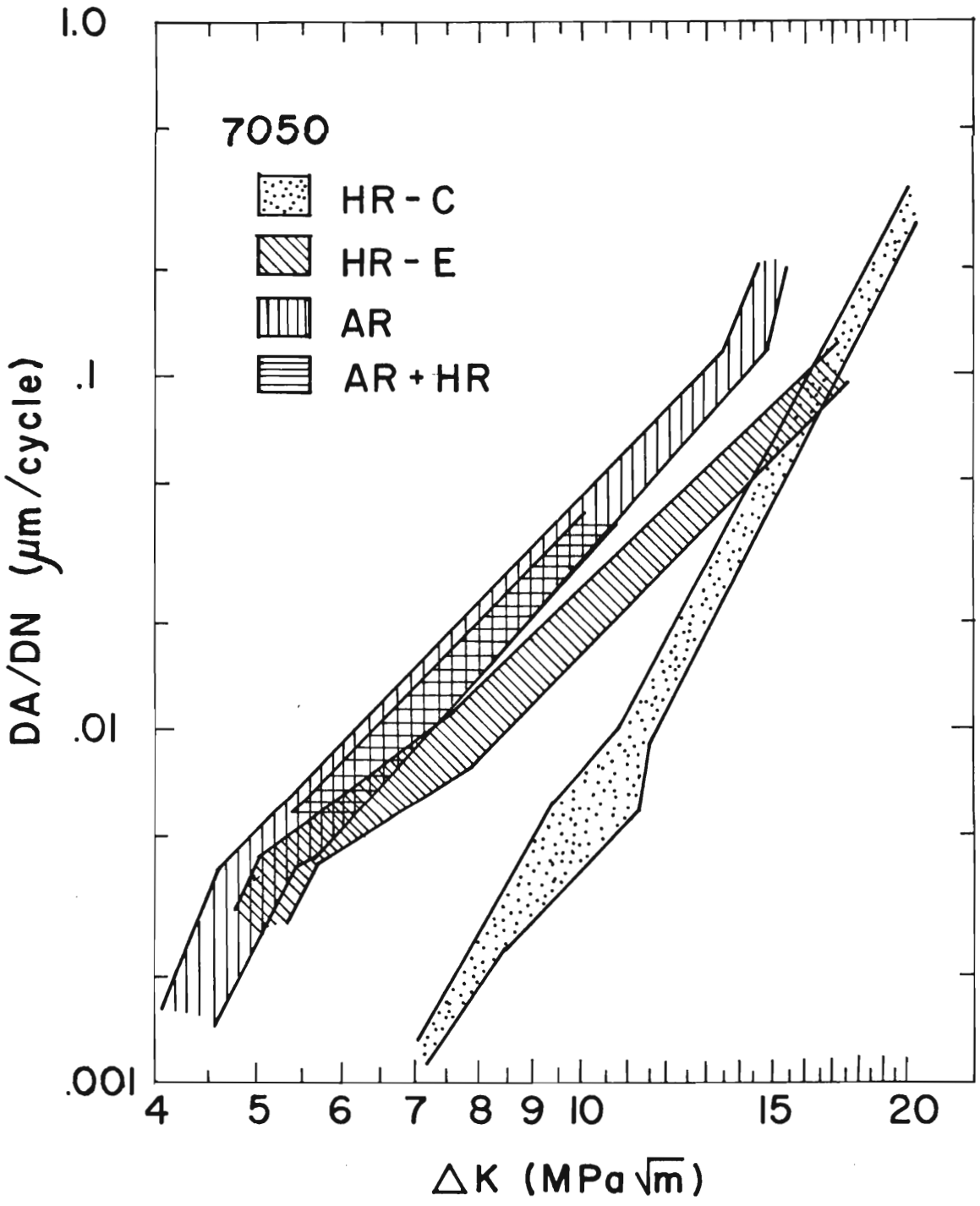

Figure 30. Fatigue Crack Propagation Data Obtained for 7050 Experimental Materials Plotted as da/dN versus ΔK.

in FCP resistance over the other materials. The data plotted in Figure 30 shows the scatter bands of the FCG data for both specimen orientations, T-L and L-T. Results for 7050 AR and 7050 HR showed no appreciable differences in crack growth rates for different specimen orientations. 7050 AR+HR showed slightly higher crack growth rates when the crack grew perpendicular to the rolling direction (L-T). Quantitative metallography showed that particle spacing was approximately the same in both L and T directions of the AR+HR plate, eliminating that possible microstructural explanation for observed differences in crack growth rates. In view of the scatter observed for FCP data of the other experimental materials, e.g., HR-C, specimen orientation probably does not have a significant effect on crack growth rates of 7050 AR+HR.

In order to determine if FCP rates for the 7050 materials are influenced by the presence of residual stresses, several sample blanks were resolutionized, quenched, and aged to the T6X1 temper. This reheat-treatment was thought necessary since the original 7050 AR and AR+HR specimens were cut from previously heat-treated plate and the HR specimens were heat-treated as small blanks. Differences in residual stresses could have contributed somewhat to the overall scatter in the FCP data. However, the data from these specimens invariably fell within the scatter band for the crack growth data collected from the original specimens. Thus, it was concluded that the major differences in crack growth rates arise from the microstructures produced by the different ingot processing methods and not from differences in the residual stresses.

The two major microstructural features which may contribute to the differences in FCP rates in this study are the grain structure (grain size and degree of recrystallization) and the volume fraction and distribution of the Al_2CuMg particles. At low ΔK values, the higher crack growth rates of the 7050 ITMT materials (AR, AR+HR) compared to the HR-C material are most likely due to the large volume fraction (>1.0%) of Al_2CuMg particles in the microstructures. Since the AR and AR+HR materials have markedly different grain structures (see Figure 5, Table 2), but comparable FCP rates, DR and grain size are probably not the most important parameters controlling crack growth in the 7050 alloy studied in this investigation. However, grain structure may have some effect on FCP rates when the volume fraction of Al_2CuMg particles is not a factor. Recent research at Alcoa[6] and this laboratory[53] also indicates that grain structure does not play a dominant role in determining FCP rates in 7050-type alloys. There is substantial evidence[1,53], however, that degree of recrystallization may influence crack growth in alloys with fewer constituent particles.

The conclusion that the undissolved Al_2CuMg particles are responsible for the higher FCP rates in the 7050 ITMT materials is supported by the SEM fractographs of Figures 31 and 32. Many areas of the ITMT fatigue fracture surfaces were found to contain large concentrations of the particles. Localized areas of intergranular fracture and areas covered with Al_2CuMg particles were the most frequent features found on the ITMT fatigue fracture surfaces as shown in Figure 31. The fracture surfaces of 7050 HR fatigue specimens,

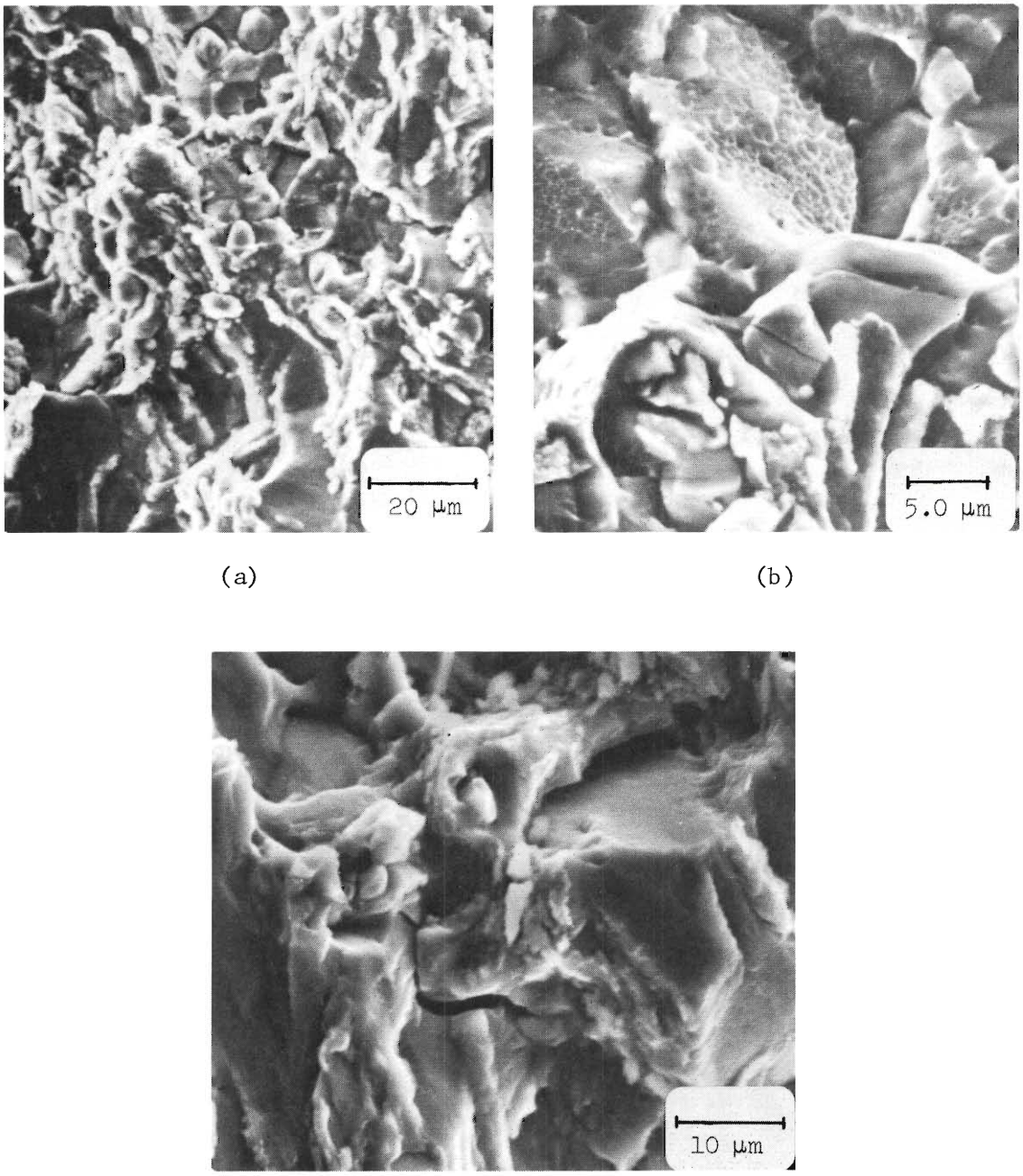

(a) (b)

(c)

Figure 31. Scanning Electron Fractographs of 7050 ITMT Crack Growth Specimens Tested in Dry Air at $\Delta K = 8.5$ MPam$^{1/2}$: (a) and (b) AR, and (c) AR+HR. Crack growth direction is vertical.

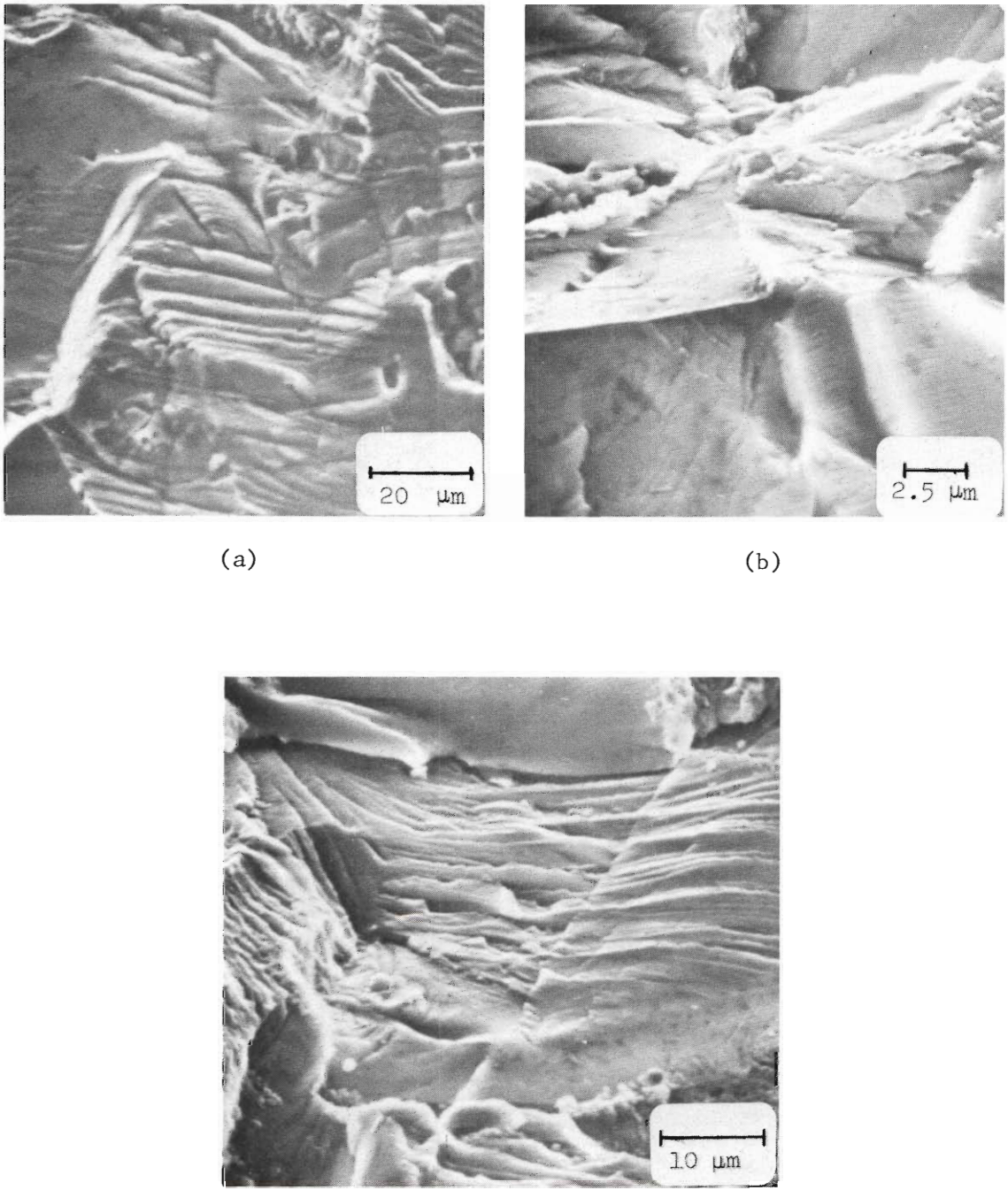

(a) (b)

(c)

Figure 32. Scanning Electron Fractographs of 7050 HR Crack Growth Specimens Tested in Dry Air at ΔK = 8.5 MPam$^{\frac{1}{2}}$. Crack Growth Direction is Vertical.

Figure 32, show the presence of ductile crack growth markings (not fatigue striations) and features which resemble irregular plateaus and ridges. Al_2CuMg particles were only observed rarely on the FCP surfaces of 7050 HR.

Other research[6] seemingly contradicts the previously stated conclusion regarding the effect of constituent particles in the 5-10 μm size range on fatigue crack growth in this investigaion. Staley and co-workers[6] offer fractographic evidence to show that large constituent particles have little effect on striation spacing and FCP rates in hot-rolled materials. However, in the more recrystallized ITMT materials, the Al_2CuMg particles are often found at grain boundaries (Figure 5), and may lead to localized intergranular fracture during fatigue crack growth as shown in Figure 31. This lower energy type of fracture would be expected to lead to the accelerated crack growth rates observed for the ITMT materials.

The position of the HR-E crack growth data on Figure 30 also supports the conclusion regarding undissolved Al_2CuMg particles and fatigue crack propagation. The microstructure, Figure 33, of the HR-E material is approximately 72% recrystallized and has a recrystallized grain size of ~.055 mm, causing to resemble the ITMT (AR+HR) microstructure more closely than that of 7050 HR. Importantly, it should be noted from Figure 33 that the volume fraction of Al_2CuMg particles (1.38%) is considerably larger in the HR-E material than in the HR-C. This is probably due to the uneven distribution of alloy elements between the center and edges of the as-cast ingot[83]. The higher

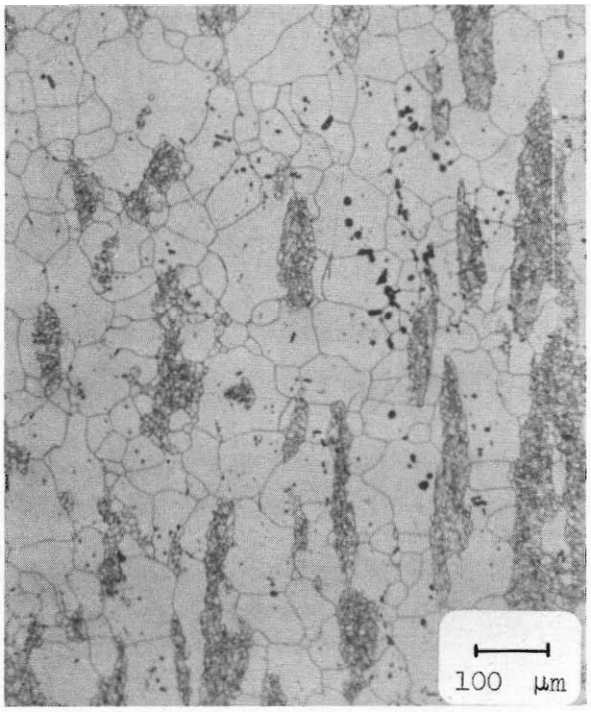

Figure 33. Microstructure of 7050 HR Material Near the Edge of the 38.1 mm Plate (HR-E).

volume fraction of Al_2CuMg in the HR-E specimens probably leads to the observed FCP rates by the same mechanism discussed previously for the 7050 ITMT materials.

The FCP rates for 7050 AR remain somewhat higher than for the HR-C materials at high ΔK values. Most research[1,6] has indicated that, as ΔK values approach K_{IC}, fatigue crack growth is affected by the same parameters that control fracture toughness. As discussed previously (see Monotonic Properties), recrystallized microstructures and constituent particles in the 1-10 μm range are both detrimental to fracture toughness in 7XXX plate material[31]. Consequently, the large Al_2CuMg volume fraction and recrystallized microstructure of the AR materials should adequately explain its observed higher FCP rates at high ΔK levels.

Alloy 7475

FCP rates for 7475 specimens tested in the T-L orientation are shown in Figure 34. 7475 HR exhibited the best resistance to fatigue crack growth, i.e., slowest FCP rates, over the range of ΔK studied. 7475 AR+HR showed slightly superior FCP resistance compared to 7475 AR. Figures 35 through 37, which show SEM fractographs of fatigue crack growth fracture surfaces, support a microstructural explanation for the observed differences in FCP resistance. At low ΔK 7475 AR fatigue fracture surfaces, Figure 35, had a very irregular fracture appearance, characterized by the presence of individual grain facets. Slip markings on the fracture surface obviously changed orientation at grain boundaries. 7475 HR low ΔK fatigue fractures, shown in Figure 36, exhibited regular ductile slip-

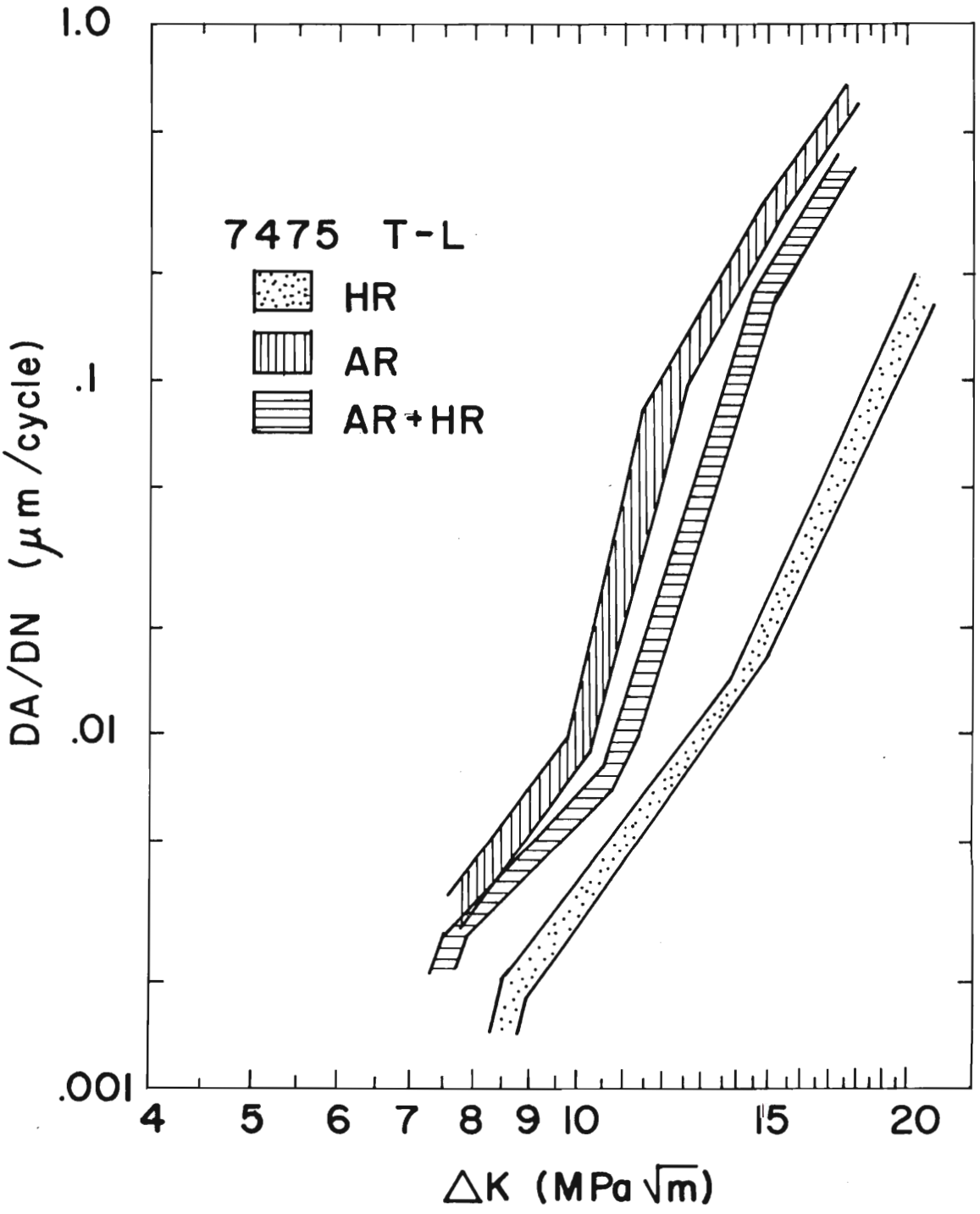

Figure 34. Fatigue Crack Propagation Data Obtained for 7475 Experimental Materials Plotted as da/dN versus ΔK.

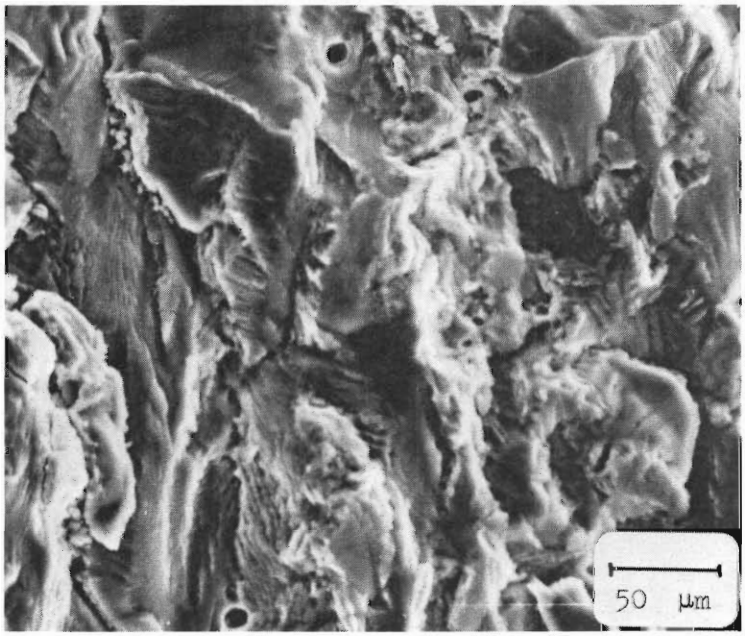

(a)

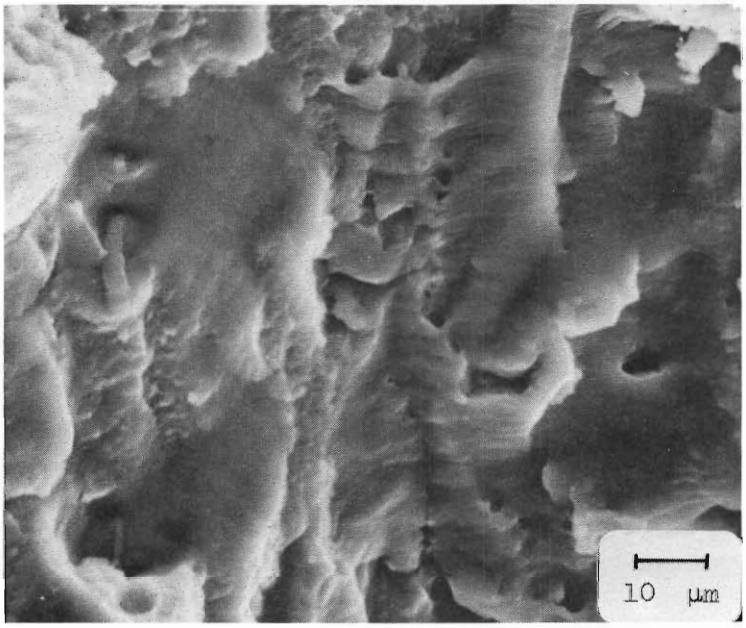

(b)

Figure 35. Scanning Electron Fractographs of 7475 AR Crack Growth Specimens Tested in Dry Air at: (a) $\Delta K = 8.5$ MPam$^{\frac{1}{2}}$, and (b) $\Delta K = 15.0$ MPam$^{\frac{1}{2}}$. Crack growth direction is vertical.

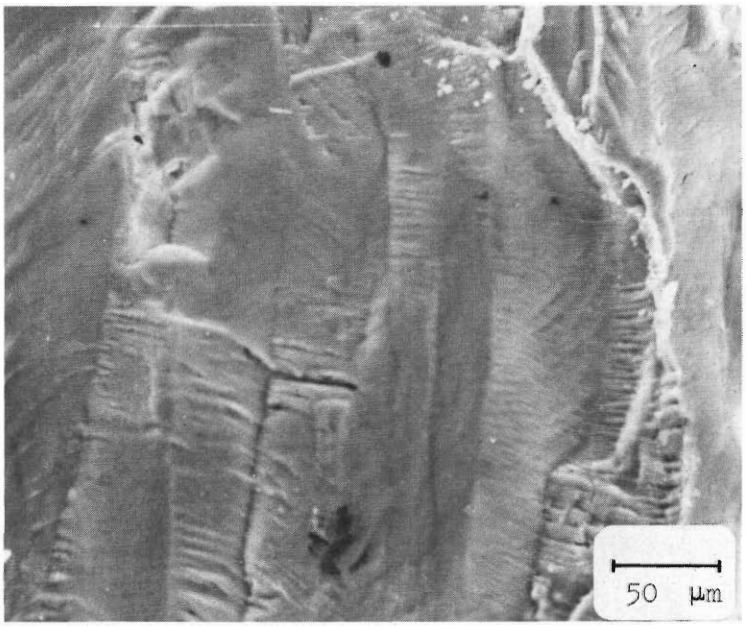

(a)

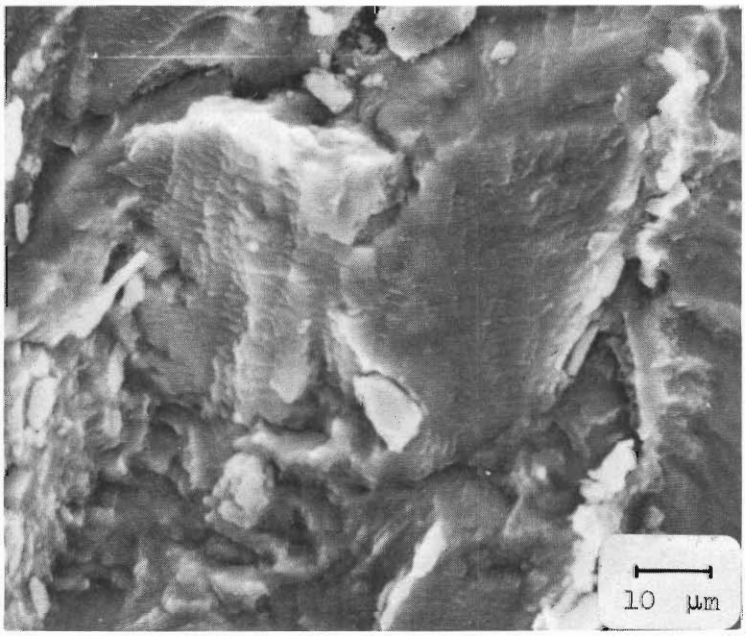

(b)

Figure 36. Scanning Electron Fractographs of 7475 HR Crack Growth Specimens Tested in Dry Air at: (a) $\Delta K = 8.5$ MPam$^{\frac{1}{2}}$, and (b) $\Delta K = 15.0$ MPam$^{\frac{1}{2}}$. Crack growth direction is vertical.

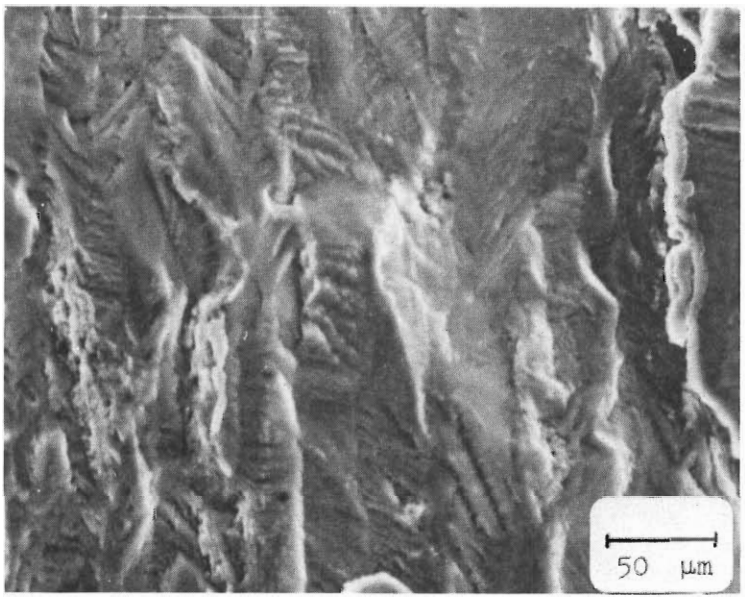

(a)

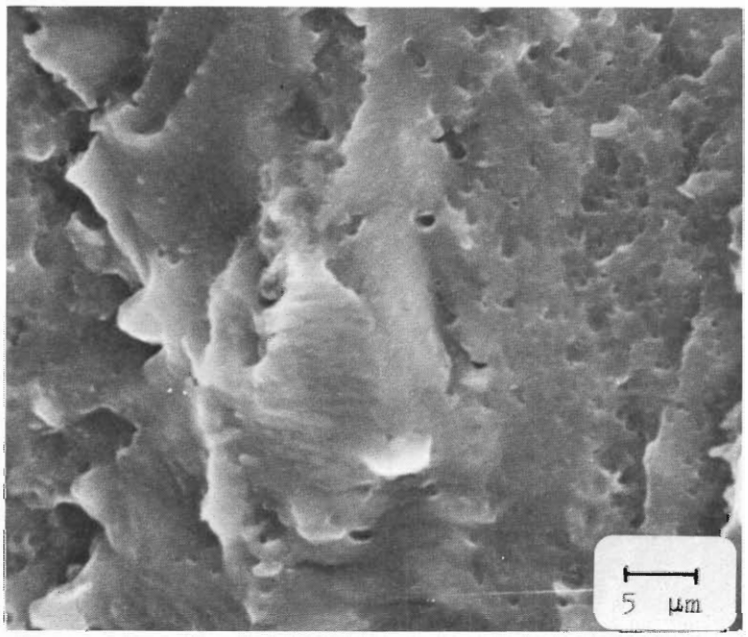

(b)

Figure 37. Scanning Electron Fractographs of 7475 AR+HR Crack Growth Specimens Tested in Dry Air at: (a) $\Delta K = 8.5$ MPam$^{1/2}$, and (b) $\Delta K = 15.0$ MPam$^{1/2}$. Crack growth direction is vertical.

markings, and were generally more featureless in appearance than 7475 AR fractures. The presence of the plateaus and ridges shown in Figure 36 is probably associated with the presence of the elongated "packets" of subgrains in the hot-rolled material. From a comparison of Figure 6(c) and Figure 36, it is evident that the width of the elongated features on the fracture surfaces is approximately the same as that of the unrecrystallized grains in the microstructure. Examination of 7475 AR+HR specimens fatigued at low ΔK, Figure 37, revealed fracture features intermediate in character between those of the other 7475 materials. FCP fractures in 7475 AR+HR were not as ductile and regular in appearance as those of 7475 HR, but were not as faceted and chaotic as those of the AR material. At higher $\Delta K(15.0\ MPam^{\frac{1}{2}})$, the FCP fracture surfaces of all three 7475 materials were somewhat more ductile in appearance. Grain facets on AR and AR+HR specimens were more rounded in appearance and fatigue striations could be observed in all three materials. The overall ranking of FCP fracture character at high ΔK, however, remained the same: 7475 AR exhibited the roughest, most irregular fracture appearance, while 7475 HR fractures were the most featureless with regular slip markings. Similar observations of FCP fracture character have been made previously[53] in fatigue studies of Al-Zn-Mg-Cu alloys with different grain structures.

It is apparent from a correlation of FCP fracture appearance and observed da/dN values that the more ductile, featureless fracture of 7475 HR promotes the best resistance to fatigue crack growth. The presence of subgrains in the hot-rolled materials tends to homogenize deformation on a microscopic scale[53] and provides for a ductile,

transgranular type fracture mode (Figures 15 and 36). This type of fracture would be expected to absorb more energy during FCP than the less ductile, faceted fracture seen in 7475 AR specimens. High-angle grain boundaries in the recrystallized material seem to provide a preferred path for crack growth, leading to a lower-energy intergranular type of fracture and higher da/dN values. The type of mechanism described above may also be responsible, in part, for the differences in FCP rates in the 7050 materials. However, due to the different volume fractions of Al_2CuMg in those materials, differences in grain structure could not be said unambiguously to affect FCP rates of 7050 in the described manner.

Recently several workers[91-93] have sought to develop predictive relationships for fatigue crack growth resistance based on measurable LCF and microstructural parameters. Due to the constraint of surrounding material, a finite volume of material at the crack tip undergoes a condition of strain-controlled cycling. As damage accumulates in this region to a level at which the cyclic ductility is exceeded, cracking occurs. Liu and Iino[91] have used Miner's cumulative damage law[94] and the Coffin-Manson relationship, Equation 4, to formulate an equation for predicting FCP rates from LCF parameters. Their approach has been modified by Majumdar and Morrow[92] and, more recently, by Chakrabortty[93] who have attempted to incorporate a microstructural parameter in their analyses. According to Chakrabortty, the microstructural parameter, ρ', should represent the distance over which slip can occur before encountering a major barrier. His equation, shown in Appendix C, has been applied

successfully to predict FCP rates in steels[93], titanium alloys[93], and 7XXX aluminum alloys[93,95].

This relationship has been applied to the 7475 fatigue data obtained in the present investigation. Since the microstructure of 7475 contains predominantly shearable precipitates, a ρ' value of one-half the average grain length in the rolling direction was chosen. It may have seemed possible to use the subgrain size for this parameter. However, it was shown previously in this work that the texture of the hot-rolled materials made the subgrains ineffectual as barriers to fatigue deformation. The LCF parameters, obtained from Equations 3 and 4, and values of ρ' and Young's Modulus for the three 7475 variants are shown in Table 6.

Before the experimental 7475 FCP data could be compared to predictions from Chakrabortty's equation, it was nceessary to account for the presence of residual stresses in the 7475 plate. Compressive residual stresses, whose values are shown in Table 6, were found by x-ray measurements to occur in the long transverse direction of the three 7475 plates. (Their presence in the materials is not entirely unexpected since the experimental plates were not given the stress-relieving stretching operation usually received by commercial plates). The occurrence of compressive stresses in the long transverse direction of the FCP specimens would be expected to slow crack growth rates in the T-L specimens used to obtain the 7475 data. Since compact tension specimens were used in the present investigation, it was not possible to correct the stress intensity factor directly with the appropriate residual stress. The calculation of K in

Table 6. Parameters for Predicting FCP Rates from the Chakrabortty[93] Equation

	7475-AR	7475-AR+HR	7475-HR
-c	0.51	0.51	0.51
ε'_f (at $2N_f$=1)	0.20	0.20	0.20
n'	0.05	0.06	0.04
k', (MPa)	1421	1497	1380
ρ', (μm)	20	65	93
E, (GPa)	71.1	71.1	71.1
Residual Stress (MPa)	36	30	48

compact tension specimens must be made from the applied load and other geometric factors, rather than from an applied far-field stress, as in the case of center-cracked specimens[49]. (This type of calculation is illustrated for the crack growth specimen of the present investigation in Appendix A). An indirect method was used to estimate the reduction in K value for a compact tension specimen caused by the presence of a compressive residual stress[96]. For a given K, a plot of σ_y versus r can be made according to Equation 6:

$$K = \sigma_y \sqrt{2\pi r} \tag{6}$$

where:

σ_y = stress perpendicular to the crack growth direction, and
r = distance from crack tip.

Such a plot is shown in Figure 38 for a K value of 10 $MPam^{\frac{1}{2}}$. After subtraction of the residual stress value, a new σ_y-r curve was obtained. The areas under the two curves were calculated for values of r up to r_{max} = 8000 μm, a point far enough from the crack tip so that σ_y is very small. By comparing the area under the two curves up to r_{max}, the effective K due to the residual stress is estimated.

Values of ΔK for FCP specimens may be corrected for residual stress in an analogous manner to the method described above. The residual stress values of Table 6 were used to correct the 7475 FCP data of the present investigation. This data is shown in Figure 39

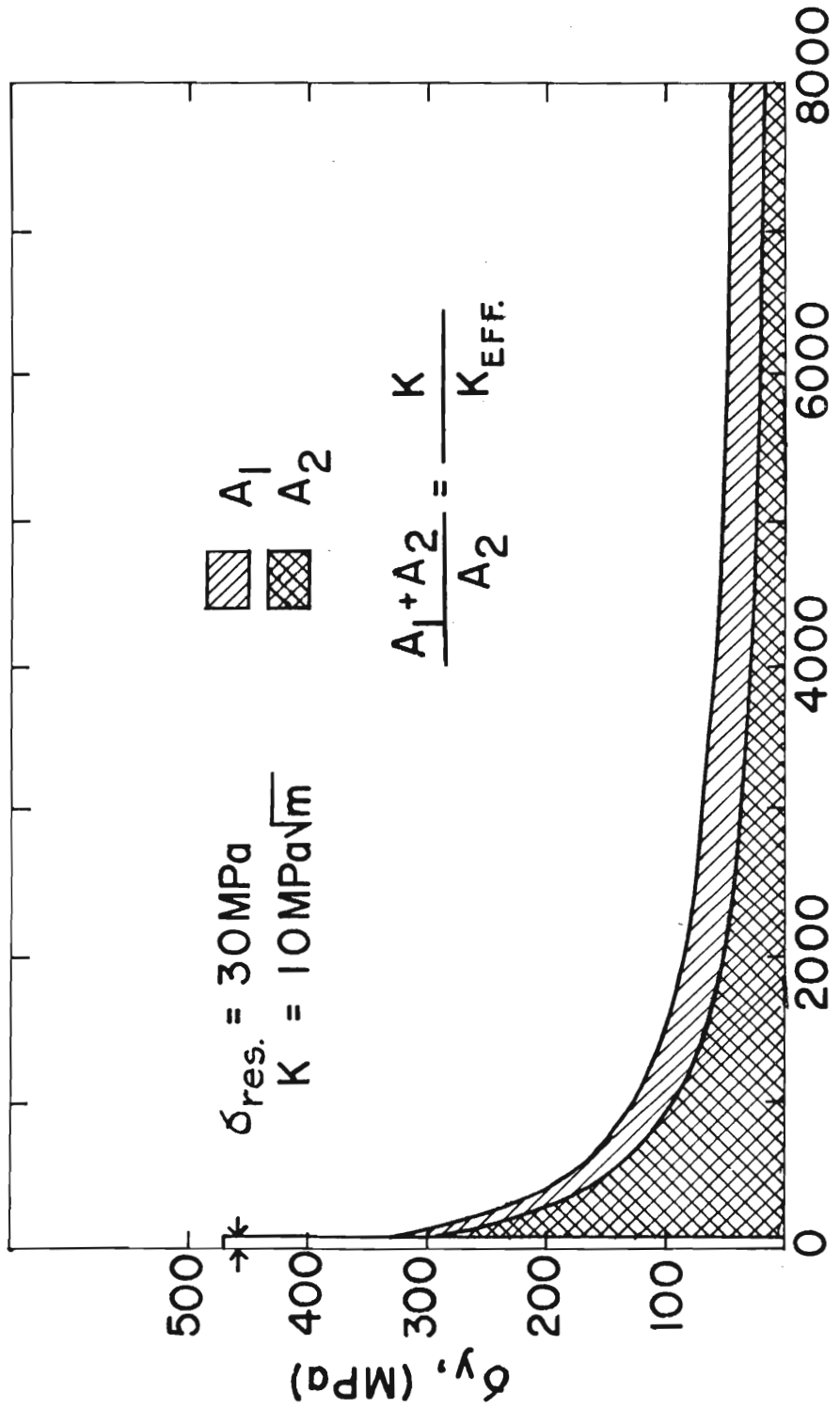

Figure 38. Schematic Diagram Showing the Correction of ΔK values in 7475 FCP Specimens to Account for Residual Stresses.

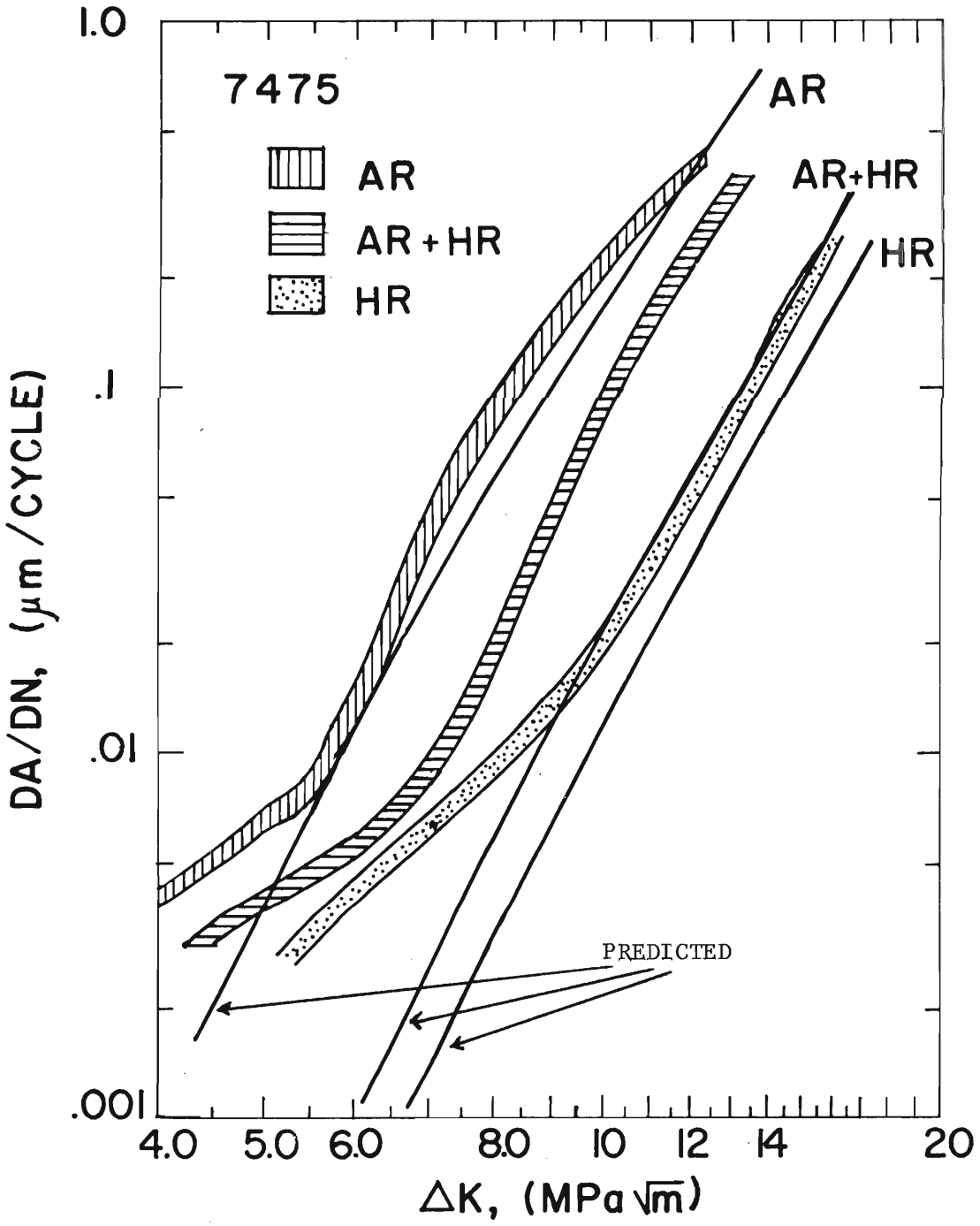

Figure 39. 7475 FCP Data Corrected for Residual Stresses and Compared to the Predictions of the Chakrabortty[93] Equation.

and compared to predictions of FCP rates made from Chakrabortty's equation. It is evident that the predictions of FCP resistance from the LCF data are in fairly good agreement with the data obtained for 7475 AR and 7475 HR at da/dN values greater than 0.01 μm/cycle. However, this agreement may be purely fortuitous. The corrections made to account for residual stresses can only be assumed to result in estimates, rather than absolute values, of ΔK since x-ray measurements of residual stresses normally involve a large amount of scatter. Furthermore, other microstructural features not accounted for by the magnitude of ρ' might have influenced FCP rates in the present investigation. Parameters such as dispersoid spacing and distribution, subgrain size, and texture could have led to some variability in this respect. It is important to note that, even though quantitative agreement with observed FCP rates was not always obtained, the relative positions of the data were correctly predicted from LCF and microstructural parameters using the relationship proposed by Chakrabortty.

CHAPTER V

CONCLUSIONS

1. The unrecrystallized microstructures of hot-rolled 7050 and 7475 exhibited the best overall combination of properties of the materials studied. For applications where total fatigue performance must be considered (i.e., resistance to crack initiation, crack growth, and unstable fracture), the HR variants of the alloys should be chosen in preference to more fully recrystallized ITMT materials.
2. Total LCF and HCF lives of the experimental materials were relatively unaffected by changes in microstructure produced by ingot processing. Some slight improvement in LCF life of 7475 AR at low strain amplitudes was indicated.
3. Crack initiation resistance of fine-grained AR materials was improved somewhat due to the virtual elimination of slip band decohesion as a crack initiation mechanism. This effect was more pronounced in the more fully recrystallized 7050 AR.
4. The texture of the HR materials led to the occurence of crack initiation and Stage 1 crack growth at slip bands in both recrystallized and unrecrystallized grains. Subgrains were not effective in preventing this type of crack initiation.
5. The HR variants of both experimental materials exhibited the best FCP resistance of the materials studied. In 7475, this improvement

was attributed to the promotion of a high-energy absorbing transgranular type of fracture by subgrains in the unrecrystallized material. High-angle grain boundaries in 7475 AR provided for a lower-energy intergranular fracture mode. Analysis of grain structure effects on FCP of 7050 was hindered by the presence of large volume fractions of Al_2CuMg in the ITMT materials.

6. The differences in microstructure observed in similar variants of 7475 and 7050 were due to the presence of different dispersoid phases and slight differences in processing schedules. 7050 materials were more fully recrystallized than their 7475 counterparts.
7. Improved homogeneity of deformation due to the fine grain size of the AR variants let to ductility improvements in 7475 and equivalent ductility in 7050 compared to the hot-rolled materials. The lack of a ductility improvement in 7050 AR was due to the occurrence of pronounced intergranular fracture.
8. The occurrence of large volume fractions of Al_2CuMg in 7050 ITMT materials was due to a slow cooling step prior to deformation at 274°C. Re-solution of these particles was not accomplished by the solution treatments used in the present investigation.
9. Al_2CuMg particles in 7050 ITMT materials were detrimental to fracture toughness and FCP resistance.
10. The occurrence of low-energy intergranular fracture in AR variants of 7050 and 7475 produced low fracture toughness values compared to the unrecrystallized or partially recrystallized

variants of the alloys.

11. The 7475 FCP data showed that the presence of compressive residual stresses in un-stretched plate material can markedly affect measured FCP rates.

12. An equation based on LCF and microstructural parameters proposed by Chakrabortty correctly predicted the relative order of FCP resistance for the three variants of the 7475 alloy.

APPENDIX A

Fatigue Crack Propagation Specimen Design

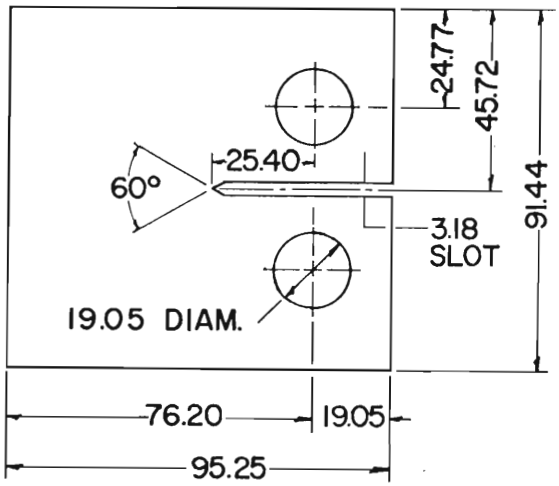

(All Dimensions in mm.)

The specimen design shown above was used to obtain fatigue crack propagation data in the present investigation. This type of specimen was used previously in an extensive FCP study by Clark and Hudak[81]. The value of ΔK is determined for this specimen by:

$$\Delta K = (1-R)\frac{YPa^{\frac{1}{2}}}{BW} \qquad (7)$$

where:

R = stress ratio,

P = maximum applied load,

a = crack length,

B = specimen thickness,

W = distance from load line to end of specimen, and

Y = calibration factor.

The value of Y for this specimen design is given by:

$$Y = 30.96-195.8(a/W)+730.6(a/W)^2-1186.3(a/W)^3+754.6(a/W)^4 \quad (8)$$

APPENDIX B

Fracture Toughness Specimen Design

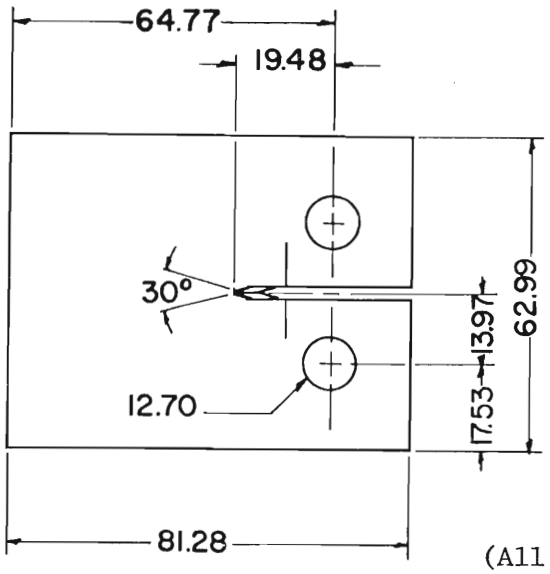

(All dimensions in mm.)

The specimen design shown above was used to obtain the fracture toughness data shown in Table 3 by workers at Frankford Arsenal[9] and Alcoa[10]. The values obtained by Alcoa are reported as K_Q, rather than K_{IC}, because of excessive precrack curvature and insufficient specimen thickness to meet ASTM plane strain requirements[82]. Specimen thickness for both investigations was 25.4 mm. The value of K for this specimen is obtained by:

$$K = \frac{YPa^{\frac{1}{2}}}{BW} \tag{9}$$

where:

$$Y = 29.60-185.5(a/W)+655.7(a/W)^2-1017(a/W)^3+638.9(a/W)^4 \tag{10}$$

APPENDIX C

Predictive Equation for Fatigue Crack Propagation

Chakraborty[93] has modified the equation of Liu and Iino[91] by considering the entire strain field and using the ρ' parameter to represent the average distance between barriers to slip. His equation is presented as:

$$\frac{da}{dN} = 4\rho' \, (2\varepsilon'_f)^{\frac{1}{c}} \sum_{n=1}^{\infty} \left[\int_{x=r+(n-1)\rho'}^{x=r+n\rho'} x^q \Delta\varepsilon_p(x)\,dx \Big/ \int_{x=r+(n-1)\rho'}^{x=r+n\rho'} x^q \, dx \right]^{-\frac{1}{c}} \tag{11}$$

where $\Delta\varepsilon_p(x)$ and X are related as

$$X = \frac{\Delta K^2}{(1+n')\pi K' E} \cdot \frac{1}{[\Delta\varepsilon_p(x)]^{n'+1} + \frac{k'}{E}\,[\Delta\varepsilon_p(x)]^{2n'}} \tag{12}$$

and $\Delta\sigma = k'(\Delta\varepsilon_p)^{n'}$

and $r = \frac{COD}{2}$, and $q = 0.5$

where c and ε'_f are the fatigue ductility exponent and coefficient respectively, and COD is the crack opening displacement, q is a parabolic averaging exponent. Other symbols have been defined previously.

BIBLIOGRAPHY

1. A. R. Rosenfield, C. W. Price, C. J. Martin, D. S. Thompson, and R. E. Zinkham: AFML Tech. Rep. TR-74-129, Part I, December, 1974.

2. M. V. Hyatt: AFML Tech. Rep. TR-73-224, September, 1973.

3. J. G. Kaufman: Design of Aluminum Alloys for High Toughness and High Fatigue Strength, presented at 40th Meeting of the Structures and Materials Panel, NATO, Brussells, Belgium, April, 1975.

4. D. S. Thompson, S. A. Levy, G. E. Spangler, and D. K. Benson: AFML Tech. Rept. TR-73-247, Vol. I, September, 1973.

5. D. S. Thompson and R. E. Zinkham: AFML Tech. Rept. TR-73-247, Vol. II, September, 1974.

6. W. G. Truckner, J. T. Staley, R. J. Bucci, and A. B. Thakker: AFML Tech. Rept. TR-76-169, October, 1976.

7. J. Waldman, H. Sulinski, and H. Markus: Met. Trans., 1974, vol. 5, pp. 573-84.

8. H. Sulinski and J. Waldman: Frankford Arsenal Summary Report, July, 1975.

9. H. Sulinski and J. Waldman: Frankford Arsenal Summary Report, July, 1976.

10. J. E. Vruggink: Tech. Rept. FA-TR 76073, April, 1977.

11. J. C. Zola: AVSCOM Rept. 76-41, October, 1976.

12. M. V. Hyatt and W. E. Quist: AFML Tech. Rept. TR-67-329, 1967.

13. J. T. Staley: Tech. Rept. Naval Air Systems Command Contract N00019-71-C-0131, May, 1972.

14. J. T. Staley: Microstructure and Toughness of High-Strength Aluminum Alloys, presented at ASTM Symposium on Properties Related to Toughness, Montreal, Canada, June, 1975.

15. J. S. Santner: AFML Tech. Rept. TR-76-200, March 1977.

16. F. Osterman: Met. Trans., 1971, vol. 2, pp. 2897-2902.

17. E. DiRusso, M. Conserva, F. Gatto, and H. Markus: Met. Trans., 1973, vol. 4, pp. 1133-1144.

18. W. H. Reimann and A. W. Brisbane: Eng. Fract. Mech., 1973, vol. 5, pp. 67-78.

19. D. S. Thompson, S. A. Levy, and D. K. Benson: Thermomechanical Aging of Aluminum Alloys, presented at 3rd International Conference on Strength of Metals and Alloys, Cambridge, England, 1973, pp. 119-123.

20. D. S. Thompson: Met. Trans., 1975, vol. 6A, pp. 671-83.

21. N. E. Paton and A. W. Sommer: Influence of Thermomechanical Processing Treatments on Properties of Aluminum Alloys, presented at 3rd International Conference on Strength of Metals and Alloys, Cambridge, England, 1973, pp. 101-108.

22. F. G. Osterman and W. H. Reimann: Thermomechanical Processing and Fatigue of Aluminum Alloys, in Achievement of High Fatigue Resistance in Metals and Alloys, ASTM STP 467, ASTM, 1970, pp. 169-187.

23. F. Mehrpay, D. L. Kudsin, and W. L. Haworth: Met. Trans., 1976 vol. 7A, pp. 761-62.

24. E. DiRusso, M. Conserva, M. Buratti, and F. Gatto: Mat. Sci. Eng., 1974, vol. 14, pp. 23-36.

25. R. E. Sanders, Jr. and E. A. Starke, Jr.: Mat. Sci. Eng., 1977, vol. 28, pp. 53-68.

26. A. Kelly and R. B. Nicholson: Progress in Materials Science, 1963, vol. 10, pp. 151-391.

27. J. Gjonnes and Chr. J. Simensen: Acta. Met., 1970, vol. 18, pp. 881-890.

28. H. Y. Hunsicker: Aluminum, vol. 1, American Society for Metals, 1967, Metals Park, Ohio, p. 124.

29. B. W. Lifka and D. O. Sprowls: ASTM STP 516, pp. 120-144, ASTM, 1972.

30. T. H. Sanders and E. A. Starke, Jr.: Met. Trans. A, 1976, vol. 7A, pp. 1407-1418.

31. A. Kelly and M. E. Fine: Acta. Met., 1957, vol. 5, pp. 365-367.

32. E. Orowan: Symposium on Internal Stresses in Metals, Institute of Metals, 1948, pp. 451-453.

33. P. B. Hirsch: J. Inst. of Metals, 1957-58, vol. 86, pp. 13-14.

34. V. Gerold: "Precipitation Hardening," Dislocation Theory--A Collective Treatise, (ed. R.F.N. Nabarro), to be published.

35. K. M. Carlsen and R. W. K. Honeycombe: J. Inst. of Metals, 1954-55, vol. 83, pp. 449-454.

36. G. Thomas and J. Nutting: J. Inst. of Metals, 1957-58, vol. 86, pp. 7-14.

37. N. Ryum, B. Haegland, and T. Lindtveit: Z. Metallkde, 1967, vol. 58, pp. 28-31.

38. S. P. Lynch: Met. Sci. J., 1973, vol. 7, pp. 93-99.

39. E. A. Starke, Jr.: Mater. Sci. Eng., 1977, vol. 29, pp. 99-115.

40. R. H. Van Stone, R. H. Marchant, and J. R. Low, Jr.: ASTM STP 556, pp. 93-124, ASTM, 1974.

41. C. S. Yen: in Metal Fatigue: Theory and Design, ed. A. G. Madayag, 1969, John Wiley and Sons, p. 117.

42. B. I. Sandor: Fundamentals of Cyclic Stress and Strain, Univ. of Wisconsin Press, Madison, 1972.

43. J. F. Tavernelli and L. F. Coffin, Jr.: Trans. ASM, 1959, vol. 51, pp. 438-50.

44. S. S. Manson and M. H. Hirschberg: in Fatigue: an Interdisciplinary Approach, Syracuse Univ. Press, 1964, p. 133.

45. T. Endo and J. Morrow: J. of Materials, 1969, Vol. 4, pp. 159-175.

46. R. J. Selines: Ph.D. Thesis, 1974, Massachusetts Institute of Technology, Cambridge, Mass.

47. M. E. Fine: Private Communication, Northwestern Univ., 1976.

48. P. C. Paris and F. Erdogan: J. of Basic Eng., Trans. ASME, 1963, Vol. 85, Series D, pp. 528-534.

49. N. E. Frost, K. J. Marsh, and L. P. Pook: Metal Fatigue, Oxford Univ. Press, London, 1974.

50. C. Calabrese and C. Laird: Mat. Sci. and Eng., 1974, vol. 13, pp. 159-174.

51. C. Calabrese and C. Laird: Mat. Sci. and Eng., 1974, vol. 13, pp. 141-157.

52. C. Laird: ASTM STP 637, pp. 3-35, ASTM, 1977.

53. F. S. Lin: Ph.D. Thesis, 1978, Georgia Institute of Technology, Atlanta, Ga.

54. M. S. Hunter and W. G. Fricke, Jr.: presented at the 58th Annual Meeting of the ASTM, 1955.

55. G. Lutjering, H. Doker and D. Munz: presented at the Third International Conf. on the Strength of Metals and Alloys, 1973.

56. J. M. Finney: Mat. Sci. and Eng., 1970, vol. 6, pp. 55-65.

57. J. C. Grosskreutz: in Fatigue and Fracture of Aircraft Structures and Materials, Proc. Air Force Conf., 1969.

58. M. E. Fine: Keynote Lecture for "Advances in Physical Metallurgy of Aluminum Alloys I" session, Spring IMD Meeting, May 1973.

59. A. W. Thompson and W. A. Backofen: Acta. Met., 1971, vol. 19, pp. 597-606.

60. C. Laird and C. E. Feltner: Trans. TMS-AIME, 1967, vol. 239, pp. 1074-1083.

61. R. C. Boettner, C. Laird, and A. J. McEvily: Trans. TMS-AIME, 1965, vol. 233, pp. 379-387.

62. C. E. Feltner and P. E. Beardmore: ASTM STP 467, pp. 77-112, ASTM, 1970.

63. C. Laird: ASTM STP 415, pp. 131-180, ASTM, 1967.

64. D. A. Meyn: Trans. ASM, 1968, vol. 61, pp.42-51.

65. R. M. N. Pelloux: Trans. ASM, vol. 62, 1969, pp. 281-285.

66. B. Tomkins and W. D. Biggs: J. Mater. Sci., 1969, vol. 4, pp. 544-553.

67. C. A. Stubbington: Metallurgia, 1963, vol. 68, pp. 109-121.

68. J. A. Feeney, J. C. McMillan, and R. P. Wei: Met. Trans., 1970, vol 1, pp. 1741-1757.

69. M. O. Speidel: NATO Advanced Study Institute on SCC, Copenhagen, 1975.

70. M. R. Louthan, Jr., G. R. Caskey, Jr., J. A. Donovan, and D. E. Rawl, Jr.: Mater. Sci. Eng., 1972, vol. 10, pp. 357-368.

71. L. H. Glassman and A. J. McEvily: NASA TN D-928, 1962.

72. T. H. Sanders, Jr., R. R. Sawtell, J. T. Staley, R. J. Bucci, A. B. Thakker: Naval Air Development Center Tech. Report 56-78-AF8, April, 1978.

73. E. A. Starke, Jr.: J. of Metals, 1970, pp. 54-63.

74. B. Avitzur: Met. Trans., 1973, vol. 4, pp. 383-386.

75. F. Osterman: Met. Trans., ibid , pp. 383-386.

76. A. J. McEvily, A. J. Clark, and A. P. Bond: Trans. ASM, 1967, vol. 60, pp. 661-671.

77. H. W. Antes, S. Lipson, and H. Rosenthal: Trans. TMS-AIME, 1967, vol. 239, pp. 1634-1642.

78. S. N. Singh and M. C. Flemings: Trans. TMS-AIME, 1969, vol. 245, pp. 1811-1819.

79. 1974 Annual Book of ASTM Standards, p. 90, ASTM, "Tension Testing of Metallic Materials," Designation E8-69, 1974.

80. D. A. Mauney: Private communication, Alcoa Technical Center, Alcoa Center, Pa., July, 1976.

81. W. G. Clark, Jr. and S. J. Hudak, Jr.: J. Testing and Eval., 1975, vol. 3, pp. 454-476.

82. 1974 Annual Book of ASTM Standards, p. 432, ASTM, "Plane-strain Fracture Toughness of Metallic Materials, Designation E399-74, 1974.

83. J. T. Staley: Private communication, Alcoa Technical Center, Alcoa Center, Pa., December, 1977.

84. T. H. Sanders, Jr. and R. R. Sawtell: Private communication, Alcoa Technical Center, Alcoa Center, Pa., March, 1977.

85. Aluminum Company of America: AFML Tech. Report AFML-TR-76-60, May, 1976.

86. J. S. Santner and M. E. Fine: Unpublished research, Northwestern University, Evanston, Ill., 1976.

87. A. Saxena and S. Antolovich: Met. Trans. A, 1975, vol. 6A, p. 1816.

88. T. H. Sanders, Jr., D. A. Mauney, and J. T. Staley: presented at 10th Annual Symposium on Materials Science, ed. R. I. Jaffee, 1975.

89. E. E. Underwood and E. A. Starke, Jr.: to be published in Proceedings of the ASTM Symposium on Fatigue Mechanisms, Kansas City, Mo., 1978.

90. R. W. Hertzberg: Deformation and Fracture Mechanics of Engineering Materials, John Wiley and Sons, New York, 1976, pp. 465-539.

91. H. W. Liu and N. Iino: Proc. 2nd Int. Conf. on Fracture, Chapman and Hall, 1969, pp. 812-823.

92. S. Majumdar and J. Morrow: Univ. Of Illinois, T and A. M. Report No. 364, 1973.

93. S. B. Chakrabortty: ONR Tech Report 78-2, May, 1978.

94. M. A. Miner: J. Appl. Mech., 1945, vol. 12A, pp. 159-164.

95. E. J. Coyne, Jr. and E. A. Starke, Jr.: accepted for publication in Int. J. Fract., 1978

96. S. B. Chakrabortty: Private communication, Georgia Institute of Technology, Atlanta, Georgia, June, 1978.

VITA

Robert Edward Sanders, Jr., the son of Mr. and Mrs. Robert E. Sanders, was born on February 2, 1952 in Columbia, South Carolina. During his high school years, he was employed by the North Augusta Star newspaper and attained the rank of Eagle Scout in the Boy Scouts of America. He graduated from North Augusta Senior High School, North Augusta, S.C., as Valedictorian of his class in June, 1970 and entered the Georgia Institute of Technology in September, 1970.

During the summer quarters of 1972-1974, he was employed by the E.I. Dupont de Nemours Company at the Savannah River Plant and Laboratory, Aiken, S.C. He graduated from Georgia Tech in June, 1974, with a Bachelor of Science degree in Ceramic Engineering. In September, 1974, he returned to Georgia Tech on a Presidential Fellowship to pursue graduate studies in Metallurgy. Under the capable direction of his thesis advisor, Dr. E.A. Starke, Jr., he received a Master of Science degree in Metallurgy in June, 1976. The title of his M.S. Thesis was "The Effect of Zirconium on the Low Cycle Fatigue Behavior of an Aluminum-Zinc-Magnesium Alloy." In May, 1977, he received the Monie A. Ferst Master's Research Award from the Georgia Tech chapter of Sigma Xi.

During the course of his Ph.D. research, he served as Resident Advisor for the Gamma Eta chapter of Beta Theta Pi. He received his

Ph.D. degree in Metallurgy from Georgia Tech in September, 1978 under the guidance of Dr. E. A. Starke, Jr. The title of his Ph.D. dissertation was "The Effect of Intermediate Thermomechanical Treatments on the Fatigue Properties of Two 7XXX Aluminum Alloys." He has co-authored (with Dr. Starke) several articles in the technical literature on the relationship between microstructure and fatigue properties of high-strength aluminum alloys.